1987

The temporal and spatial acoustical response of a point-driven

Stevens, James Gerard.

NAVAL POSTGRADUATE SCHOOL
Monterey, California

THESIS

THE TEMPORAL AND SPATIAL ACOUSTICAL RESPONSE
OF A
POINT-DRIVEN, FLUID-LOADED PLATE

by

James Gerard Stevens

March 1987

Thesis Advisor: Alan B. Coppens

Approved for public release; distribution is unlimited

Y CLASSIFICATION OF THIS PAGE

REPORT DOCUMENTATION PAGE

ORT SECURITY CLASSIFICATION NCLASSIFIED)	1b. RESTRICTIVE MARKINGS
URITY CLASSIFICATION AUTHORITY	3 DISTRIBUTION / AVAILABILITY OF REPORT Approved for public release; distribution is unlimited
LASSIFICATION / DOWNGRADING SCHEDULE	
ORMING ORGANIZATION REPORT NUMBER(S)	5 MONITORING ORGANIZATION REPORT NUMBER(S)
ME OF PERFORMING ORGANIZATION l Postgraduate School	6b OFFICE SYMBOL (If applicable) 71
	7a NAME OF MONITORING ORGANIZATION Naval Postgraduate School
RESS (City, State, and ZIP Code) erey, California 93940-5000	7b ADDRESS (City, State, and ZIP Code) Monterey, California 93940-5000
E OF FUNDING / SPONSORING ANIZATION	8b OFFICE SYMBOL (If applicable)
	9 PROCUREMENT INSTRUMENT IDENTIFICATION NUMBER
RESS (City, State, and ZIP Code)	10 SOURCE OF FUNDING NUMBERS

PROGRAM ELEMENT NO	PROJECT NO	TASK NO	WORK UNIT ACCESSION NO

E (Include Security Classification)
EMPORAL AND SPATIAL ACOUSTICAL RESPONSE OF A POINT-DRIVEN, FLUID-LOADED PLATE

ONAL AUTHOR(S)
ens, James G.

E OF REPORT	13b TIME COVERED	14 DATE OF REPORT (Year, Month, Day)	15 PAGE COUNT
r's Thesis	FROM _____ TO _____	1987 March	125

LEMENTARY NOTATION

COSATI CODES			18 SUBJECT TERMS (Continue on reverse if necessary and identify by block number)
D	GROUP	SUB-GROUP	(Point-driven fluid-loaded plate, plexiglass plate, Lloyd's mirror, method of images, Arctic wave types)

RACT (Continue on reverse if necessary and identify by block number) The radiated acoustic field from a driven, fluid-loaded plate was determined several years ago. However, current ional problems force a re-examination in the light of certain acoustic anomalies. The types of waves that propagate in a solid plate are reviewed for their relative ance. Experimental models were constructed in an anechoic acoustic tank in an t to model the aforementioned anomalies.

It is found that the effect of a plexiglass plate placed at the boundary of a -of-images geometry is that of a phase delay only. Therefore, mode conversion from ssional waves to flexural waves is thought to be insignificant.

A second experiment is described in which a plexiglass plate was driven with a small udinal vibrator. Experimental radiation patterns suggest that of a quasi-piston. lass is an acoustically slow media, therefore the coincidence effect is not possible. r, its absorption of acoustic waves make it a poor choice for experiments where wave ation is important.

IBUTION / AVAILABILITY OF ABSTRACT CLASSIFIED/UNLIMITED ☐ SAME AS RPT ☐ DTIC USERS	21 ABSTRACT SECURITY CLASSIFICATION (unclassified)
ME OF RESPONSIBLE INDIVIDUAL ciate Professor Alan B. Coppens	22b TELEPHONE (Include Area Code) 408-646-2941 — 22c OFFICE SYMBOL 61Cz

M 1473, 84 MAR 83 APR edition may be used until exhausted
All other editions are obsolete

SECURITY CLASSIFICATION OF THIS PAGE

Approved for Public Release; distribution is unlimited

The Temporal and Spatial Acoustical Response of a Point-Driven, Fluid-Loaded Plate

by

James Gerard Stevens
Lieutenant, United States Navy
B.S., The Ohio State University, 1979

Submitted in partial fulfillment of the requirements for the degrees of

MASTER OF SCIENCE IN ENGINEERING ACOUSTICS

and

MASTER OF SCIENCE IN SYSTEMS TECHNOLOGY
(ANTI-SUBMARINE WARFARE)

from the

NAVAL POSTGRADUATE SCHOOL
MARCH 1987

ABSTRACT

The radiated acoustic field from a point-driven, fluid-loaded plate was determined several years ago. However, current operational problems force a re-examination in the light of certain acoustic anomalies.

The types of waves that propagate in a solid plate are reviewed for their relative importance. Experimental models were constructed in an anechoic acoustic tank in an attempt to model the aforementioned anomalies.

It is found that the effect of a plexiglass plate placed at the boundary of a method-of-images geometry is that of a phase delay only. Therefore, mode conversion from compressional waves to flexural waves is thought to be insignificant.

A second experiment is described in which a plexiglass plate was driven with a small longitudinal vibrator. Experimental radiation patterns suggest that of a quasi-piston. Plexiglass is an acoustically slow media, therefore the coincidence effect is not possible. Further, its absorption of acoustic waves make it a poor choice for experiments where wave propagation is important.

Thesis Disclaimer

The reader is cautioned that computer programs developed in this research may not have been exercised for all cases of interest. While every effort has been made, within the time available, to ensure that the programs are free of computational and logic errors, they cannot be considered validated. Any application of these programs without additional verification is at the risk of the user.

TABLE OF CONTENTS

LIST OF FIGURES

LIST OF SYMBOLS
(ROMAN ALPHABET)

a_i	Antisymmetric mode of order i
A	Amplitude
B,D	Bending stiffness
C	Integration contour
c	Speed of sound
c_b	Bending wave speed
c_L, c_p	Longitudinal wave speed
c_o	Speed of sound in fluid
c_s	Shear wave speed
d	Depth of source, plate thickness (Brekhovskikh)
E,Y	Young's modulus
f, f_c	Frequency, coincidence frequency
F_o	Amplitude of point-force source
G,G'	Shear modulus, modified shear modulus
h,H	Plate thickness
H_o	Hankel function
k	Wave number
ko	Wave number in fluid
k_f	Flexural wave number
$k_\perp$, $k_\parallel$	Perpendicular and parallel wave number components
m	Mass density per unit area
p, $\underline{p}$, P	Pressure, pressure (phasor), pressure (magnitude)
r, R, r_-, r_+	Range, characteristic impedance
$\underline{R}$	Reflection coefficient
$\underline{s}_i$	Symmetric mode of order i
t	Time, plate thickness
u	Particle velocity vector
$u_\perp$	Perpendicular component of the velocity
$v_\perp$	Perpendicular component of plate velocity
$\underline{w}$	Perpendicular plate displacement integration variable
x,y,z	Cartesian coordinate distances

LIST OF SYMBOLS
(GREEK ALPHABET)

β	Fluid loading factor
Γ_p	Plate shear parameter
η	Loss factor
θ	Angle, defined locally
λ, λ_o	Wavelength, wavelength in fluid
λ_c	Wavelength at coincidence
λ_f	Flexural wave length
ρ_o	Density of fluid
ρ_m	Density of plate
$\rho_s = t\rho_m$	Density per unit area
σ	Poisson's ratio
τ	Phase delay
$\phi, \phi(x,y,x,t)$	Scalar displacement potential, azimuthal angle
$\vec{\psi}, \vec{\psi}(x,y,z,t)$	Vector displacement potential
ω, ω_c	Radian frequency, radian coincidence frequency

Vector Operations

∇	The gradient
∇^2	The LaPlacian
∇ x	The curl
$\nabla^4 = \nabla^2\nabla^2$	The Biharmonic operator

I. INTRODUCTION

A. THESIS INTRODUCTION

The experiments on which this thesis is based were attempts to physically model a sound source mounted on the ice in the Arctic using a sheet of plexiglass and piezoelectric transducers in an anechoic water tank. Specifically, the sound field radiated into the fluid was of interest.

There are many wave types that propagate in a solid and along a solid-fluid interface. Each was examined for its relative importance, so that attention could be concentrated on those that are more important to the radiation of sound into the water from a sound source mounted on the ice. The Ewing and Press [Ref. 1] method of solution covers wave propatation in ice far from the source. Stein [Ref. 2] considered radiation from sound sources mounted on the ice.

Two experiments were performed. The first was an investigation on the effect of a plate placed at the free boundary of the classic method-of-images (Lloyd's mirror) geometry. Waves emanating from a source near a pressure-release boundary will develop an interference pattern with waves reflected from the boundary that can be detected by a receiver. It is hypothesized that a

plate placed at the boundary will affect the interference pattern.

In the second experiment performed, the source was attached to the ice in an attempt to duplicate the "acoustic mode," named by Stein [Ref. 2, p.100], of the Arctic ice sound propagation. The theoretical development of the chapter uses the Mindlin-Timoshenko thick plate equations to explain the effects of coincidence and fluid loading on the radiated sound field from a point-driven, fluid-loaded plate.

B. BACKGROUND

The classical two-dimensional theory of flexural waves in elastic bars in vacuo, using Lagrange's equation, was solved in 1889 by Lord Rayleigh under the assumption that the wavelengths were long with respect to the thickness of the plate. Thus, the equations are invalid for high frequency waves or for sharp transients. There are two effects that were neglected: rotatory inertia and transverse shear deformation. Later, however, Rayleigh introduced into the equations the effect of rotatory inertia, but because transverse shear deformation was not included, this correction was too large. Timoshenko [Ref. 3] included the effect of transverse shear deformation in a study of flexural waves of bars.

Mindlin [Ref. 4] in a study of flexural waves in plates included the effects of both rotatory inertia and shear deformation in his now classic paper in which are developed the so-called Mindlin-Timoshenko thick plate equations. Dyer [Ref. 5], using the Mindlin-Timoshenko equations, showed the effects of transverse shear to be important even for thin plates. Skudrzyk et al [Ref. 6] developed a theory of flexural waves in a driven plate similar to that of the theory of reverberation in room acoustics.

In 1966, David Feit [Ref. 7] calculated the acoustic pressure radiated into a fluid by an infinite plate driven by a point force, using the Mindlin-Timoshenko thick plate equations. His solution used the saddle point method of steepest descent to evaluate the pressure integral. Stuart [Ref. 8] explored the solution of the Mindlin-Timoshenko equations with then-new insights concerning the so-called leaky waves emanating from the plate. He asserted that previous discrepancies in the saddle point technique solution (a coincidence frequency lower than predicted, and small but unaccounted for lobes in the far-field pattern below coincidence) were due to neglected poles occurring near the saddle point, called leaky wave poles, and that these influence the far-field pressure.

Creighton [Ref. 9] contradicted these findings, demonstrating that ". . . the far-field contributions associated with . . . the leaky waves may be altered merely by a change in the integration path . . ." and that the contributions decayed exponentially with depth into the water and did not represent physically meaningful free modes, except for subsonic surface waves.

As the theory of waves in a plate developed, so did the theory of wave propagation in the ice. The theory of propagation of elastic waves in a floating ice sheet was given by Press and Ewing [Ref. 1], by considering the ice as an infinite plate and using classical wave theory. Press and Ewing [Ref. 10] then extended their results to include the effects of the air. A further discussion of their work as a whole is found in Ewing, Jardetzky, and Press [Ref. 11].

In a recent study Stein [Ref. 2] used the Ewing and Press method of solution, but solved the problem with the aid of modern computer algorithms. The bulk of the study was that of the propagation speeds of the various modes. His data taken from Arctic and freshwater lake ice experiments corraborate with the predicted transient arrival times and propagation losses.

C. WAVES IN A SOLID

There are several wave types that may propagate in a

solid and others that occur at a solid-fluid interface. A study of the applicability of each type found in the literature was done and is included here to give the reader a sense of wave types that are relevant to the problem of modeling a sound source mounted on the ice generating a sound field in the underlying water by the excitation of the ice.

Propagation of waves in solids can be distinguished from that in fluids by the solid's ability to restore shear. This leads to two wave equations:

$$\nabla^2 \phi = \frac{1}{c_p^2} \frac{\partial^2 \phi}{\partial t^2} \tag{1.1a}$$

for the scalar displacement potential which describes longitudinal motion, and

$$\nabla^2 \vec{\psi} = \frac{1}{c_s^2} \frac{\partial^2 \vec{\psi}}{\partial t^2} \tag{1.1b}$$

for the vector displacement potential which describes shear wave motion. The potentials $\phi(x,y,z,t)$ and $\vec{\psi}(x,y,z,t)$ are related to the particle velocity vector $\vec{u} = u_x\hat{i} + u_y\hat{j} + u_z\hat{k}$ by

$$\vec{u} = \nabla\phi + \nabla \times \vec{\psi} \tag{1.2}$$

An excellent depiction of some of the different types of acoustic waves, along with their speeds, is given by Ver and Holmer [Ref. 12, p. 273] and it is from this source that Figure 1.1 is taken.

Longitudinal waves are waves that propagate along the direction of compression and dilatation in the plate. The thickening and thinning of the plate seen in Fig.1.1a is a consequence of a non-zero Poisson's ratio.

Shear waves are solutions to the additional wave equation that governs waves in solids:

$$\nabla^2 \vec{\psi} = \frac{1}{c_s^2} \frac{\partial^2 \vec{\psi}}{\partial t^2}$$

where $c_s^2 = \frac{G}{\rho}$ as in Fig. 1.1b

$\vec{\psi}$ = vector potential of particle displacement in a solid.

Two types of shear waves are found in the literature: SH and SV waves are the designations given them in texts on seismological wave propagation. SV, shear waves polarized vertically, denotes waves for which the shearing motion is perpendicular to the plane of the plate. It is this wave that is depicted in Fig. 1b. SH, shear waves horizontally polarized, denotes waves for which the shearing motion is parallel to the plane of the plate.

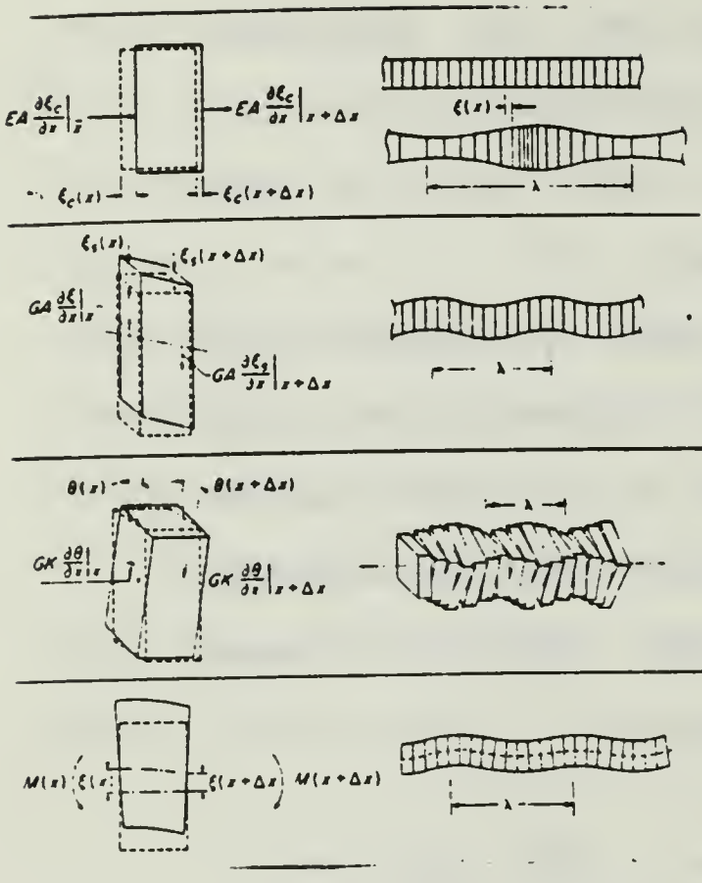

a. longitudinal wave

$$c_p = \sqrt{\frac{Y}{\rho(1-\sigma^2)}}$$

b. shear wave

$$c_S = \sqrt{\frac{G}{\rho}}$$

c. torsional wave

$$c_T = \sqrt{\frac{GK}{\rho I}}$$

d. bending (flexural) wave. (thin plte theory: see text)

$$c_b = \sqrt[4]{\frac{\omega^2 Y t^2}{12\rho(1-\sigma^2)}}$$

Figure 1.1. Wave Types in Solids and Their Speeds (After Ver and Holmer)

Y = Young's modulus, which relates the stress to the strain produced,

σ = Poissons ratio,which relates lateral expansion to its longitudinal shortening due to a compressive stress,

G = the shear modulus, which relates shearing stress to shearing strain produced,

I = the moment of inertia,

K = a torsional stiffness factor, which relates a twist to the shearing strain produced,

ρ = the solid's density,

t = the solid's thickness, and

ω = the radian frequency of the motion.

Torsional waves, Fig. 1c, result from a twisting force applied to a solid. This wave can be generated in bars, where the y and z dimensions are similar. Torsional waves are not be easily excited in a plate; they will not be further considered in this study.

Flexural waves, or bending waves, are a more complex motion than the previous ones considered, because of the complicated stresses set up when a plate is bent. The bending of a plate compresses the plate on the inside of the bend and expands the plate on the outside. Due to this compression and expansion, a Poisson's ratio effect is introduced.

As with any wave, the energy of a flexural wave is composed of two parts, potential energy and kinetic energy. The potential energy is made up of two deflections: flexural deformation, and shear deformation. The kinetic energy also has two contributions, linear (or translatory) inertia, and rotatory inertia.

The classical two-dimensional theory of flexural motions in thin elastic plates leads to the wave equation [Ref. 4, p. 31]

$$D\nabla^4 \underline{w} + \rho h \frac{\partial^2 w}{\partial t^2} = 0 \qquad (1.3)$$

where $D = \frac{Yh^3}{12(1-\sigma^2)}$, and here

h = plate thickness

$\underline{w}$ = the plate particle motion

This equation relates only the flexural deformation to the linear (or translatory) inertia as the two opposing forces. The Mindlin-Timoshenko equation relates the linear and rotatory inertia as the driving forces to the flexural and transverse shear deformation as the restoring forces. (This was what was referred to earlier as "correcting" for rotatory inertia and transverse shear.) The Mindlin-Timoshenko equation is

$$\left(\nabla^2 - \frac{\rho}{G'} \frac{\partial^2}{\partial t^2}\right)\left(D\nabla^2 - \frac{\rho h^3}{12} \frac{\delta^2}{\partial t^2}\right) \underline{w} + \rho h t \frac{\partial^2}{\partial t^2} \underline{w} = 0 \qquad (1.4)$$

where

$$G' = \frac{\pi^2}{12} \frac{Y}{2(1+\sigma^2)}$$

h = plate thickness.

The $\frac{\rho}{G'} \frac{\partial^2}{\partial t^2}$ term is the contribution of transverse shear.

The $\frac{\rho h^3}{12} \frac{\partial^2}{\partial t^2}$ term is the contribution of rotatory inertia.

Note that if these terms are neglected, the classical equation (Eq. 1.3) results.

The Mindlin-Timoshenko theory is used when analyzing "thick" plates, i.e., plates whose thickness exceeds $\lambda_s/20$, where λ_s is the shear wave length. [Ref. 13, p. 215]

Of key importance to this study is the effective phase speed for flexural motions as a function of frequency. Ross, assuming a harmonic disturbance of a homogeneous plate in vacuo, gives an equation for the flexural wave speed c_b as

$$(1- \Gamma_p(\frac{\omega}{\Omega_p}))^2(\frac{c_b}{c_p})^4 + (\Gamma_p+1)(\frac{\omega}{\Omega_p})^2(\frac{c_b}{c_p})^2 - (\frac{\omega}{\Omega_p})^2 = 0 \quad (1.5)$$

where

Γ_p = the plate shear parameter

$\doteq 2.65\ (1 + \frac{3}{5}\ \sigma + \frac{3}{4}\ \sigma^2)$

Ω_p = the reference angular frequency,

$\equiv \frac{c_p\ 12}{t}$

ω = the angular frequency of the flexural wave

c_p = the plate longitudinal wave speed, given in Fig. 1.1a.

Equation 1.5 can be solved by applying the quadratic equation to solve for the variable $(\frac{c_b}{c_p})^2$. It is a difficult function of the other parameters, but can be

represented accurately in terms of approximate solutions at low, intermediate and high frequencies.

At low frequencies, the flexural wave speed is approximated by

$$c_{bl} \doteq \sqrt[4]{\frac{\omega^2 \gamma t^2}{12\rho(1-\sigma^2)}} \tag{1.6}$$

which is that given in Fig. 1.1d, and represents the flexural wave speed in thin elastic plates, given by the classical wave equation, Equation 1.3. This equation is valid when

$$\Gamma_p \left(\frac{\omega}{\Omega_p}\right)^2 << 1$$

In the intermediate frequency range, the flexural wave speed is approximated by

$$c_{bi} \doteq c_{bl} \cdot \left[\frac{\left(1+\left(\frac{\omega}{\Omega_p}\right)^2\right)^{1/2} - 2\,\frac{\omega}{\Omega_p}}{1 - \Gamma_p \left(\frac{\omega}{\Omega_p}\right)^2}\right]^{1/2} \tag{1.7}$$

In the high frequency range, the flexural wave phase velocity predicted by the Mindlin-Timoshenko theory tends to the Rayleigh wave velocity [Ref. 13, p. 248], which is a value slightly less than the shear wave velocity. The expression for the high frequency

flexural wave speed is

$$c_{bh} \doteq 0.76\left(1 + \frac{2}{5}\,\sigma\right) c_s \qquad (1.8)$$

This equation is valid when

$$\Gamma_p \left(\frac{\omega}{\Omega_p}\right) >> 1.$$

Heretofore we have discussed waves propagating in a solid. Waves can also propagate along the boundary of a solid-fluid interface in much the same manner as do surface waves on the ocean. These waves are Rayleigh waves (for a half-solid), Lamb waves (for a plate), Stonely waves, Love waves, and Crary waves.

Rayleigh waves ". . .represent elastic perturbations propagating near the free boundary of a solid and decaying with depth" [Viktorov, Ref. 14, p. 1]. Figure 1.2 is a depiction of the instantaneous deformation associated with a Rayleigh wave.

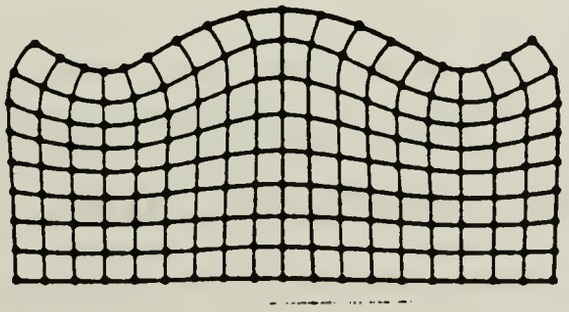

Figure 1.2 Depiction of a Rayleigh Wave (after Viktorov)

Rayleigh waves propagate along the surface of a solid at a free boundary, such as an air-ice boundary or an air-plexiglass boundary. The wave decays exponentially in the z-direction into the solid, and if the decay constant is not large, the motion of the wave may appear at the lower (in this case, water) boundary. Furthermore, the Rayleigh wave is supersonic with respect to the fluid, therefore this motion would radiate sound into fluid (see Chapter III for an explanation on the importance of relative sound speeds to radiation into the fluid.)

The discussion of Rayleigh waves is included because, as mentioned above, in the high frequency limit flexural waves degenerate to Rayleigh surface waves for a plate in vacuo. However, Stein shows that at low frequencies there is no coupling of the Rayleigh wave with the flexural wave there would be for a plate in a vacuo[1]. Moreover, the types of sources being considered would not generate Rayleigh waves, hence they will not be further considered.

Lamb waves ". . . refer to elastic perturbations propagating in a solid plate (or layer) with free

---

[1]There is a growing debate among the cognoscenti concerning the importance of the Rayleigh wave in Arctic ice [Ref. 15].

boundries, for which displacements occur both in the direction of wave propagation and perpendicular to the plane of the plate." [Ref. 13, p. 67]. They are also called the "normal modes" of a plate, and can be symmetrical (s) or antisymmetrical (a) relative to the center plane of the plate. Note that the zero-order symmetric and antisymmetric modes are the longitudinal and flexural waves, respectively. Figure 1.3 depicts the zero-order Lamb waves. These two modes are of key importance to this study.

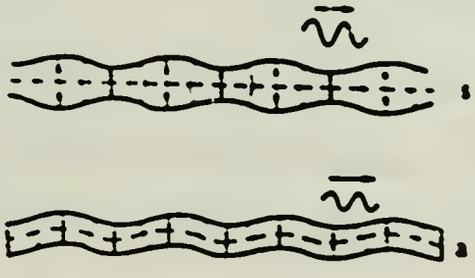

Figure 1.3 Lamb Wave Propagation (after Viktorov)

Another wave that can exist at an interface between two media is a Stonely wave. According to Ewing, Jardetzky and Press [Ref. 11, p. 112] they are modified Rayleigh waves that exist when the shear wave velocities in the two media are nearly equal. Stein [Ref. 2, p. 69] states that they can also exist along the boundary between an elastic medium and a high density,

acoustically slow fluid or elastic medium, and that the Stonely wave is the high frequency asymptote of the first anti-symmetric mode along the ice-water interface. That is, they are Rayleigh waves along the solid-fluid interface. However, absorption in Artic ice is high at the frequencies for which Stonely waves exist [Ref. 2, p. 190] and therefore the Stonely wave is not important to this study.

Two other wave types concerning propagation of sound in ice are described in the literature. Love waves and Crary waves. Both are shear waves. Love waves are SH waves that are generated due to discontinuities in the ice. Stein [Ref. 2 p. 100] notes that ". . . unless there is a discontinuity . . . . they will not radiate nor can they couple to other modes." Discontinuities in the ice are not considered in this study, therefore Love waves will not be considered.

Crary waves are a type of SV wave discovered by Crary in seismic experiments on a floating ice island. They were generated after an ice "event", a small explosive charge mounted in the ice. According to Ewing, Jardetzky and Press [Ref. 11, p. 299], this wave has the following characteristics:

"1. phase velocity is near the speed of compressional waves in the plate;

2. travel time is intermediate between that for P (compressional) waves and that for SH waves;
3. principal [amplitude] is [observed] on longitudtudinal horizontal seismograph; amplitudes are much smaller on vertical and practically absent on transverse horizontal;
4. frequency is almost constant, increasing very slightly with time."

Stein [Ref. 2, p. 93] again discusses these waves, but has found the attenuation to be at least 0.1 dB/m in the horizontal for the Arctic. Thus, these waves will not be observed at appreciable distances. Further, because of their small vertical amplitude and velocity less than that of the fluid, (characteristic 3 of above) they do not impart acoustic energy to the underlying fluid. For these reasons, Crary waves will not be further considered.

So far in this chapter, the types of waves that propagate in a solid, namely Arctic ice, have been discussed without regard to their origin. That is, they have been assumed to be plane waves, far from their source. As these waves propagate, they may be coupled into the surrounding medium, creating acoustic radiation.

Additional radiation may be generated when the waves are excited by a localized force. This is a result of

the flexural motion having a spatial gradient of displacement in the ice, which plane waves do not. Stein [Ref. 2 p. 96] has named this mode of acoustic radiation the "acoustic mode."

Figure 1.4 is a depiction of the first antisymmetric mode, the flexural wave, in a solid. At this point, far from the source, it can be seen why the flexural wave does not radiate[2]: it travels subsonically with respect to the water and there is cancellation of radiation from adjacent positive and negative pressure peaks. (In actuality, because of geometric spreading, there is incomplete cancellation and some radiation does exist.) However, when these waves are excited by a localized force (Fig. 1.5) there is incomplete cancellation and

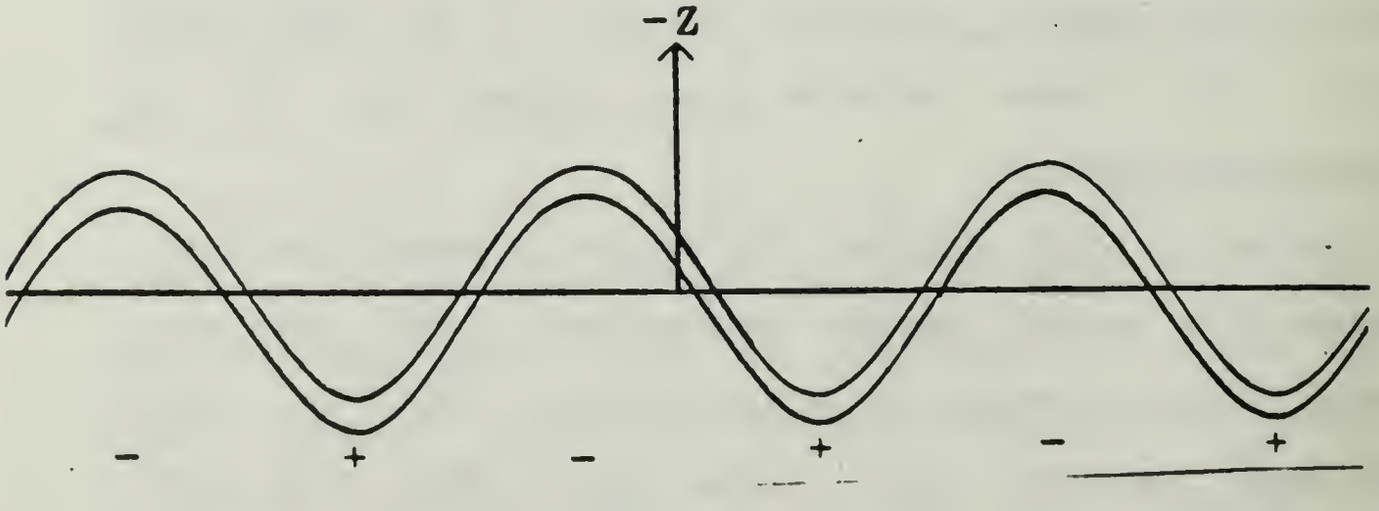

Figure 1.4 Flexural Wave Propagation

[2]A flexural wave below coincidence will not radiate. The coincidence frequency is that frequency above which the plate vibrations can couple to the fluid. See Chapter 3 for a further discussion.

radiation occurs. Note that this acoustic mode is still a flexural wave. A further discussion of this mode found in Chapter III.

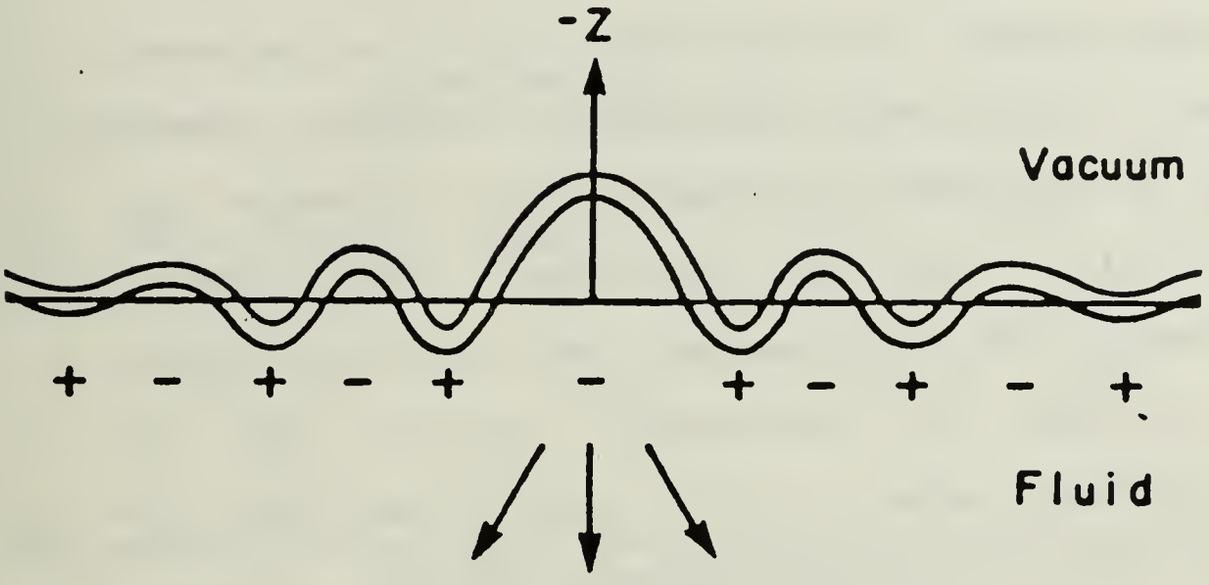

Figure 1.5 Flexural Wave Propagation From a Point Source (after Stein)

D. SUMMARY

In this chapter, the many types of waves found in a solid (ice) have been discussed. As was indicated earlier, only a few have real importance in the Artic, and therefore modeling in the lab should be attempted only for these. Stein [Ref. 2 p. 107] has concluded that the three modes of propagation of importance are the first symmetric and antisymmetric modes, and the acoustic mode. All other aforementioned waves are neglected because either they are highly attenuated in the Arctic at the frequencies of concern or there is a lack of a source with which to generate them.

II. A LLOYD'S MIRROR EXPERIMENT

A. INTRODUCTION

In this chapter, an experiment will be discussed that tested the following hypothesis: a plate introduced at an air-water interface will influence the acoustic field in the water half-space. More simply, the reflection of a spherical wave from an ideal boundary develops an interference pattern with the original incident wave. It is hypothesized that the plate will effect this Lloyd's mirror pattern.

B. THE METHOD OF IMAGES

The method of images is a well-known technique for predicting the radiation pattern of an acoustic source near a fluid interface. For continuity, a brief description of the theory of the acoustic Lloyd's mirror will be presented. The following description is based on that given by Sanders and Coppens [Ref. 16].

If a source of spherical waves is placed on the z-axis a distance d below a pressure-release boundary, as shown in Fig. 2.1, the acoustic radiation from this source in the absence of the boundary can be specified as

$$\underline{p}_s = \frac{A}{r_-} \, e^{j(\omega t - k r_-)} \qquad (2.01)$$

where $r_- = \sqrt{(h-d)^2 + R^2}$

As a result of the boundary, there must be an additional wave present to describe the reflection:

$$\underline{p}_r = -\frac{A}{r_+} e^{j(\omega t - kr_+)} \tag{2.02}$$

where $r_+ = \sqrt{(h+d)^2 + R^2}$

The total field is, then: (2.03)

$$\underline{p}_s + \underline{p}_r = \underline{p} = A\left(\frac{1}{r_-} e^{-jkr_-} - \frac{1}{r_+} e^{-jkr_+}\right)e^{j\omega t}$$

The acoustic field will show strong interference effects because the two waves $\underline{p}_s$ and $\underline{p}_r$ must travel along different paths to reach the receiver.

The geometry is simplified if the assumption

$$r >> d\cos\theta \tag{2.04}$$

is made. Then, r_+ and r_- can be replaced by

$$r_+ \approx r+\Delta r \tag{2.05}$$

$$r_- \approx r-\Delta r$$

$$\Delta r \approx d\sin\theta$$

with 2.04, 2.03 becomes

$$\underline{p}(r,\theta,t) = \frac{A}{r} e^{j(\omega t - kr)}\left[\frac{e^{jk\Delta r}}{1-\frac{\Delta r}{r}} - \frac{e^{-jk\Delta r}}{1+\frac{\Delta r}{r}}\right]$$

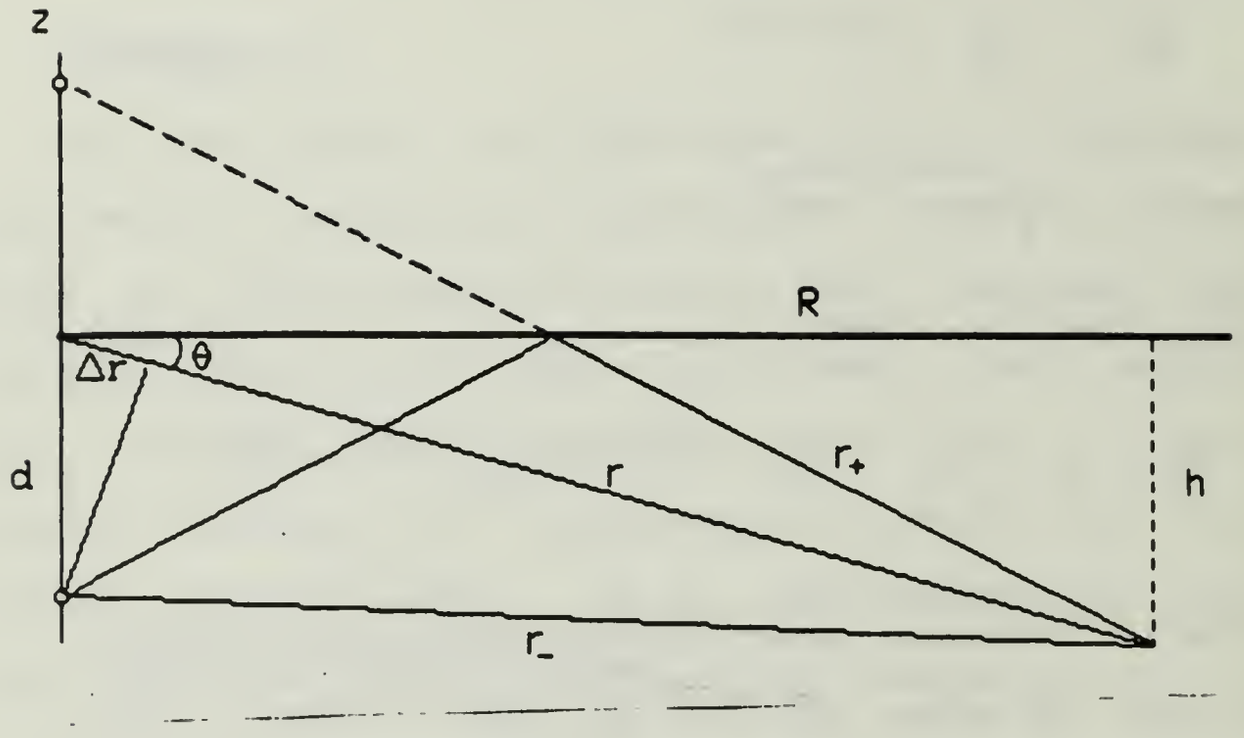

Figure 2.1 Lloyd's Mirror Geometry

Thus when a simple harmonic acoustic wave in the the water is incident on a plane, perfectly reflecting pressure release boundary, the reflected wave is a mirror image of the incident wave which leads to an interference pattern in the medium below the boundary.

This interference pattern may be observed by different methods. The receiver can be placed at a fixed horizontal range from the source and moved downward to show the nodes and antinodes from the pattern. It might also be placed at a fixed slant range from the source and swept through an arc about the source. Or, it might

be held at a constant depth and moved away from the source in horizontal range. Lastly, and want was done in the experiment, the source and receiver can be held in a fixed position and the frequency of the source swept, observing the response of the receiver. The interference of the incident and reflected waves produce maxima and minima in the frequency response of the receiver.

C. THE EFFECT OF THE PLATE

The effect of the plate[3] on the incident wave can be best seen by reverting to simple ray theory. Consider the following problem: an incident wave in water, represented by ray $\underline{p}_i$, impinges on a plate of different characteristic impedance r_2, as shown in Fig. 2.2. The ray (now $\underline{p}_a$) is refracted as it traverses into the plate. It reflects from the top of the plate at z = H (now $\underline{p}_b$), traverses the plate and then is refracted back into the water as $\underline{p}_r$. Note that while the wave is in the plate, it is considered as a compressional (longitudinal) wave.

---

[3]An infinite plate forced by an incident sound wave at any frequency, even below its coincidence frequency, will radiate sound, although a bending wave of the plate itself, below coincidence, will not. [Ref. 12, p. 280]

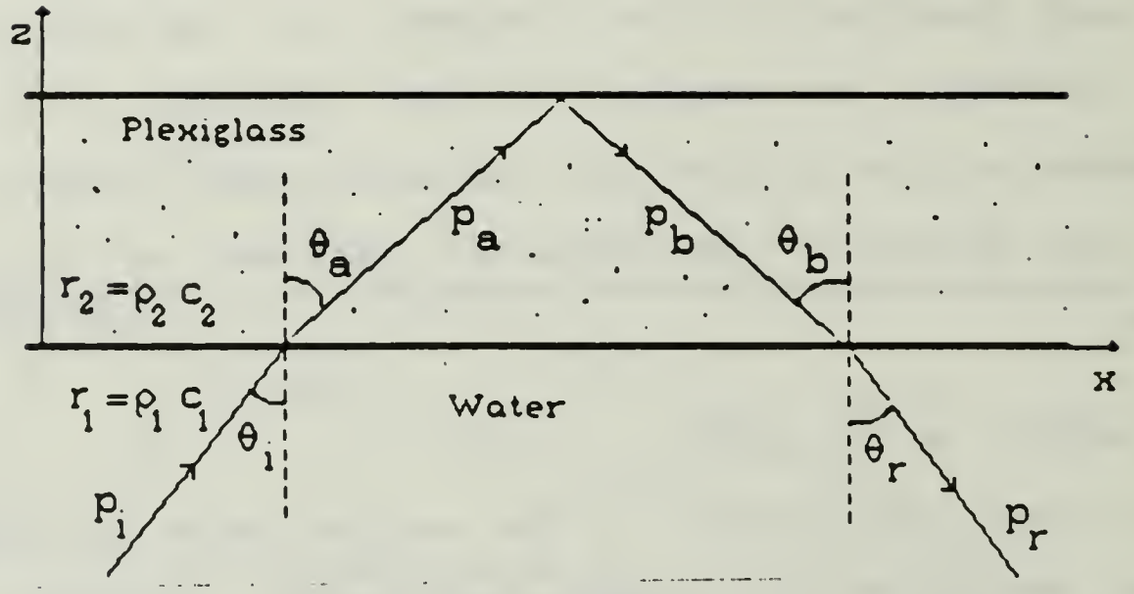

Figure 2.2 Ray Traversing Through a Plate

The four waves may be represented as (considering only two dimensions):

$$\underline{p}_i = \underline{P}_i \, e^{j(\omega t - k_1 \sin\theta_i x - k_1 \cos\theta_i z)} \tag{2.1}$$

$$\underline{p}_a = \underline{P}_a \, e^{j(\omega t - k_2 \sin\theta_a x - k_2 \cos\theta_a z)} \tag{2.2}$$

$$\underline{p}_b = \underline{P}_b \, e^{j(\omega t - k_2 \sin\theta_b x + k_2 \cos\theta_b z)} \tag{2.3}$$

$$\underline{p}_r = \underline{P}_r \, e^{j(\omega t - k_1 \sin\theta_r x + k_1 \cos\theta_r z)} \tag{2.4}$$

The boundary conditions are:

at $z = 0$, continuity of pressure requires

$$\underline{p}_i(x,o) + \underline{p}_r(x,o) = \underline{p}_a(x,o) + \underline{p}_b(x,o) \tag{2.5}$$

Also at z=0, the condition of continuity of normal velocity, requires (taking into account direction of propagation)

$$\underline{u}_i(x,o)\cos\theta_r - \underline{u}_r(x,o)\cos\theta_r = \underline{u}_a(x,o)\cos\theta_a - \underline{u}_b(x,o)\cos\theta_b \tag{2.6}$$

The boundary at z = H is pressure release, therefore

$$\underline{p}_a(x,H) + \underline{p}_b(x,H) = 0 \tag{2.7}$$

For each plane wave, we have

$$\frac{\underline{p}}{\underline{u}} = \pm r \tag{2.8}$$

With Snell's Law, $\frac{\sin\theta_r}{c_1} = \frac{\sin\theta_a}{c_2}$, (2.9)

and since the angle of incidence equals the angle of reflection, we have

$$\theta_i = \theta_r \equiv \theta_1 \quad \text{and} \quad \theta_a = \theta_b \equiv \theta_2 \tag{2.10}$$

If each value of $\underline{u}$ in 2.6 is replaced with the appropriate value of p/r , and from 2.10, subscription are changed, then:

$$\frac{\cos\theta_1}{r_1}[\underline{p}_i(x,o)-\underline{p}_r(x,o)] = \frac{\cos\theta_2}{r_2}[\underline{p}_a(x,o)-\underline{p}_b(x,o)] \tag{2.12}$$

or

$$\underline{p}_i(x,o)-\underline{p}_r(x,o) = \frac{r_1}{r_2}\frac{\cos\theta_2}{\cos\theta_1}(\underline{p}_a(x,o)-\underline{p}_b(x,o)) \tag{2.13}$$

Apply 2.1 through 2.4 to 2.5 , and drop the $e^{j\omega t}$,

$$(\underline{P}_i+\underline{P}_r)e^{-jk_1\sin\theta_1 x} = (\underline{P}_a+\underline{P}_b)e^{-jk_2\sin\theta_2 x} \qquad (2.14)$$

and do the same to 2.13,

$$(\underline{P}_i-\underline{P}_r)e^{-jk_1\sin\theta_1 x} = \frac{r_1}{r_2}\frac{\cos\theta_2}{\cos\theta_1}(\underline{P}_a-\underline{P}_b)e^{-jk_2\sin\theta_2 x} \qquad (2.15)$$

Apply the boundary condition at z=H (Equation 2.7), and dividing through by $e^{-jk_2\sin\theta_2 x}$ gives

$$\underline{P}_a e^{-jk_2\cos\theta_2 H} + \underline{P}_b e^{+jk_2\cos\theta_2 H} = 0 \qquad (2.16)$$

Algebraic manipulation of 2.14 - 2.16 then leads to the reflection coefficient $\underline{R}$:

$$\underline{R} = \frac{\underline{P}_r}{\underline{P}_i} = \frac{\left(1 - \frac{r_1}{r_2}\frac{\cos\theta_2}{\cos\theta_1}\right) - \left(1 + \frac{r_1}{r_2}\frac{\cos\theta_2}{\cos\theta_1}\right) e^{-j2k_2\cos\theta_2 H}}{\left(1 + \frac{r_1}{r_2}\frac{\cos\theta_2}{\cos\theta_1}\right) - \left(1 - \frac{r_1}{r_2}\frac{\cos\theta_2}{\cos\theta_1}\right) e^{-j2k_2\cos\theta_2 H}} \qquad (2.17)$$

where θ_1 and θ_2 are related by Snell's Law (.9), and

$$\cos\theta_2 = \sqrt{1 - \left(\frac{c_2}{c_1}\right)^2 \sin^2\theta_1} \qquad (2.18)$$

D. VALIDATION OF EQUATION 2.17

In the limit as $H \to 0$, Equation 2.17 reduces to $\underline{R} = -1$. This is to be expected, because when $H \to 0$ the r layer disappears and the incident wave is [2] reflected off a purely pressure-release boundary, where the reflected wave is 180° out of phase with the incident, and hence $\underline{R} = -1$.

In the limit as $\theta_1 \to 0$, that is, normal incidence, Equation 2.17 reduces to:

$$\underline{R_1} = \frac{-r_1 \cos k_2 H + j r_2 \sin k_2 H}{r_1 \cos k_2 H + j r_2 \sin k_2 H} \qquad (2.19)$$

Comparing Equation 2.19 with Equation 6.12 of Kinsler et al [Ref. 17]

$$\underline{R} = \frac{[1 - \frac{r_1}{r_3}]\cosh_2 H + j(\frac{r_2}{r_3} - \frac{r_1}{r_2})\sinh_2 H}{(1 + \frac{r_1}{r_3})\cosh_2 H + j(\frac{r_2}{r_3} + \frac{r_1}{r_2})\sinh_2 H} \qquad (2.20)$$

where r_3 is characteristic impedance of the fluid above the place. In the limit $r_3 \to 0$, that is, assuming a vacuum above the plate, 2.20 reduces to 2.19.

Finally, comparison of 2.12 with Brekhovskikh [Ref. 18] yields additional validation. His coordinate system

...is inci
...through medium 2 and

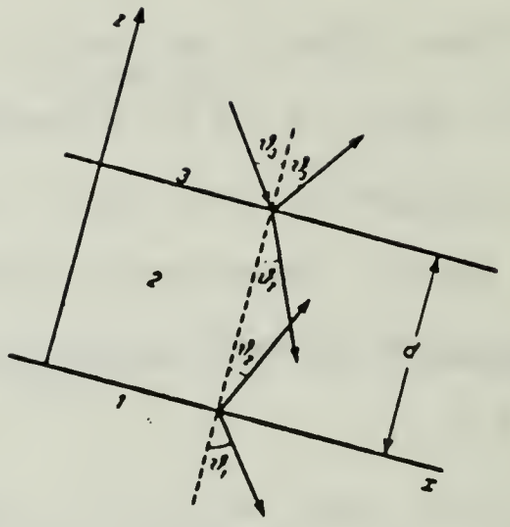

Figure 2.3 Brekhovskikh's Coordinate System (from Brekhovskikh [Ref. 18])

Define the normal impedance as

$$Z_i = \frac{\rho_i c_i}{\cos\theta_i} \qquad i = 1,2,3$$

and define

$$\alpha_2 = k_2 \cos\theta_2 \tag{2.21}$$

Brekhovskikh found [Ref. 18, Equation 5.10]

$$\underline{R} = \frac{(Z_1+Z_2)(Z_2-Z_3)e^{-j\alpha_2 d}+(Z_1-Z_2)(Z_2+Z_3)e^{j\alpha_2 d}}{(Z_1+Z_2)(Z_2+Z_3)e^{-j\alpha_2 d}+(Z_1-Z_2)(Z_2-Z_3)e^{j\alpha_2 d}} \tag{2.22}$$

(2.23)

which reduces to [Ref. 18, Equation 5.18]

$$\underline{R} = \frac{V_{23} + V_{12} e^{zj\alpha_2 d}}{1 + V_{23} V_{12} e^{zj\alpha_2 d}} \tag{2.24}$$

where $V_{12} = \frac{Z_1 - Z_2}{Z_1 + Z_2}$, $V_{23} = \frac{Z_2 - Z_3}{Z_2 + Z_3}$ (2.25)

Assuming $Z_1 = 0$ (in vacuo), then $V_{12} = -1$, and .27 reduces to

$$\underline{R} = \frac{(1 - \frac{Z_3}{Z_2}) - (1 + \frac{Z_3}{Z_2}) e^{zj\alpha_2 d}}{(1 + \frac{Z_3}{Z_2}) - (1 - \frac{Z_3}{Z_2}) e^{zj\alpha_2 d}} \tag{2.26}$$

changing to previous notation and noting that $d = -H$, equation 2.26 becomes 2.17:

$$\underline{R} = \frac{\left(1 - \frac{r_1}{r_2} \frac{\cos\theta_2}{\cos\theta_1}\right) - \left(1 + \frac{r_1}{r_2} \frac{\cos\theta_2}{\cos\theta_1}\right) e^{-zjk_2 \cos\theta_2 H}}{\left(1 + \frac{r_1}{r_2} \frac{\cos\theta_2}{\cos\theta_1}\right) - \left(1 - \frac{r_1}{r_2} \frac{\cos\theta_2}{\cos\theta_1}\right) e^{-zjk_2 \cos\theta_2 H}}$$

E. VALIDATION OF THE PLANE WAVE ASSUMPTION

Thus far, the reflection coefficient of an oblique incident plane wave off a finite layer has been calculated and validated against previously known theory and limiting cases. However, one question still needs to be

addressed before this equation is put to use. That is, the validity of the plane wave assumption made above, Equation 2.8, needs to be established.

The solution for a point source near a boundary is addressed in two works. Officer's [Ref. 19] solution is in the form of three integrals for each of the three regions. However, the integrals are difficult to compute. Officer does give ". . . the condition under which the plane wave reflection coefficient may be taken as a valid approximation for the reflection of an accident spherical wave. This condition is that

$$\frac{c_1}{\omega R_1 \left[\frac{c_1^2}{c_2^2} - \sin^2\theta\right]^{3/2}} << 1 \quad " \qquad (2.27)$$

where R_1 is the distance from point of reflection to the receiver.

The second work that addresses this problem is Brekhovskikh. From Brekhovskikh, the geometric optics approximation (in which a spherical wave is relected off a layer with the same reflection coefficiient as a plane wave) is valid when the distances of the source and the receiver from the boundary are large compared with the wavelength. [Ref. 18 p. 256] In the experiment run, this assumption is valid above f = 50kHz.

Lastly, for completeness, the extent of the near field should be calculated. From Ziomek [Ref. 20], the maximum radial extent r of the near field of the source is given by:

$$r > \frac{\pi R^2}{\lambda} \qquad (2.28)$$

where

R is the maximum radial dimension of the transmit transducer.

For the experiment done here, the following values were used in equations 2.27 and 2.28:

c_1 = 1481 m/s

c_2 = 1992 m/s

θ_1 = 42.27°

R_1 = 0.5 m

Equation 2.27 requires that f >> 14.8 kHz for the plane wave assumption to be valid. From 2.28, for the radiation from the transmitting LC-10 to be in the far-field prior to reaching the plate requires f < 1.01 MHz. Therefore for the frequency range of interest (50-100 kHz) both conditions are satisfied.

F. APPLICATION OF EQUATION 2.17

Upon close inspection of Equation 2.17, it can be seen that the reflection coefficient is a phasor of unit magnitude with a phase delay that is a function of

frequency. This is intuitively true because of the conditions imposed on the problem: the boundary condition at the top of the plate, $Z = H$, is a pressure release, perfectly reflecting plane; the medium is assumed to be lossless. Since it is perfectly reflecting, there is no refracted wave at the upper boundary and there is no loss of signal. If the medium is lossless there is no loss of signal as the wave travels through the plate. Thus, the reflection is of unit magnitude with a phase angle, that is $\underline{R} = 1 \cdot e^{j\tau}$.

The phase angle τ of $\underline{R}$ is, from Equation 2.17,

$$\tau = \tan^{-1} \frac{\left(1+\frac{r_1}{r_2}\frac{\cos\theta_2}{\cos\theta_1}\right)\sin[2k_2H\cos\theta_2]}{\left(1-\frac{r_1}{r_2}\frac{\cos\theta_2}{\cos\theta_1}\right)-\left(1+\frac{r_1}{r_1}\frac{\cos\theta_2}{\cos\theta_1}\right)\cos[2k_2H\cos\theta_2]}$$

$$- \tan^{-1} \frac{\left(1-\frac{r_1}{r_2}\frac{\cos\theta_2}{\cos\theta_1}\right)\sin(2k_2H\cos\theta_2)}{\left(1+\frac{r_1}{r_2}\frac{\cos\theta_2}{\cos\theta_1}\right)\cos(2k_2H\cos\theta_2)} \qquad (2.29)$$

In the experiment to be described, the following parameters were used in Equation 2.29:

$$r_1 = \rho_1 c_1 = [998 \tfrac{kg}{m^3}]\,[1481 \text{ m/s}] = 1.48 \times 10^6 \tfrac{Pa \cdot s}{m}$$

$$r_2 = \rho_2 c_2 = [1200 \tfrac{kg}{m^3}]\,[1992 \text{ m/s}] = 2.39 \times 10^6 \tfrac{Pa \cdot s}{m}$$

$$H = 3.18 \times 10^{-3} \text{ m}$$

From the geometry of the setup,

$$\theta_1 = \tan^{-1} \frac{d_{rcvr}}{d_{rcvr} + d_{source}} = \tan^{-1} \frac{.5m}{.55m} = 42.3°$$

where d_{rcvr} and d_{source} are the receiver and source depths, respectively. A plot of the phase angle caused by the plate, Equation 2.29, as a function of frequency with the parameters shown in Figure 2.4 above is in Figure 2.4. Note the conventional of a negative angle producing a phase delay in the signal.

In the frequency range of interest, f = 0 to 100 kHz, τ decreases from 0° at f = 0Hz, to -104° at f = 100,000 kHz.

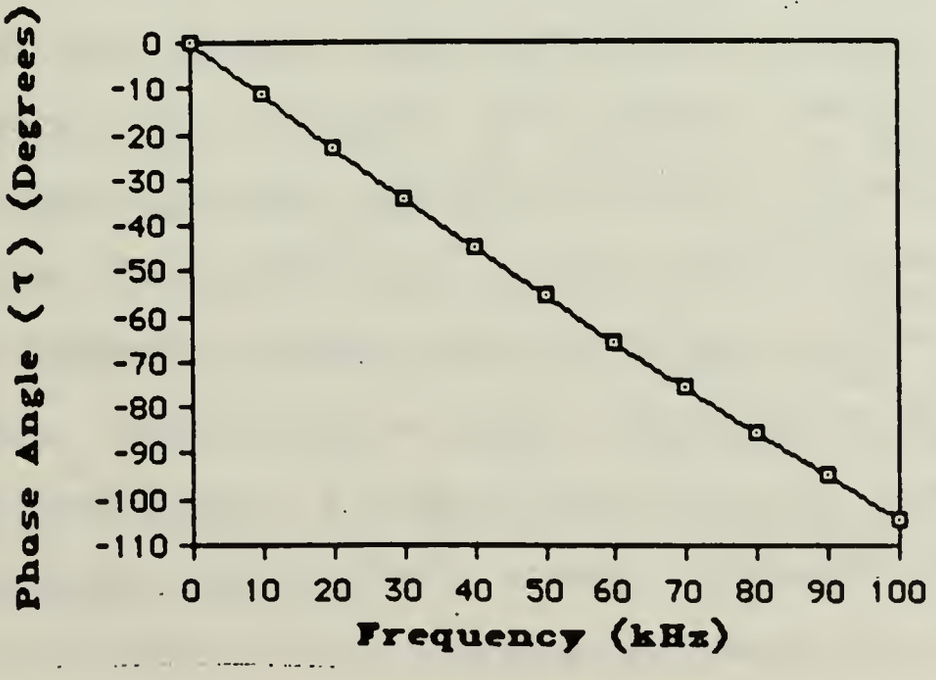

Figure 2.4 Phase Delay Caused By the Plate

The phase delay caused by the plate will be manifested by a shift in the frequency of the nodes and antinodes of the interference pattern. It can be shown that the frequency shift Δf caused by the phase delay τ is:

$$\Delta f = - \frac{c_o \tau}{4 \pi \Delta r} \qquad (2.30)$$

where

Δr = difference in path lengths between the direct and reflected signals

τ = phase delay caused by the plate, as obtained from Equation 2.29,

c_o = speed of sound in the fluid.

G. DESCRIPTION OF EXPERIMENT

Two small LC-10 transducers were placed in the water, one acting as a source, the other as a receiver, and were connected to a Hewlett Packard 4162A frequency analyzer as shown in Figure 2.5. A periodic chirp signal of 0-100 kHz was applied to the source transducer, and the received response was measured and plotted. The LC-10 transducers were assumed to have a flat response throughout the frequency range. While the response curves of the LC-10 show the response to be fairly flat up to 100-kHz, the assumption is really not tested, since the response of the transducers themselves

is not being tested, rather the difference in response with and without the pressure of the plate.

The response of the receiving transducer showed the maxima and minima in the pressure at its location due to the boundary. The response was measured for the water-air boundary, and without changing the location of the two transducers, the plate was introduced and the response was remeasured.

H. EXPERIMENTAL RESULTS

The results of the experiment can be seen from Figures 2.6 and 2.7. Figure 2.6 is a plot of the frequency response of the receiving hydrophone with fixed geometry with no plate present; the classic Lloyd's mirror experiment. Note the frequency pattern of the nodes and antinodes. When the plate was placed in position without moving source or receiver, the positions of these nodes and antinodes shift to the right, higher in frequency, as can be seen in Figure 2.7. This was predicted as the manifestation of the phase angle caused by the plate. The change in the frequency of the nodes increases linearly with frequency, corresponding to the increased phase angle.

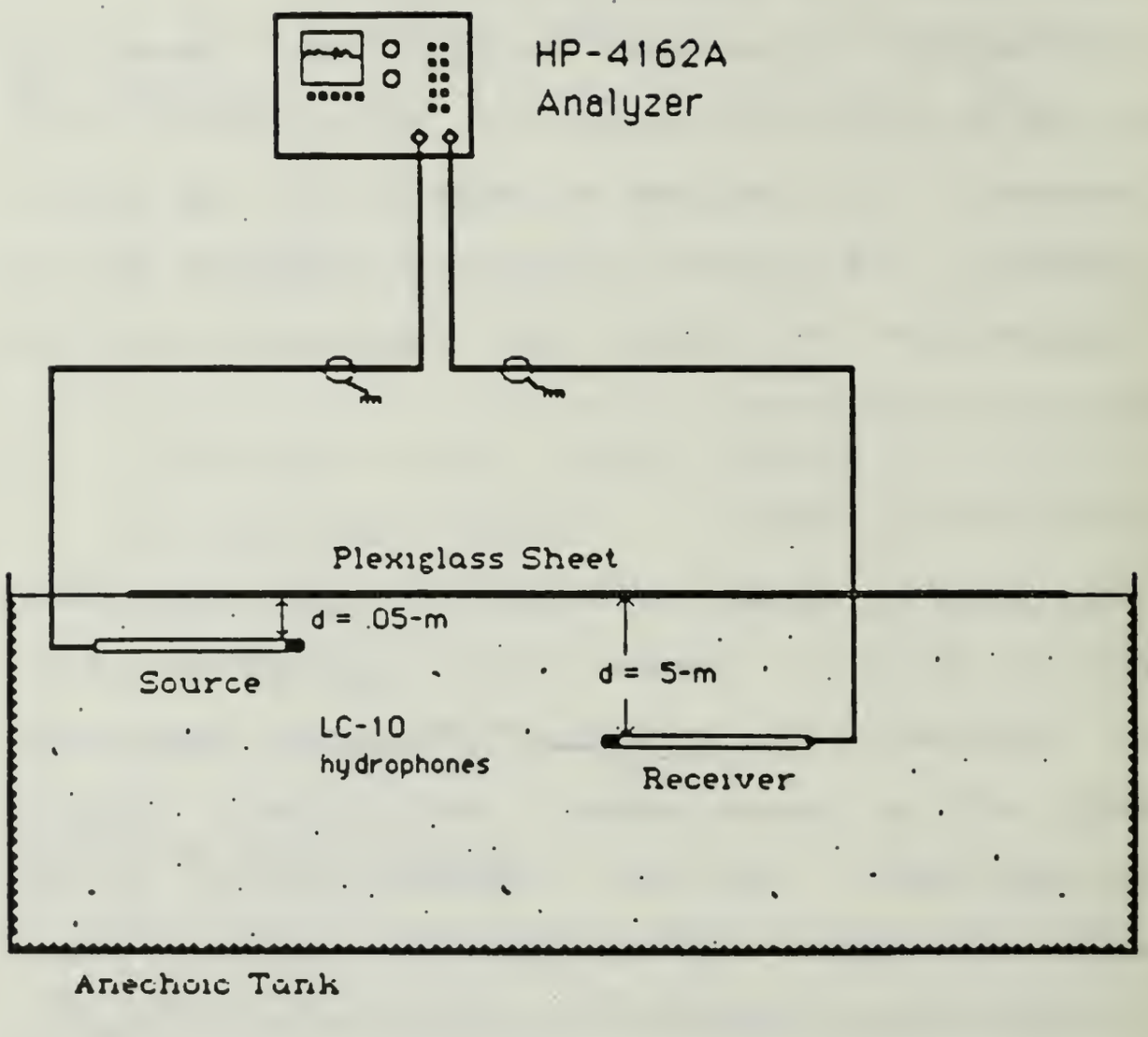

Figure 2.5. Lloyd's Mirror Experiment set-up

Table 2.1 shows a comparison of the predicted nodal shift to the nodal shift obtained experimentally. τ was obtained from Figure 2.4. The predicted frequency shift was obtained from Equation 2.30.

TABLE 2.1

f_{node}	τ	$\Delta f_{predicted}$	$\Delta f_{exp.}$
37 kHz	-42°	1 kHz	1.02 kHz ± .13
56	-62	1.5	2.01 ± .43
75	-81	1.9	2.24 ± .37
93	-100	2.3	2.50 ± .39

The data of Table 2.1 are shown in Figure 2.8. The size of the error bars of the experimental data are due to the inaccuracies in reading the frequencies of the nodes. Note, however, that in all cases the experimental data agreed with prerdicted values of the frequency shift within the accuracies of measurement, so on a qualitative level, at least, the theoretical predictions of the nodal shifts are supported.

In further comparison of Figures 2.6 and 2.7, it can be seen that although the pattern has been shifted in frequency, there is no change in the amplitudes of the maxima and only a small change in some of the minima of the frequency response pattern when the plate is

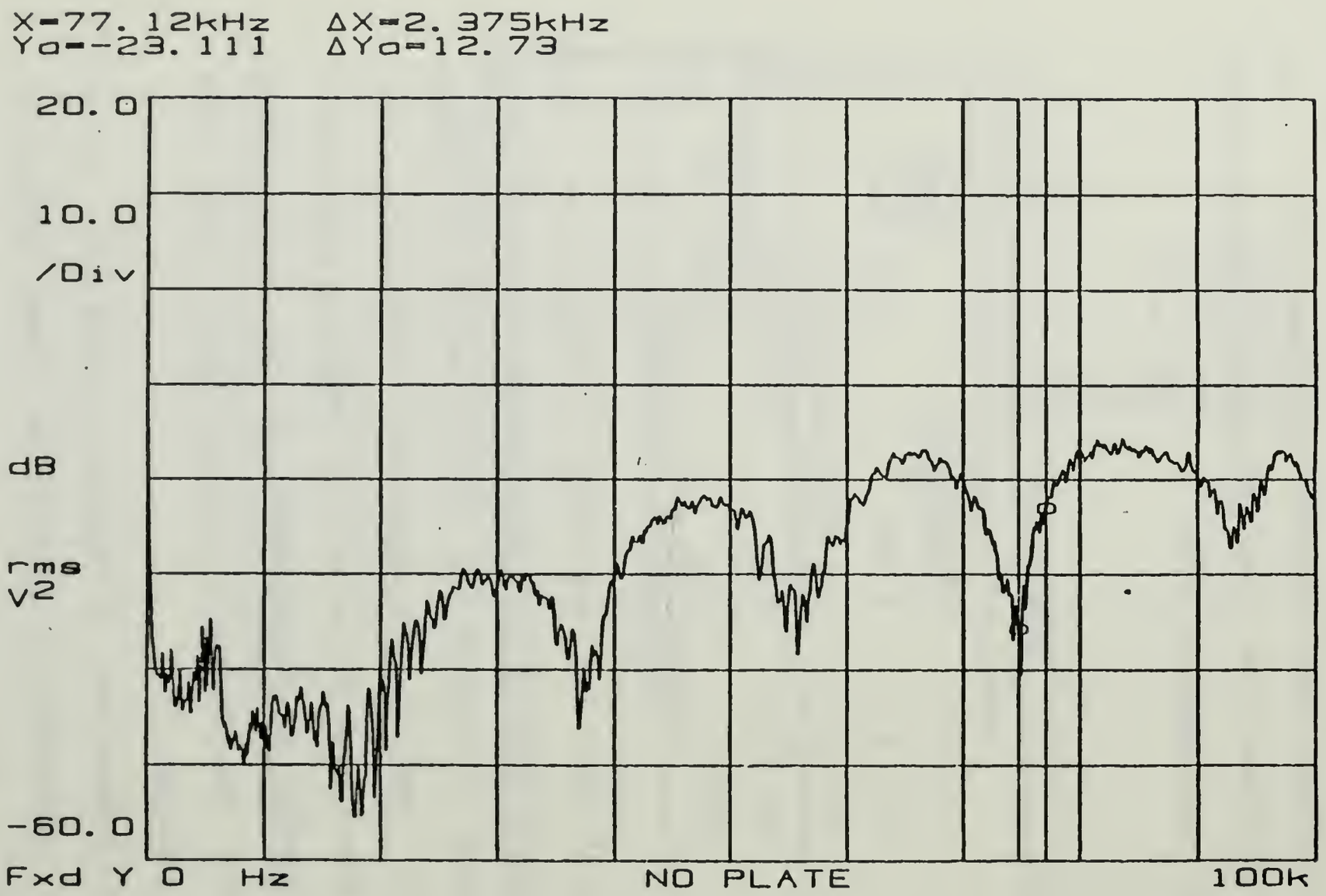

Figure 2.6. Frequency response, free boundary

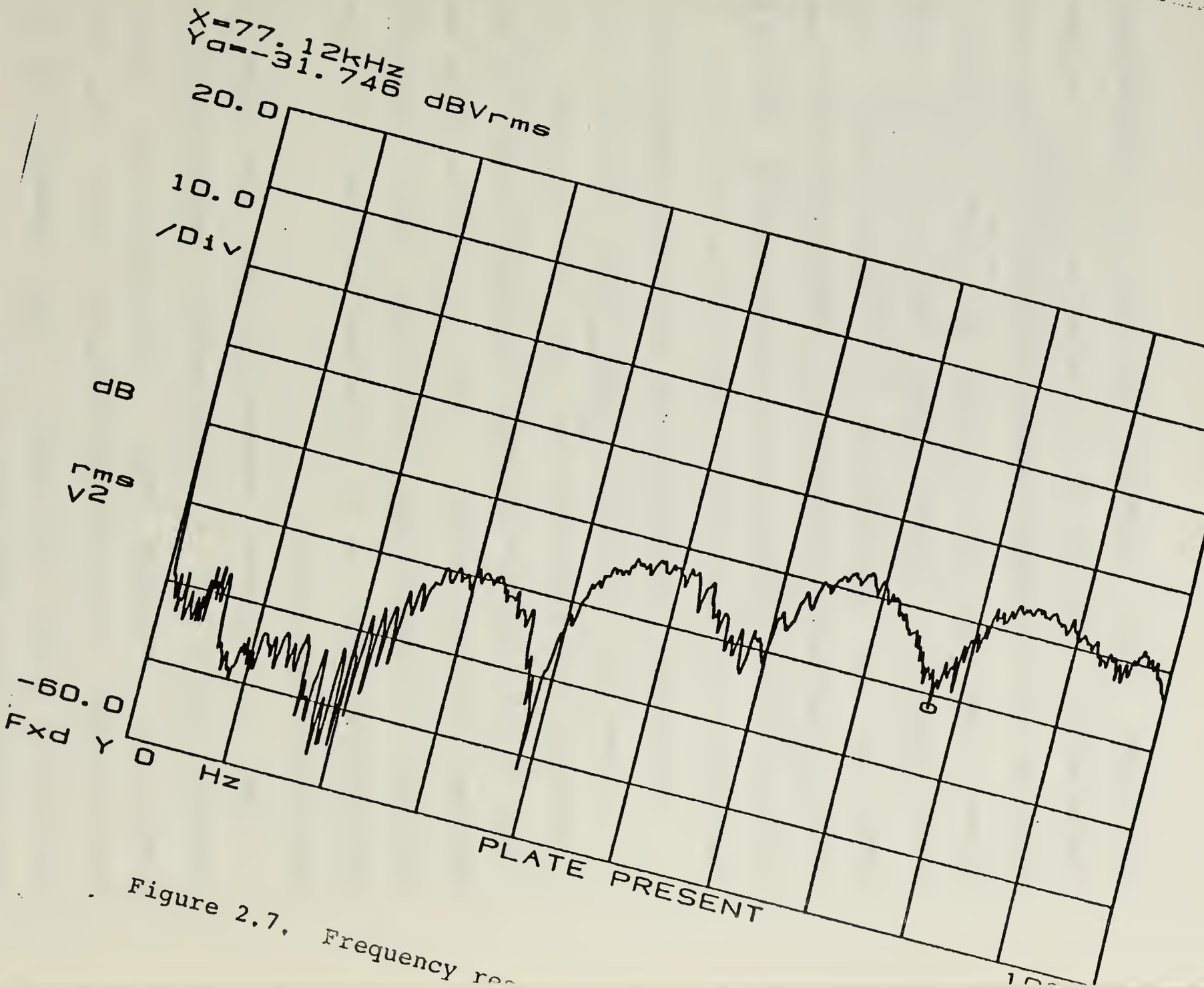

Figure 2.7. Frequency re

introduced. This suggests that there is insignificant change in the amplitude of the reflected signal, as predicted by the reflection coefficient $\underline{R}$ having a magnitude of one. From this, it is inferred that there is insignificant translation of the incident wave into plate wave modes other than longitudinal. The ray-method used in deriving the reflection coefficient $\underline{R}$ assumes that the compressional wave incident at the plate boundary remains a comressional (or longitudinal) wave in the plate.

A change in the mode of the wave from compressional to, for instance, flexural or shear, would involve a loss of energy in the reflected wave, which would be seen as a change in the amplitude of the maxima and minima of the frequency response pattern. Since very little change was observed, it appears that the incident wave remained a compressional wave as it traversed the plate and re-entered the fluid below.

Thus, it has been demonstrated that the effect of placing a plate into a fixed-geometry method-of-images problem is to introduce only a phase delay into the reflected signal, causing a related upward shift in the frequencies of maxima and minima in the pressure for the fixed source and receiver positions.

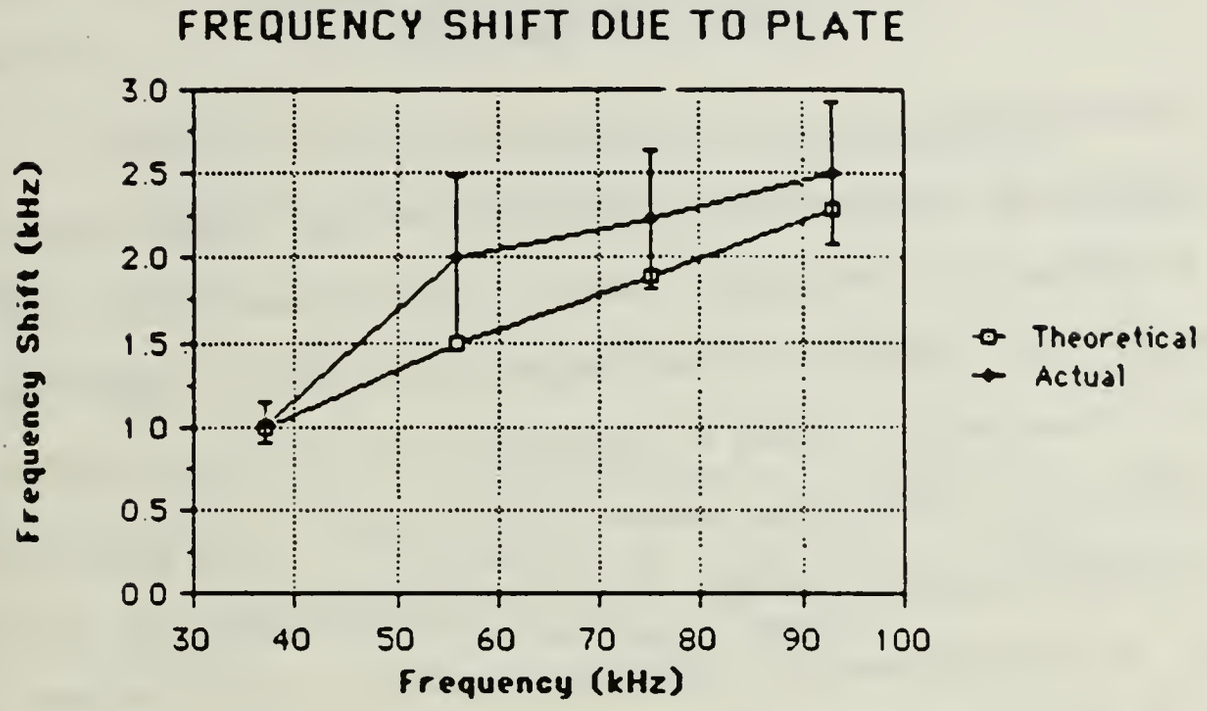

Figure 2.8 Frequency Shift due to Plate

III. RADIATION FROM A POINT DRIVEN FLUID-LOADED PLATE

A. INTRODUCTION

Chapter II treated the effects on the sound field from a source in the water when a plexiglass plate is placed on the surface. This chapter will deal with the acoustic radiation from a plate driven by a source attached to it. When the source is driving the plate, it excites the "acoustic mode" of sound propagation in the plate, as described in Chapter I. From the previous discussion, the acoustic mode leads to radiation away from the plate caused by the spatial gradient of the amplitude of the flexural wave excited by the source.

The principal references for the theoretical description of the problem are Feit [Ref. 7] and Ross [Ref. 21]. A computer program was written to compute the radiation pattern from the driven plate at various frequencies. An experiment was conducted to obtain actual radiation patterns from a plexiglass plate placed on the water.

B. THEORETICAL DEVELOPMENT

As was seen in the background section of Chapter One, the theory concerning the point-driven fluid-loaded plate is well known, and its full development will not

be given here. However, for continuity, key points leading to an understanding of the solution will be summarized.

1. Radiation from a Propagating Flexural Wave

A flexural wave propagates in a plate with wave number k_f where

$$k_f = \frac{\omega}{c_b} \tag{3.1}$$

When this plate is in contact with a fluid, vibrations of the plate will be imparted to the fluid, producing waves in the fluid of wave number k_o where

$$\vec{k}_o = \vec{k}_\perp + \vec{k}_\parallel \tag{3.2}$$

where $\vec{k}_\perp$ and $\vec{k}_\parallel$ are the wave numbers perpendicular and parallel to the plane of the plate, respectively.

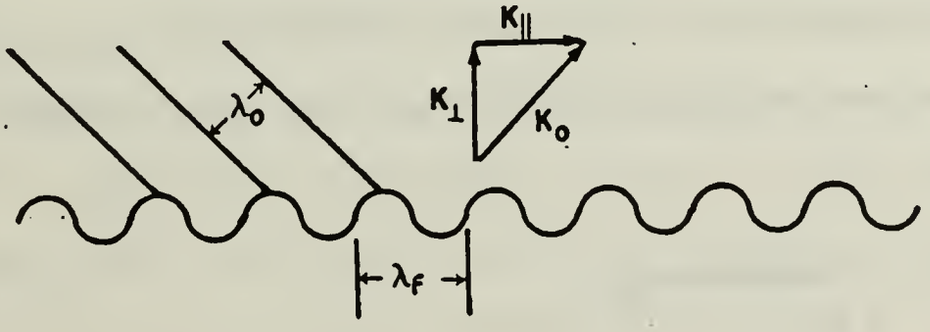

Figure 3.1 Sound Radiation from a Flexural Wave of a Plate

The length of this vector is given by

$$k_o^2 = k_\perp^2 + k_\parallel^2 \tag{3.3}$$

the component parallel to the plate is

$$\sqrt{k_o^2 - k_\perp^2} \tag{3.4}$$

and from Snell's Law this must be equal to k_f . This leads to [Ref. 20, p. 163]

$$k_\perp = \sqrt{k_o^2 - k_f^2} \tag{3.5}$$

From the boundary conditions at the interface, the normal components of particle velocity must be equal,

$$v_{\perp_f} = u_{\perp_o} \tag{3.6}$$

where $v_{\perp_f}$ refers to the perpendicular component of the plate particle velocity and $u_{\perp_o}$ is the fluid particle velocity perpendicular to the plate.

From these conditions, it can be shown that [Ref. 21 p. 163] the acoustic pressure $\underline{p}$ on the plate due to the fluid is:

$$\underline{p} = -j\omega\rho_o c_o \frac{k_o}{\sqrt{k_o^2 - k_f^2}} \underline{w} \tag{3.7}$$

where $\underline{w}$ is the normal displacement of the flexural wave. Equation 3.7 gives the acoustic pressure $\underline{p}$ on the plate attributable to fluid loading. Note that $\underline{p}$ is dependent on the relative values of k_o and k_f .

This leads to the important effect of coincidence. When $k_f > k_o$, the expression for the fluid pressure is real, which represents mass-loading [Ref. 21 p. 163] and acoustic power is not radiated into the fluid. When $k_o = k_f$, the condition of coincidence is reached. The expression for the radiated acoustic pressure from the flexural wave would seemingly predict infinite pressure. (This cannot, however, occur, because fluid loading prevents the two speeds from being exactly equal [Ref. 21 p. 163]) When $k_f < k_o$, the expression for the fluid pressure in Equation 3.7 is imaginary, so the effect is that of a radiation resistance, [Ref. 21 p. 163] and the propagating wave radiates power away from the plate.

The coincidence frequency is obtained by equating the wave numbers of the flexural wave in the plate and the compressional wave in the fluid and solving for frequency w_c . But because, the flexural wave speed varies with frequency and formulae for the flexural wave speed depend on whether thin plate or thick plate approximations are used, there are different forms for the solution for the coincidence frequency.

As there were three approximations for the flexural wave speed (Equations 1.6 - 1.8), there are three formulae for the coincidence frequency. In the low

frequency limit, or thin-plate theory, the coincidence frequency is given by:

$$\omega_{ci} = \frac{12\ c_o^2}{t\ c_p} \qquad (3.8a)$$

In the intermediate frequency range, the coincidence frequency cannot be easily solved for implicitly, but is given by the solution of:

$$\frac{\omega_{ci}}{\Omega_p} \frac{\left(1 + \left(\frac{\omega_{ci}}{\Omega_p}\right)^2\right)^{1/2} - 2\frac{\omega_{ci}}{\Omega_p}}{1 - \Gamma_p\left(\frac{\omega_{ci}}{\Omega_p}\right)^2} = \frac{c_o^2}{c_p^2} \qquad (3.8b)$$

In the high frequency range, the coincidence frequency can be given by:

$$\omega_{ch} \doteq \frac{c_p\ 12}{t} \frac{c_o^2}{c_p^2 - \frac{5}{2}\ c_o^2} \qquad (3.8c)$$

Note here that if $c_p < \sqrt{\frac{2}{5}}\, c_o$, Equation 3.8c is negative, which implies that coincidence cannot be reached. Recall that the high frequency asymptote of the flexural wave speed is the Rayleigh wave speed, a value somewhat less than the shear wave speed. If this speed is less than the speed of sound in the fluid, the condition of $k_o = k_f$, or coincidence, cannot be reached.

2. Radiation from a Point Source

Heretofore, we have discussed the flexural wave itself radiating power from the plate. The conclusion that no power is radiated below coincidence applies only to infinite plane bending waves on an infinite plate. If excited by a localized force even below coincidence, sound will be radiated because the waves in the plate have divergence [Ref. 20 p. 169].

The pressure at a field point (R, ϕ, θ) from a point-driven fluid-loaded plate can be, in a derivation by Feit [Ref. 7, p. 1492], eventually expressed in the form (3.9)

$$\underline{p}(R,\phi,\theta)= \frac{F_o k_o^2}{4\pi}\int_C H_o^{(1)}(k_o R\sin\phi\sin w)e^{jk_o R\sin\phi\cos w}V(w)\sin w\,dw$$

where

$p(R,\phi,\theta)$ = acoustic pressure in spherical coordinates with the source at the origin,

R = the slant distance from the source,

ϕ = the azimuthal angle,

θ = the circumferential angle measured in the plane of the plate,

w = the variable of integration,

k_o = the wave number in the fluid,

C = contour of integration shown in Figure 3.2,

F_o = the amplitude of the source.

$H_o^{(1)}$ = the zero-order Hankel function of the first kind, and

V(w) = a complicated formula that relates the vibrating field of the plate to the water through the Mindlin-Timoshenko thick plate equation. V(w) contains the poles of the integral in Equation 3.10.

The solution of the integral was obtained by Brekhovskikh [Ref. 18, pp. 242-258] and is given by Feit [Ref. 7, Equation 24]. Ross, however, gives a more useful form of Feit's solution:

$$p(R,\phi)= \frac{jk_o F_o \cos\phi}{2\pi R} \quad x \tag{3.10}$$

$$\left[1-j\,\frac{\cos\phi}{\beta}\,\frac{\left(\frac{\omega}{\omega_c}\right)^2\left(\sin^2\phi-\left(\frac{c_o}{c_p}\right)^2\right)\left(\sin^2\phi-\Gamma_p\left(\frac{c_o}{c_p}\right)^2\right)}{1+\left(\frac{\omega}{\omega_c}\right)^2\left(\frac{c_o}{c_p}\right)^2\Gamma_p\left(\sin^2\phi-\left(\frac{c_o}{c_p}\right)^2\right)}\right]^{-1}$$

where Γ_p is the plate shear parameter, given by

$$\Gamma_p \approx 2.65\left(1+\frac{3}{5}\,\sigma+\frac{3}{4}\,\sigma^2\right) \tag{3.11}$$

and β is the fluid loading factor, given by Equation 3.13, which is discussed fully in the next section.

The bracketed term in Equation 3.10 along with the $\cos\phi$ can be described as a directivity function $H(\omega,\phi)$. This directivity function was encoded in FORTRAN and the program (given in Appendix A) was used to generate plots of theoretical directivity patterns

at several different frequencies. From these figures (Figures 3.5-3.11) the coincidence effect can be readily observed. The figures were based on thin plate theory, and cover frequencies from below to above coincidence. They represent a hypothetical plate and are presented for a discussion on the effects of coincidence and fluid loading. They will be discussed in section E1 of this chapter.

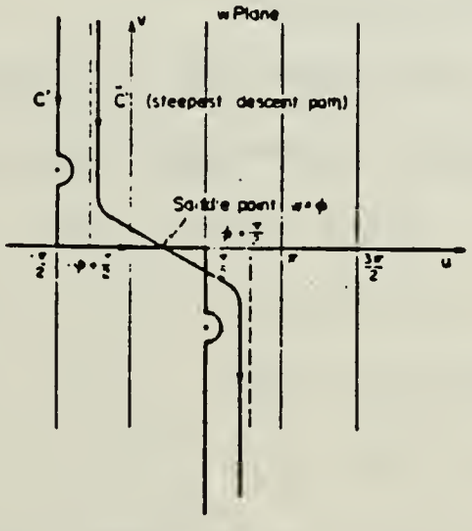

Figure 3.2 Integration Path of Integral of Equation 3.9 (from Feit)

C. THE EFFECT OF FLUID LOADING

Although Equation 3.10 is valid for all ranges of plate and fluid parameters and frequencies, the expression may be simplified greatly and further insight may be obtained by considering the effect of fluid loading.

The fluid loading factor, β, is the ratio of the specific acoustic impedence of the fluid to the mass reactance per unit are of the plate. Ross [Ref. 20 p. 166] defines it as

$$\beta = \frac{\rho_o c_o}{\omega \rho_p t} \tag{3.12}$$

where

ρ_o = density of the fluid

c_o = speed of sound in the fluid

ω = radian frequency of the flexural wave

ρ_p = density of the plate

t = thickness of the plate

Applying the formula for the thin plate coincidence frequency, Equation 3.8a, the fluid loading factor becomes

$$\beta = \frac{1}{\sqrt{12}} \frac{\rho_o}{\rho_p} \frac{c_p}{c_o} \frac{\omega_c}{\omega} \tag{3.13}$$

where

c_p = the plate longitudinal wave speed, given in Figure 1.1a,

ω_c = the coincidence frequency.

A fluid loading factor much less than 1 corresponds to light fluid loading, which occurs, for example, in a metal plate in air. A fluid loading factor much greater than 1 corresponds to heavy fluid loading found, for example, a plexiglass plate on water. The effect of

fluid loading can best be seen by considering four general cases: frequency below coincidence, light and heavy fluid loading; frequency above coincidence, light and heavy loading.

When $\omega<\omega_c$ and $\beta<<1$, a case of light fluid loading, the radiation pattern is that of a small baffled piston, or monopole-type radiation, non-directive. For this case, Equation 3.10 reduces to [Ref. 7 p. 1492]

$$p(r,\phi,\theta) = \frac{\rho_o F_o}{2\pi\rho_p t} e^{jkoR} \qquad (3.14)$$

Ross [Ref. 20 p. 170] states that the radius of this piston is the sum of the radius of the surface over which the force is applied and a quarter of the flexural wavelength. Ver and Holmer [Ref. 12 p. 278] give a slightly different form. They state that for a plate driven by point source, the equivalent radius of the baffled piston is 0.286 λ_c , where λ_c is the flexural wavelength at coincidence.

When, $\omega<\omega_c$ and $\beta>>1$, heavy fluid loading, the point force acting on a thin plate radiates sound as through the plate were not there, representing dipole-type radiation, and the radiation pattern is cosinusoidal. Equation 3.10 reduces to [Ref. 7 p. 1492]:

$$p(R,\phi) = \frac{-jk_o F_o}{2\pi R} e^{jkoR} \cos\phi \qquad (3.15)$$

When $\omega > \omega_c$ and $\beta << 1$, the radiation pattern is still cosinusoidal [Ref. 21 p. 171].

When $\omega > \omega_c$ and $\beta >> 1$, Equation 3.10 can be reduced only slightly, and gives the interesting radiation patterns corresponding to the flexural wave radiation and radiation from the driving piston.

D. THE EFFECT OF STRUCTURAL ABSORPTION[4]

Above coincidence, then, the absorption of the flexural wave as it propagates through the plate will effect the radiation pattern. Feit [Ref. 7, p. 1494] states this and states that (without proof) the far field pressure maximum is reduced by 5 dB for a loss factor, η=0.1. (See Equation 3.18 for the definition of the loss factor η .) Ungar [Ref. 22, p. 453] lists a loss factor typical of plexiglass of η = 0.02 to 0.04 in the audio frequency range. Therefore, it is expected that the decrease in predicted peak pressure amplitude due to the absorption of the flexural wave will be less than 5 dB.

An experiment was conducted to quantify the loss factor for the plate used in the experiment. This was done also to investigate the effects of the reflection of the flexural wave from the edge of the plate, i.e.,

---

[4]Although the effect is the same, the term absorption is perhaps more correct than damping as the term damping implies additional materials applied to the plate.

of the infinite plate assumption. An accelerometer was used to measure the decay in amplitude at various distances r away from the source, and for various frequencies.

Quantitative results were difficult to obtain. This was due to the method of data collection. The accelerometer was positioned at various test points along the plate. However, the coupling between the plate and accelerometer was crucial, and obtaining the same coupling between the data measurements in a non-destructive test was impossible using this technique.

A proper, (through destructive) test would have been to drill holes into the plate at the test points and bolt the accelerometer to the plate at the test points using equal torquing. However, only qualitative results were desired, so this was not done. Other techniques are possible. They include resonance -Q measurements, which would work for smaller samples of material, and optical-acoustic methods.

An attempt was made to develop Schladni patterns on a small piece of plexiglass, of material properties similar to that used in the experiment. The small sample (approximately 10 cm by 20cm) was suspended above a loudspeaker driven well in excess of 120 dB re 20 Pa at frequencies above and below the calculated modal frequencies of the plexiglass sample. No Schladni

patterns were induced. (Other samples, for instance of metal, did produce Schladni patterns using this technique.)

Qualitatively, the effect of the plexiglass loss factor η was very apparent. Refer to Figure 3.3 which is a plot of flexural wave attenuation, after correction for cylindrical spreading. As the accelerometer was moved farther away from the source, the corrected amplitude of the flexural wave steadily decreased with range, dropping 40 dB by the end of the plate for the frequencies of interest. No reflections of the pulse off the edges were observed.

Ver and Homer [Ref. 12, p. 276] give the losses in power radiated from the plate due to absorption to be

$$e^{-\eta k_f R/2}$$

where k_f = flexural wave number (3.18)

R = range from rource

η = loss factor of the plate material

using this, with the 100 kHz absorption curve (the only one straight enough to be trusted) yields $\eta \sim 0.03$ which is consistent with the values of Ungar [Ref. 21, p. 453].

According to Junger and Feit [Ref. 13, p. 249], the effects of structural damping on the far-field pressure pattern are accounted for, for small loss factors, by

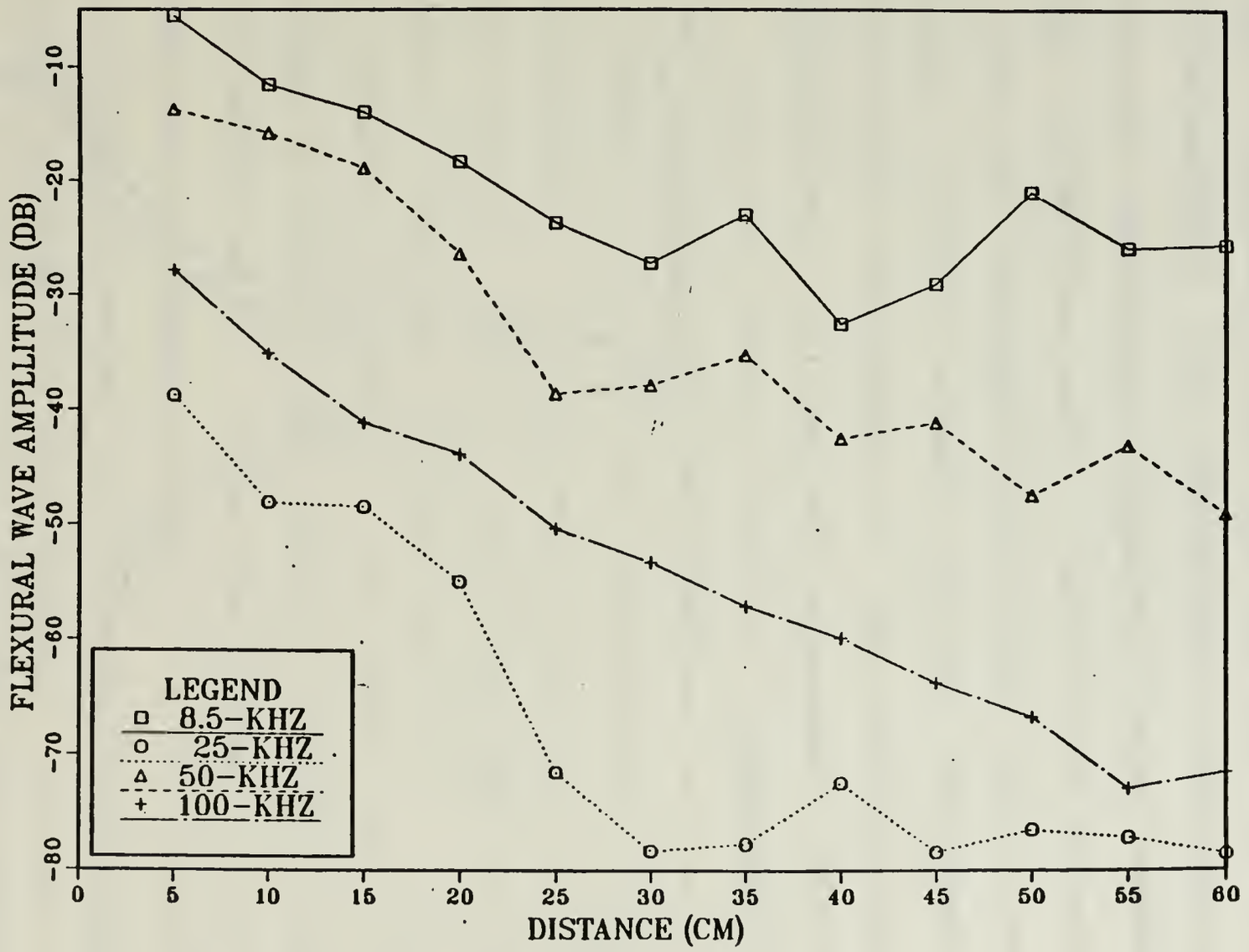

Figure 3.3. Flexural wave excess attenuation vs range

multiplying c_p in Equation 3.10 by $(1-j\eta)^{1/2} \approx (1-1/2\ j\eta)$, or ω_c by $(1+ 1/2\ j\eta)$. They further state that damping plays no significant effect on the maximum pressure of the radiation field below coincidence. This is also intuitively true because below coincidence the propagating flexural wave does not radiate and therefore its absorption has no effect. Above coincidence, they state (as Feit did in his earlier work) that the effect is to reduce the far-field pressure maximum. Figure 3.4, taken from Feit [Ref. 7, p. 1494], show the effect of structural damping on the far-field of a point-excited thin plate.

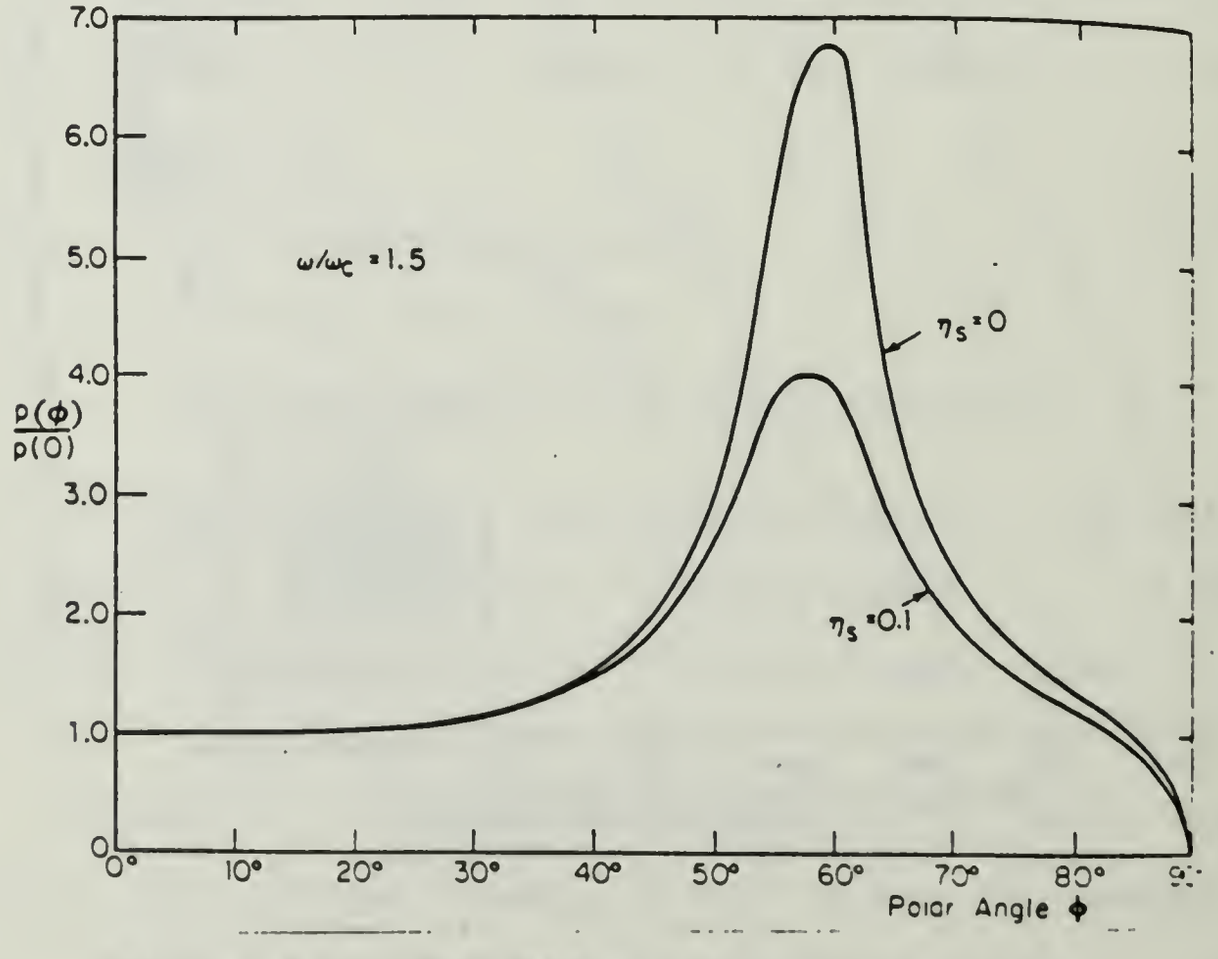

Figure 3.4, The Effect of Damping on the Far-Field Pressure (from Feit)

E. DISCUSSION OF THEORETICAL PLOTS

1. The General Effects of Increasing Frequency

Figures 3.5 to 3.11 were generated from the program given in Appendix A. They show the radiation directivity pattern $H(\phi)$, normalized to the on-axis pressure, for a frequency range from below coincidence to above coincidence.

The plate parameters used in these figures were those of a hypothetical plate and fluid combination. They do, however, show quite well the effects of increasing frequency on the radiation pattern in the fluid. Thin-plate theory was assumed, and the ratio of ω/ω_c was the parameter that was varied.

Figures 3.5 to 3.7 show the directivity patterns below coincidence. Far below coincidence, Figure 3.5, the radiation from the plate is cosinusoidal, with maximum radiation at $\phi = 0°$ and minimum radiation at $\phi = 90°$. It was shown in Section B1 of this chapter that below coincidence an infinite plane propagating flexural wave will not radiate sound. It was shown in Section C that the radiation pattern should be that of a low frequency small radius piston mounted on an infinite baffle. This is revealed in these first three figures. Note that as the coincidence frequency is approached, the pattern changes into a wider (Figures 3.7 and 3.8) pattern.

As the frequency of the source becomes larger than the coincidence frequency, the phase speed of the propagating flexural wave exceeds that of the fluid, and therefore the propagating flexural wave can radiate energy away from the plate. This is seen in Figures 3.9 and 3.10.

Well above coincidence, Figure 3.11, a third lobe is predicted. This, according to Feit, is the " . . . nonpropagating near-field deflection of the plate . . . . itself becoming a propagating wave." [Ref. 7, p. 1493]

Feit, in a later work with Junger [Ref. 13, p. 248], state that thick plate theory yields larger values for the angles at which the propagating flexural wave radiates and smaller values of peak pressure. That is, the lobes in the pattern will be at a greater angle and have a smaller value. Figure 3.11, from Feit and Junger, show a comparison of the size of the pressure lobe and the angle at which it appears for thin-plate theory and thick-plate theory. The figure neglects the effect of structural damping.

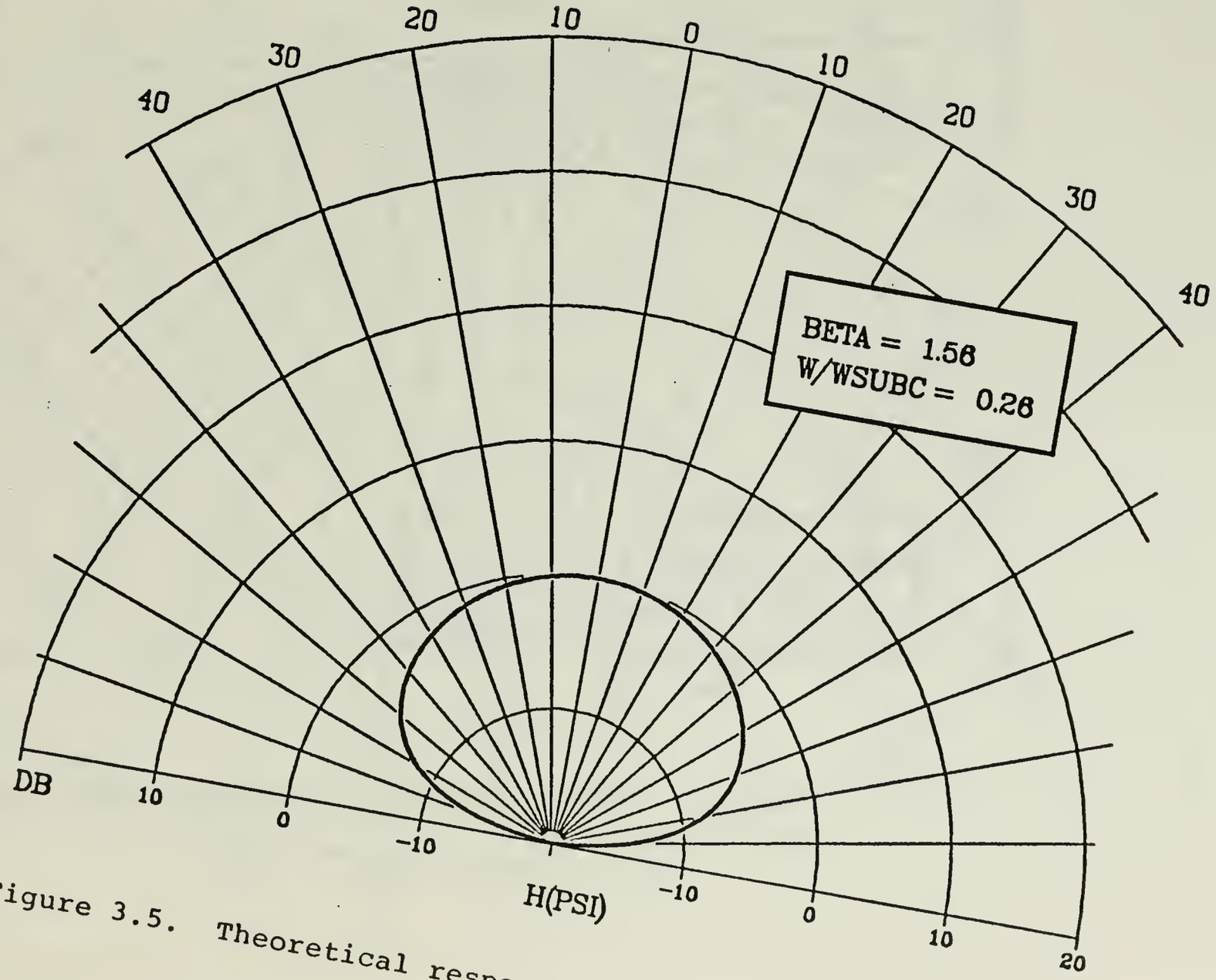

Figure 3.5. Theoretical response, $\omega/\omega_C = 0.26$

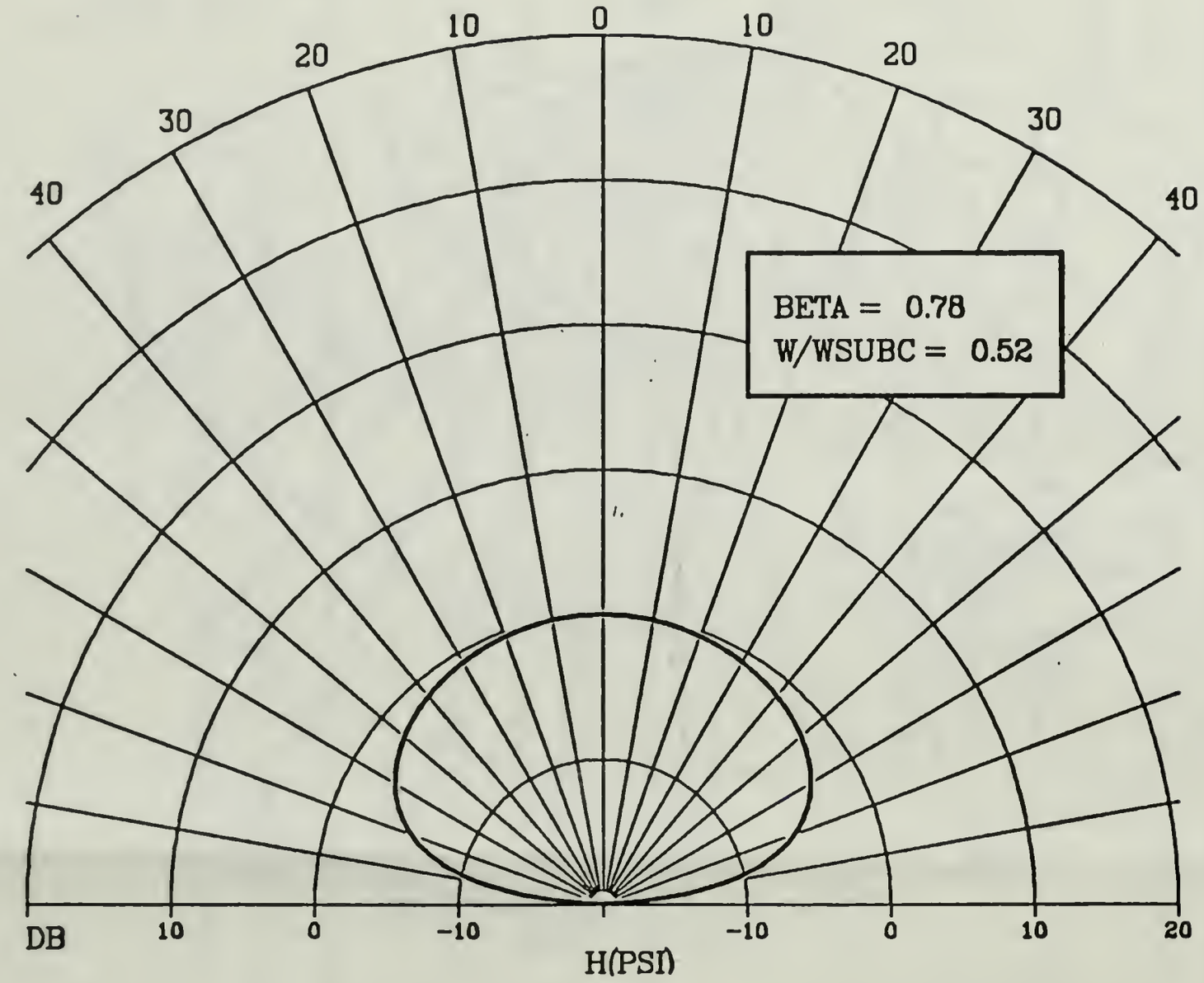

Figure 3.6. Theoretical response, $\omega/\omega_c = 0.52$

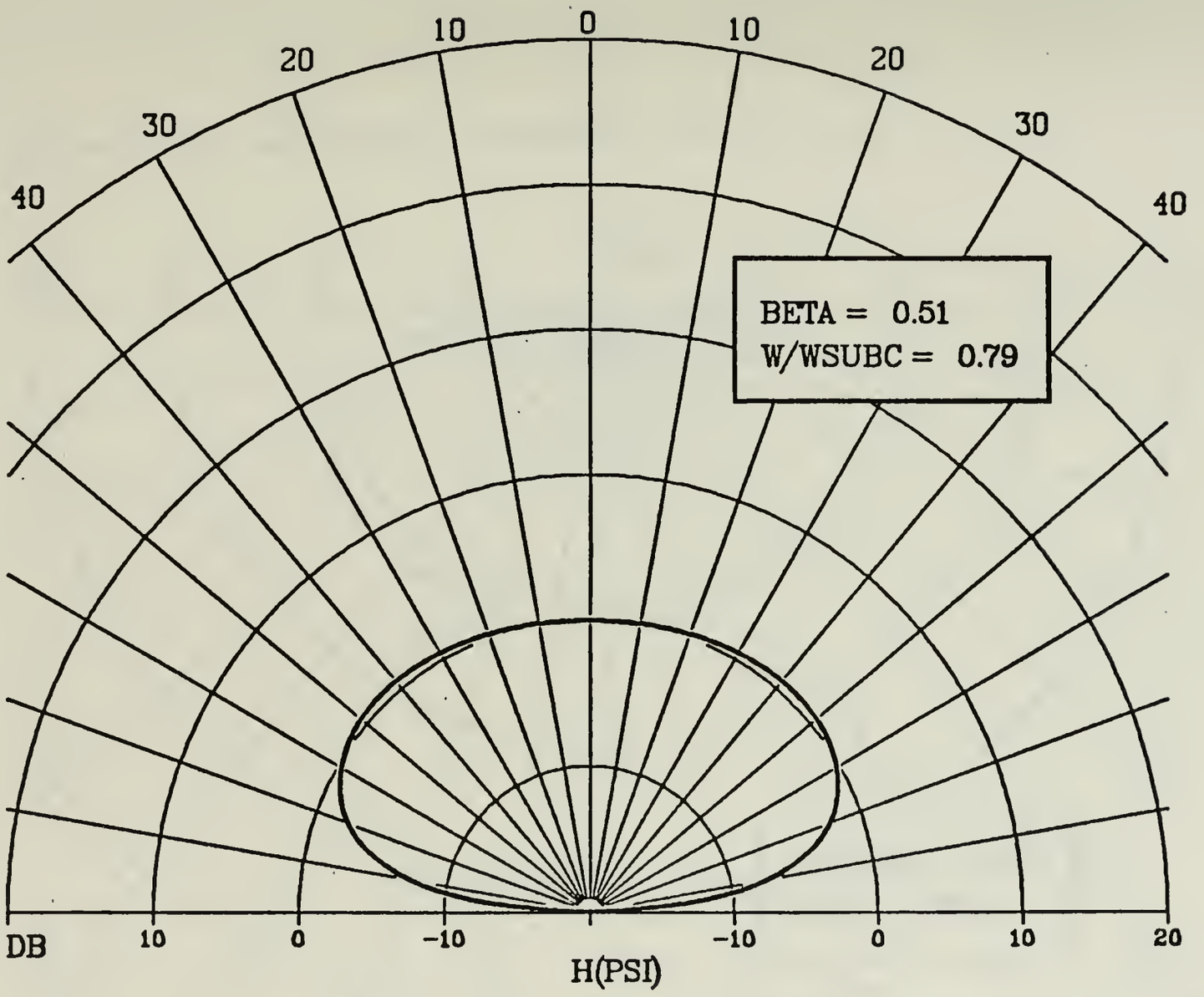

Figure 3.7. Theoretical responce, ω/ω_C = 0.79

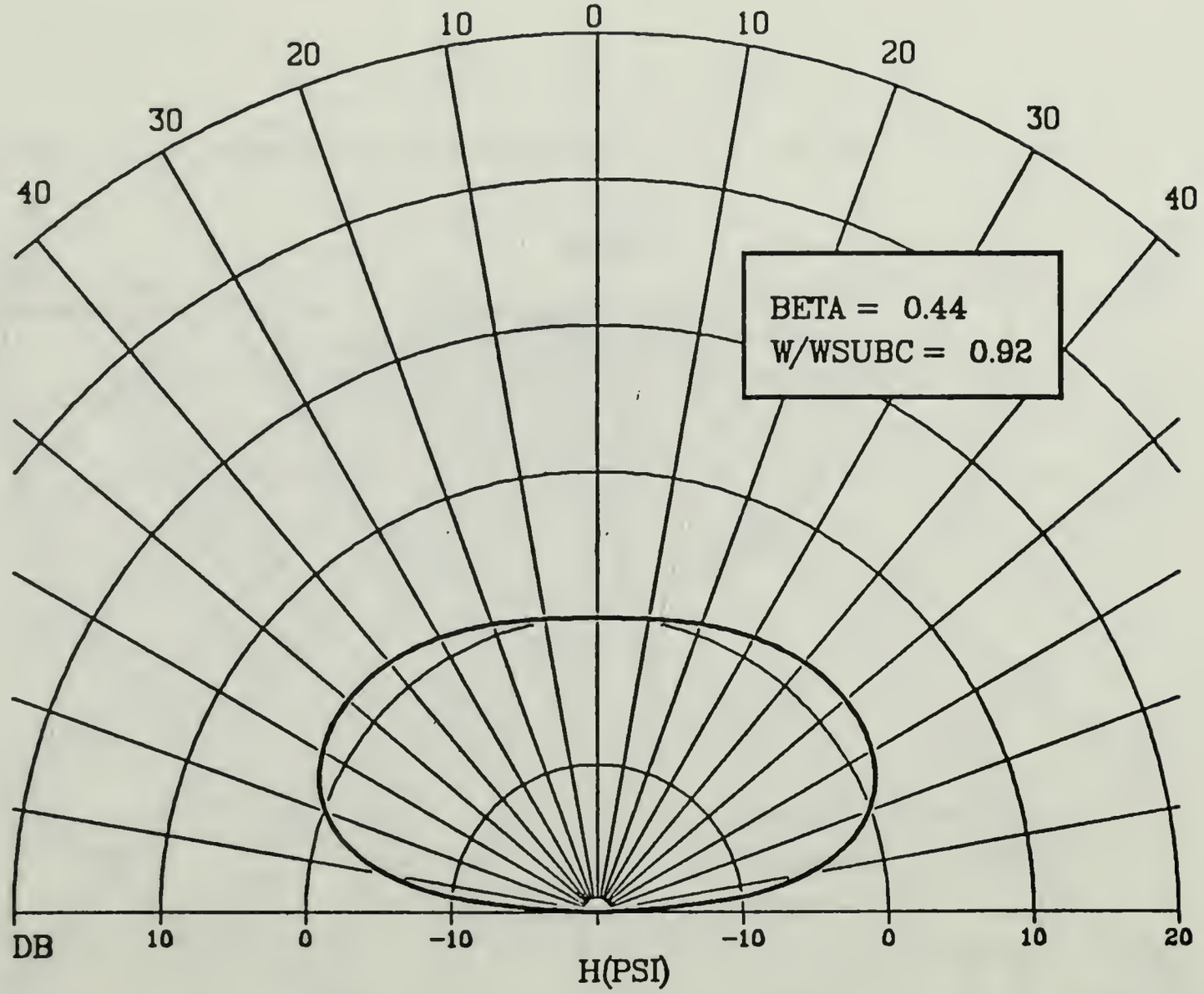

Figure 3.8. Theoretical response, $\omega/\omega_c = 0.92$

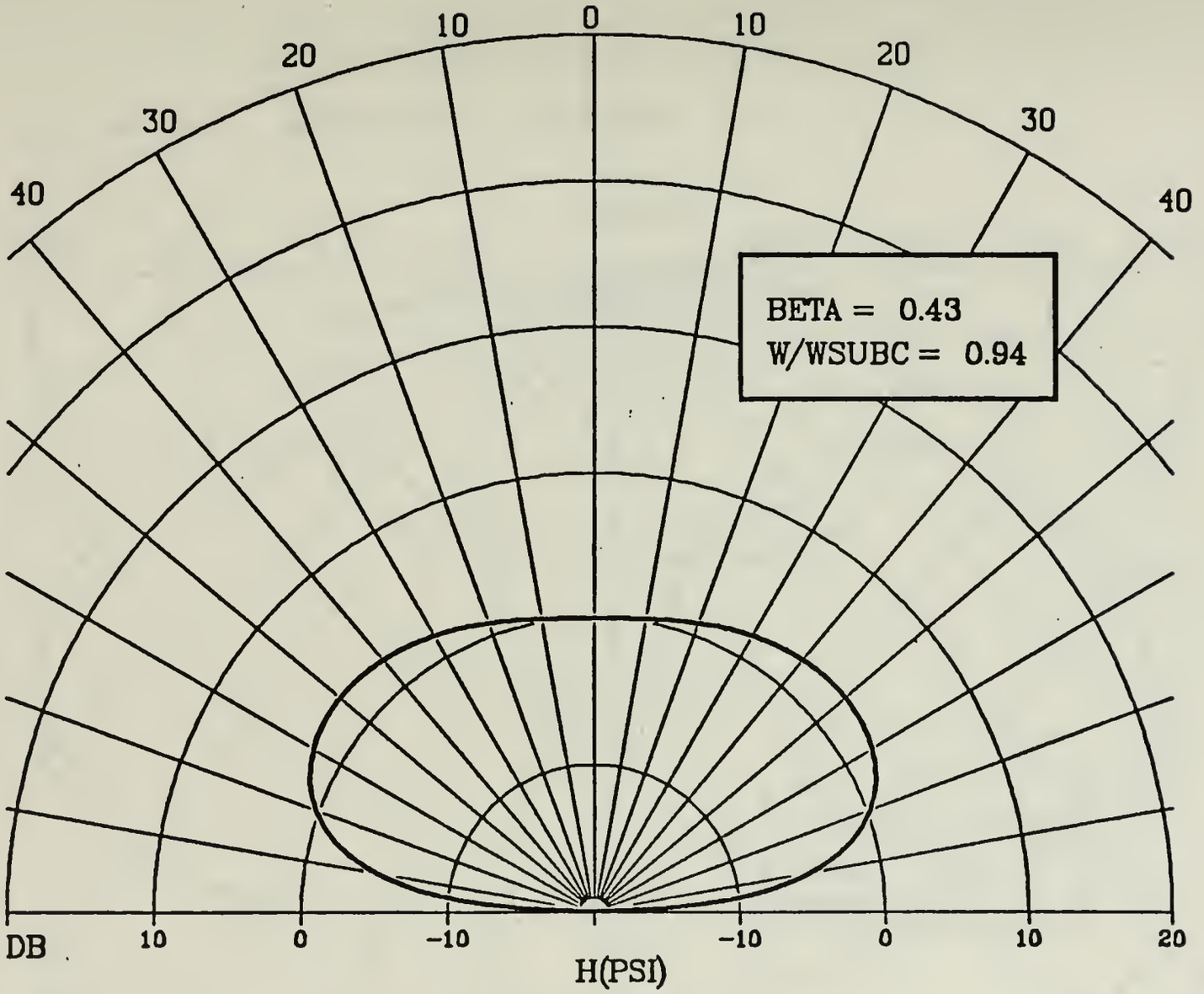

Figure 3.9. Theoretical response, $\omega/\omega_c = 0.94$

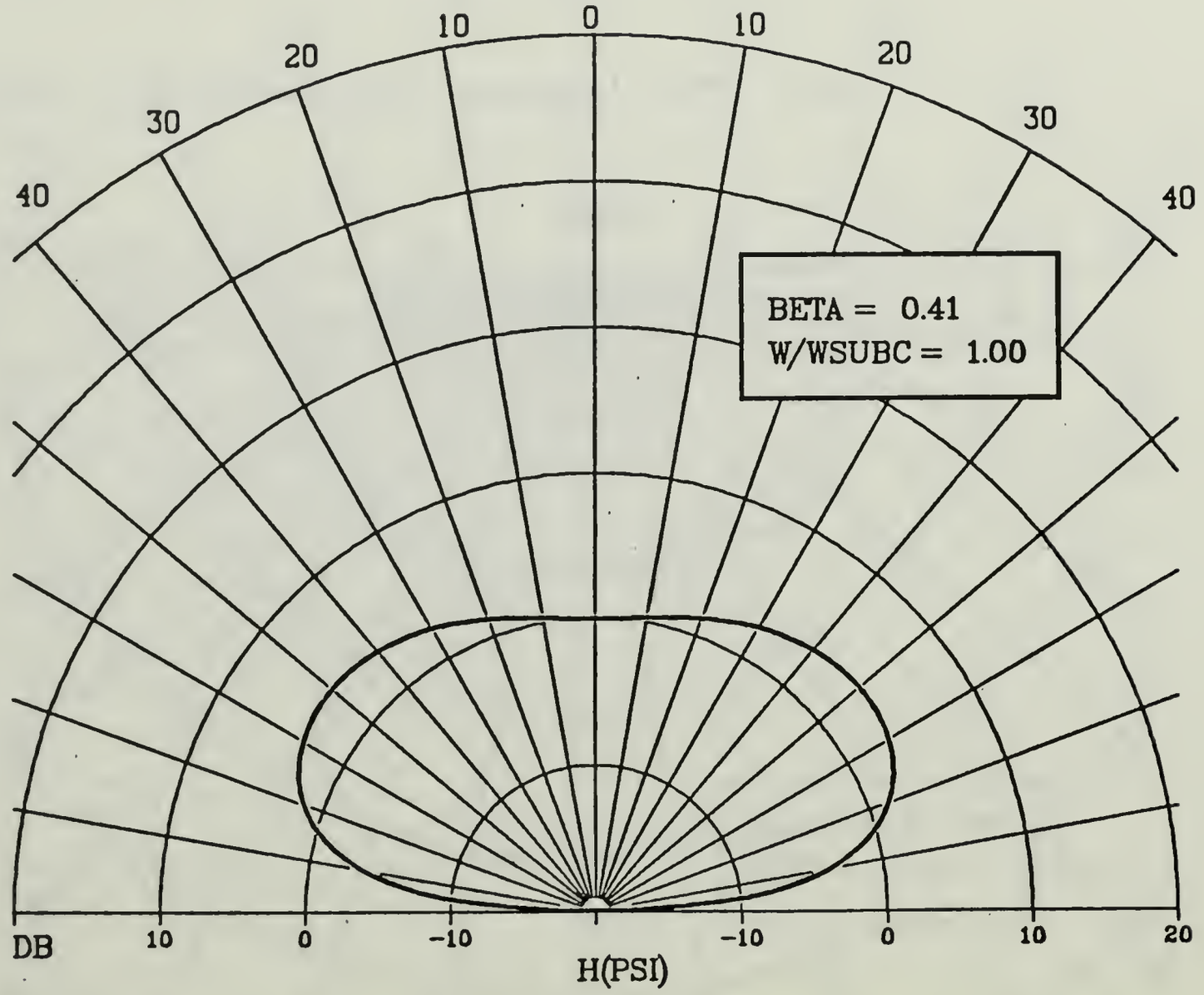

Figure 3.10. Theoretical response, $\omega/\omega_c = 1.0$

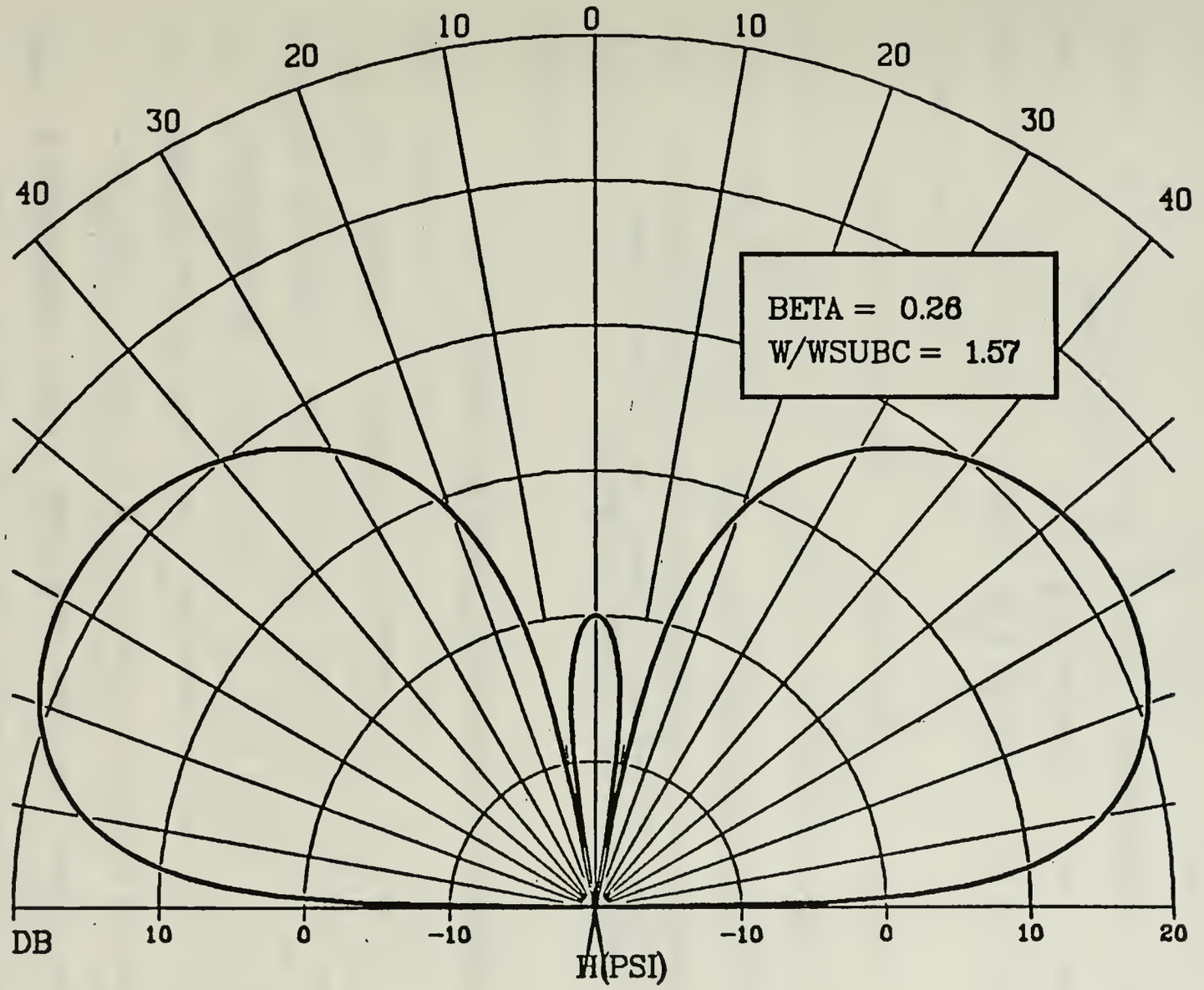

Figure 3.11. Theoretical response, $\omega/\omega_c = 1.57$

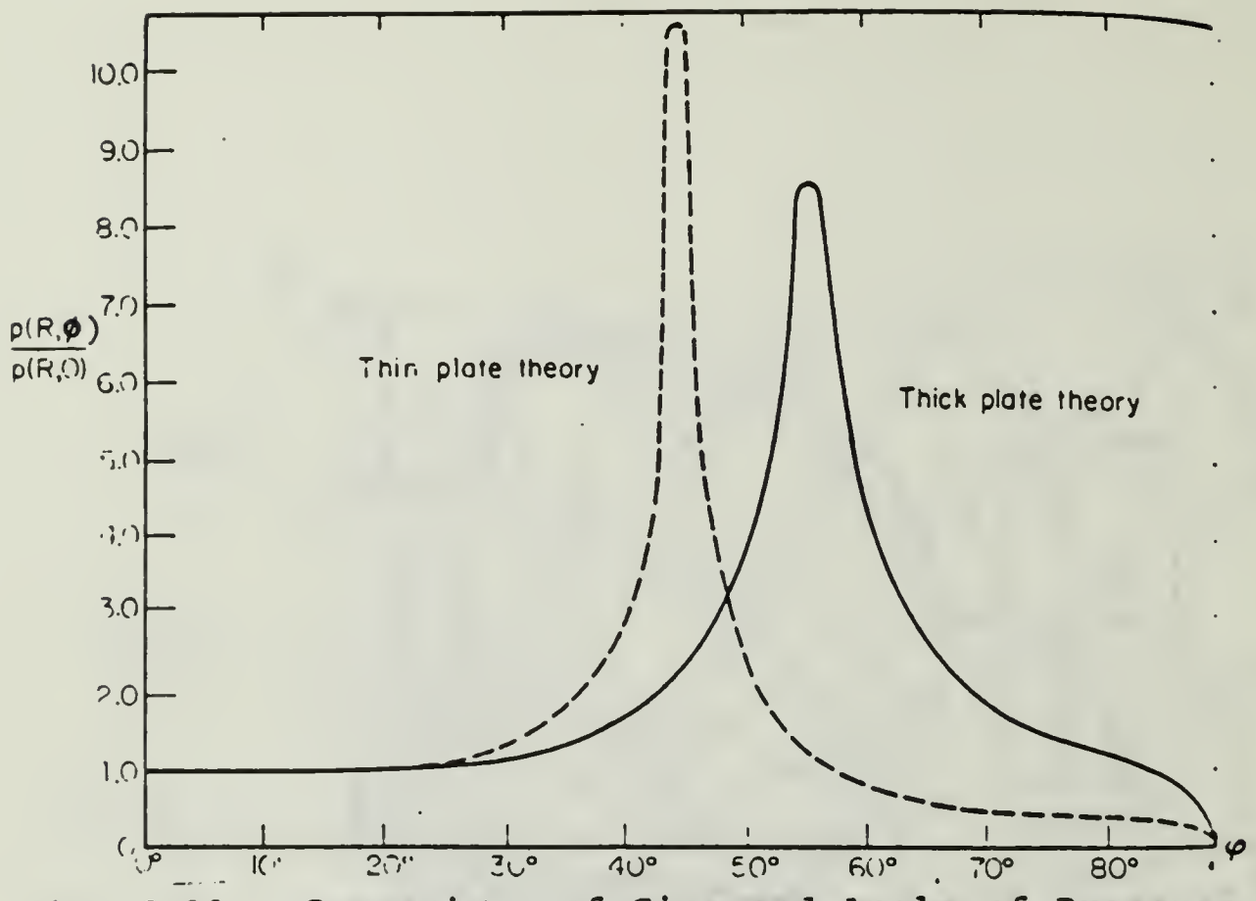

Fig. 3.11. Comparison of Size and Angle of Pressure Lobes, Thin-Plate Theory vs. Thick-Plate Theory (From Junger and Feit)

2. The Effect of the Fluid Loading Factor, β

The plots of the previous section showed the general trend in the radiation pattern when frequency is increased for a given set of thin-plate parameters. However, there are subtle changes that take place in the patterns when different parameters are used. The density of the plate can be measured with reasonable accuracy, and Poisson's ratio should be somewhat similar among plexiglass samples. However, Young's modulus and the exact effect of Poisson's ratio in the wave speed formula may vary. Additionally, Equation 3.10 lends

itself better to changing certain parameters than others. The parameter chosen for variation was the fluid loading factor, β , for fixed ratios of ω_c/ω . Figures 3.13 to 3.21 are the results of these runs. The effect of varying the fluid loading factor β as follows. Increasing the fluid loading smooths the radiation pattern, reducing the peaks and making the coincidence effect less dramatic.

Below coincidence, fluid loading should not have a great effect on the radiation pattern. This is seen in Figures 3.13 thru 3.15. A change in the fluid loading factor β for a frequency ratio of $\omega_c/\omega = 2$ below coincidence has a minimal effect on the radiation pattern.

At coincidence, the effects of fluid loading on the radiation pattern can be seen: for light fluid loading, Figure 3.16 shows a well-developed radiation pattern, but as β is increased (Figures 3.17 and 3.18) the radiation pattern is less pronounced and the off-axis pressure gain not as great.

Similarly, above coincidence, $(\omega_c/\omega) = 0.86$, as seen in Figures 3.19 through 3.21, the increase in fluid loading causes a less dramatic radiation pattern.

The importance of β is noticeable. Even though in the computer runs β was never "much less than one"

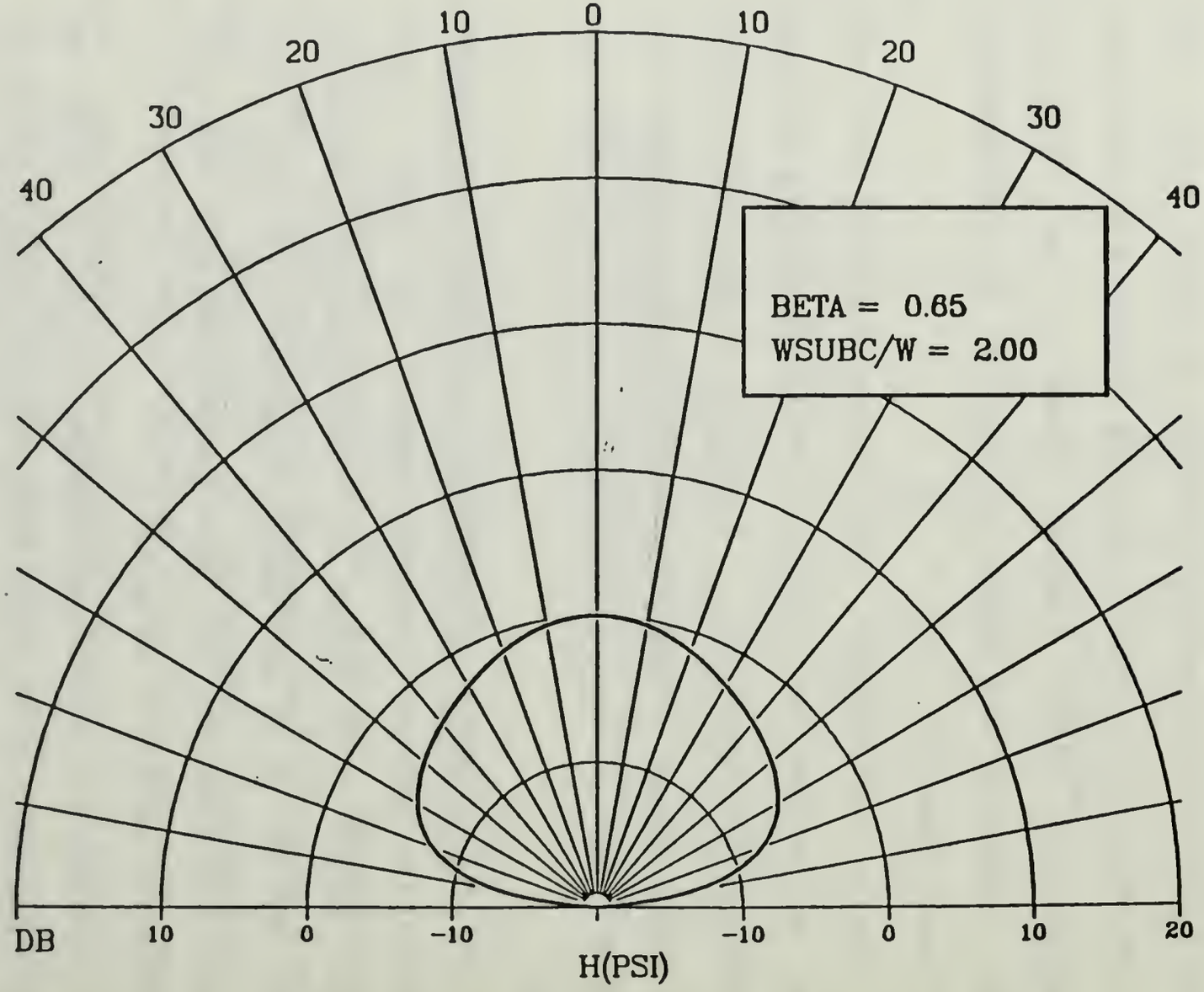

Figure 3.13 Theoretical response, $\beta = 0.65$, $\omega_c/\omega = 2$

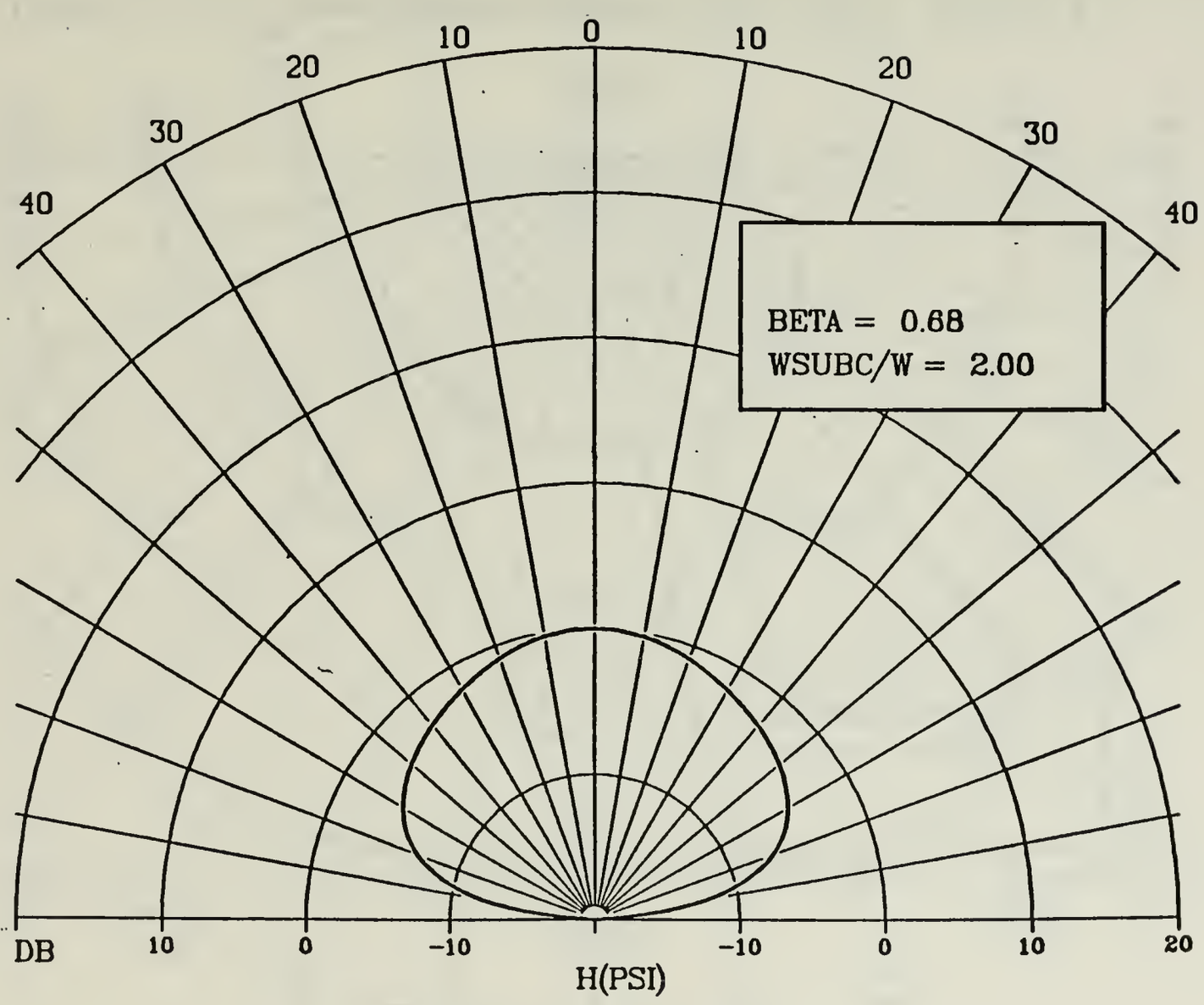

Figure 3.14 Theoretical response, $\beta = 0.68$, $\omega_c/\omega = 2$

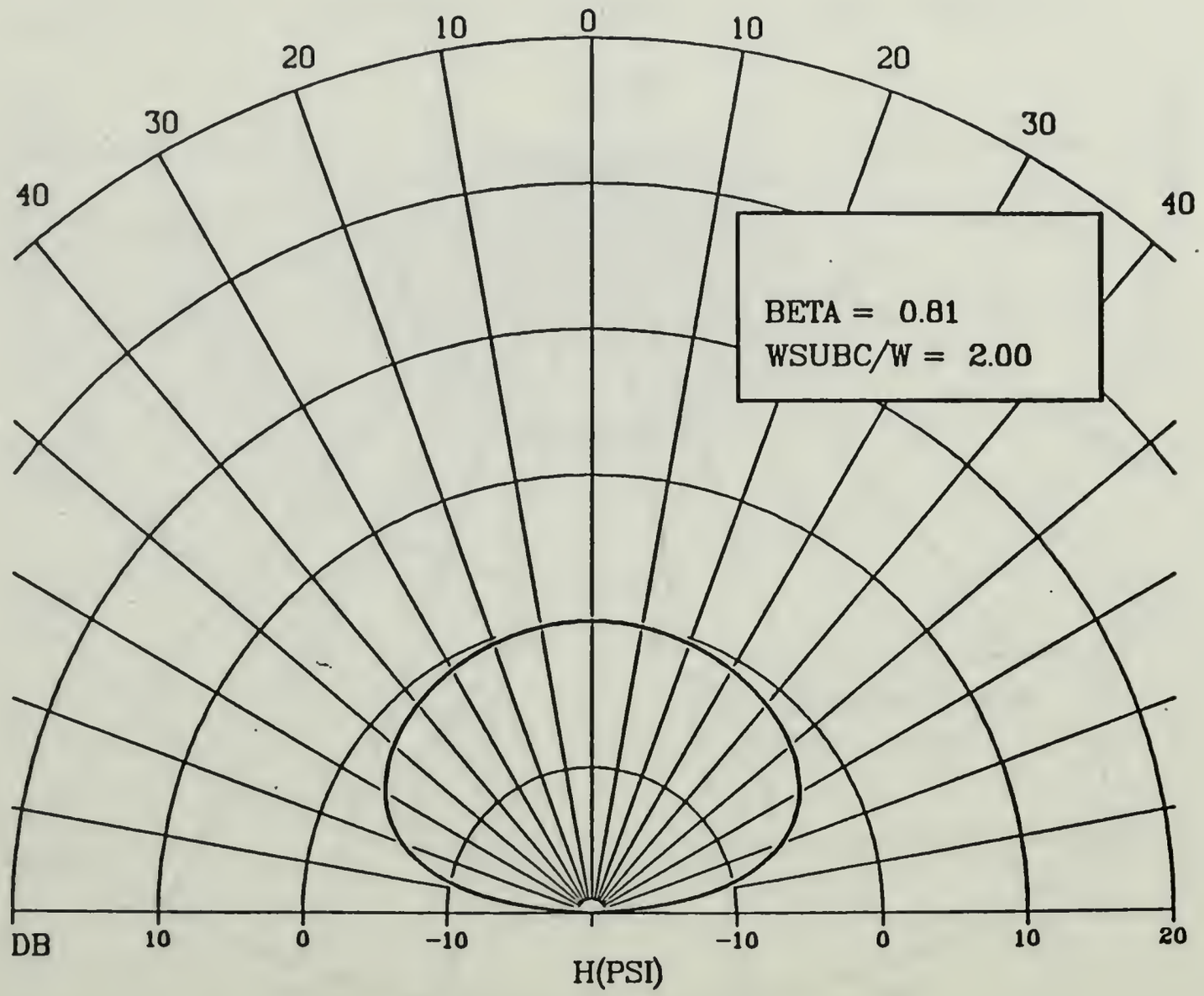

Figure 3.15 Theoretical response, $\beta = 0.81$, $\omega_c/\omega = 2$

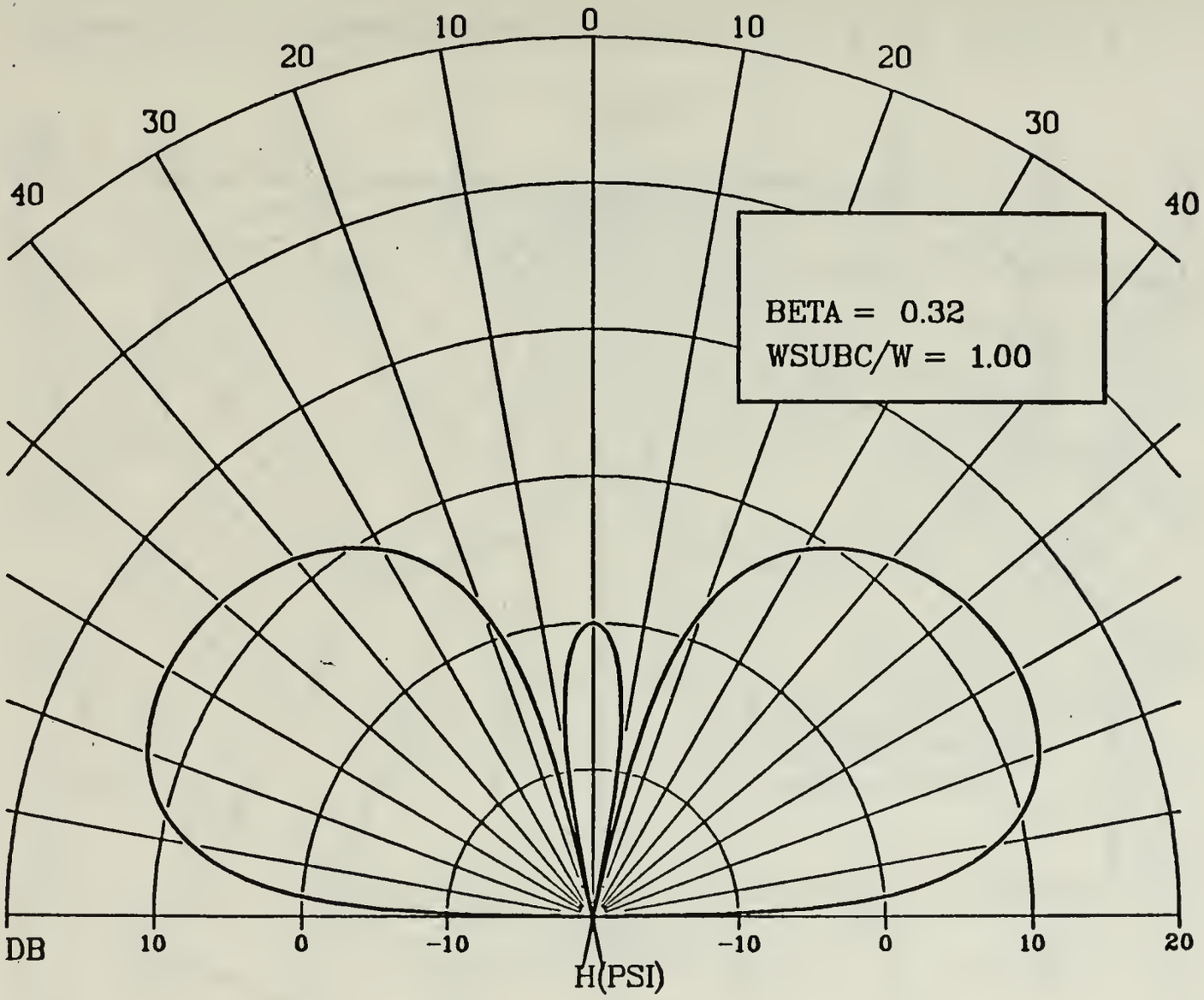

Figure 3.16 Theoretical response, $\beta = 0.32$, $\omega_c/\omega = 1$

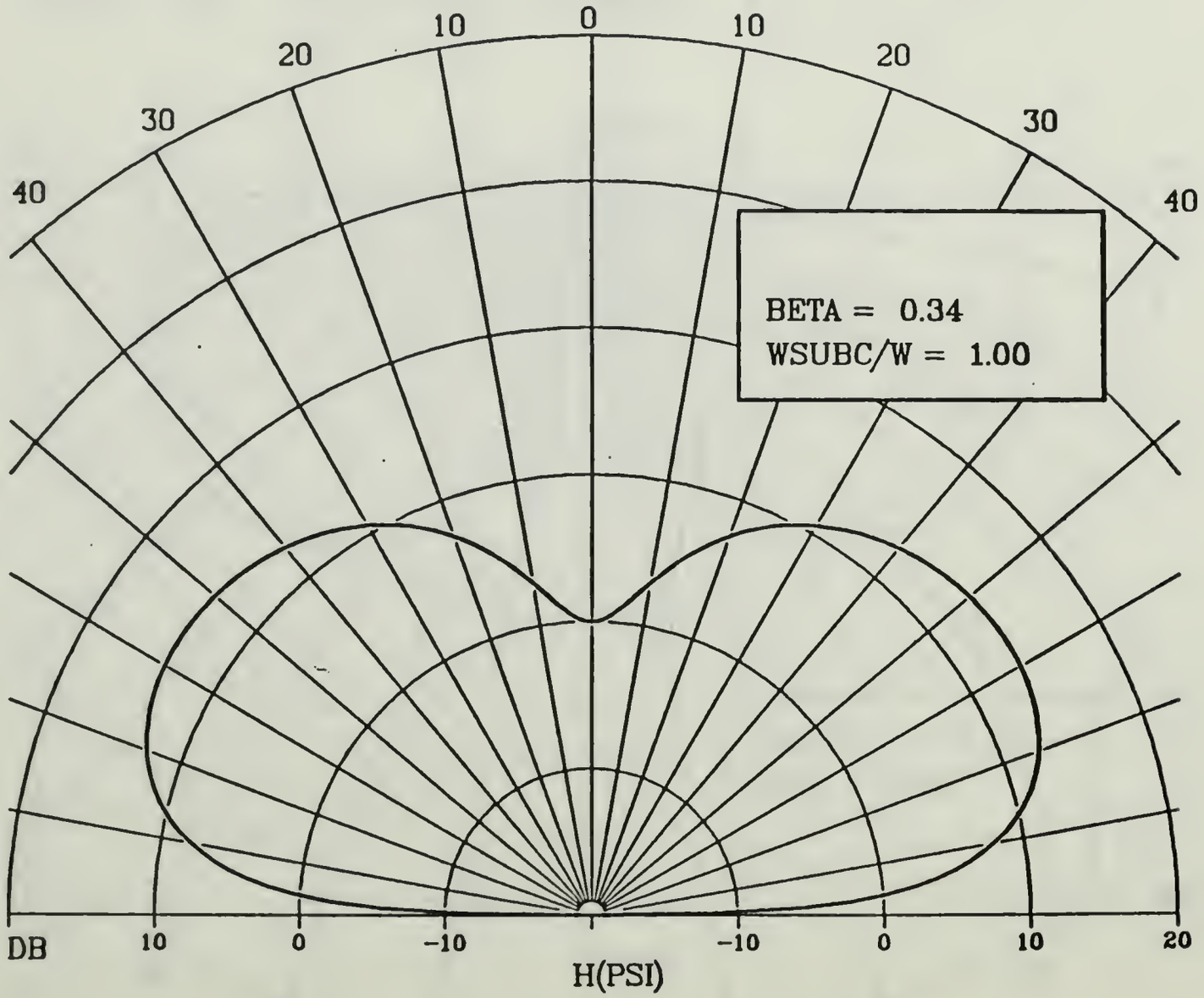

Figure 3.17 Theoretical response, $\beta = 0.34$, $\omega_c/\omega = 1$

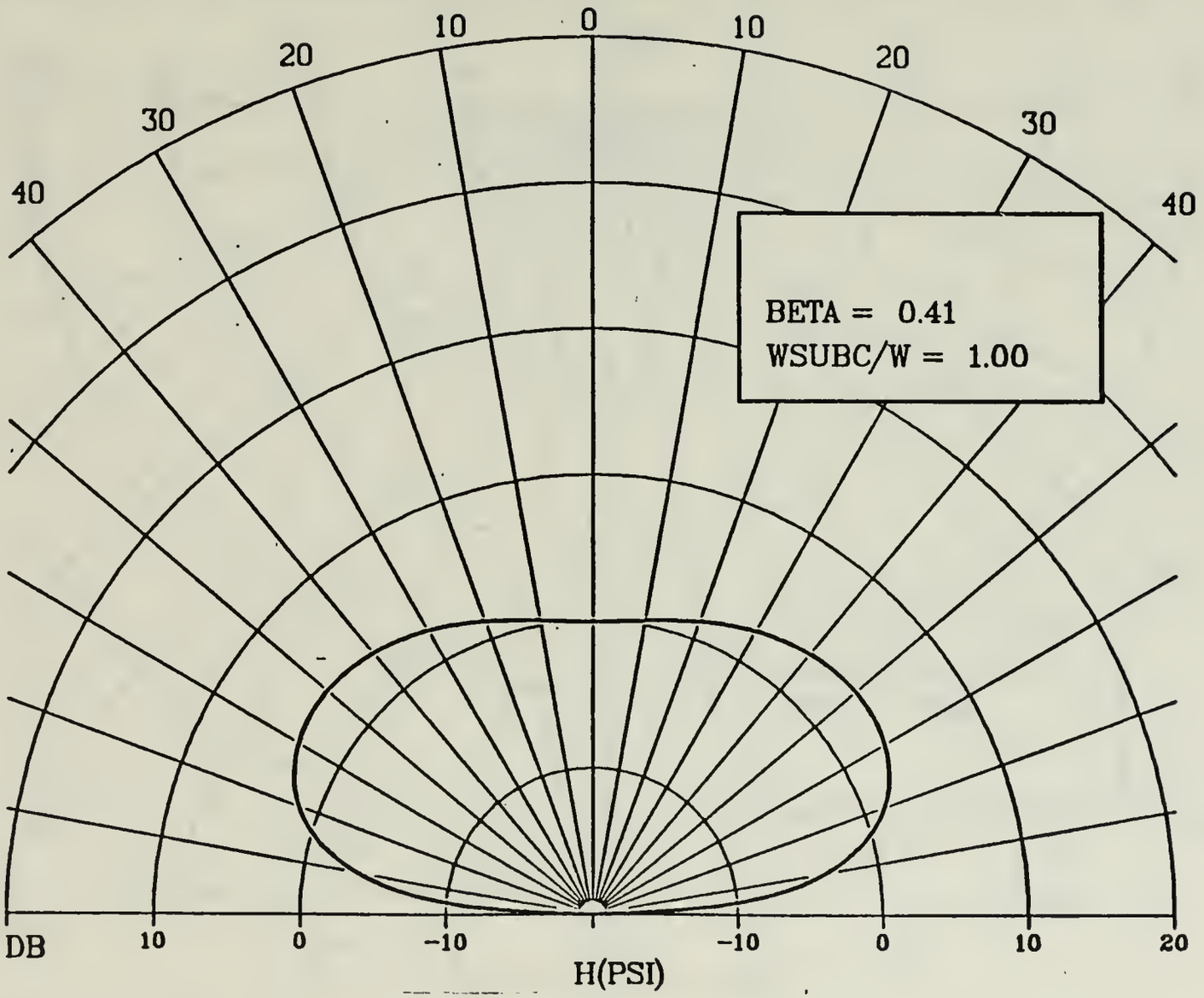

Figure 3.18 Theoretical response, $\beta = 0.41$, $\omega_c/\omega = 1$

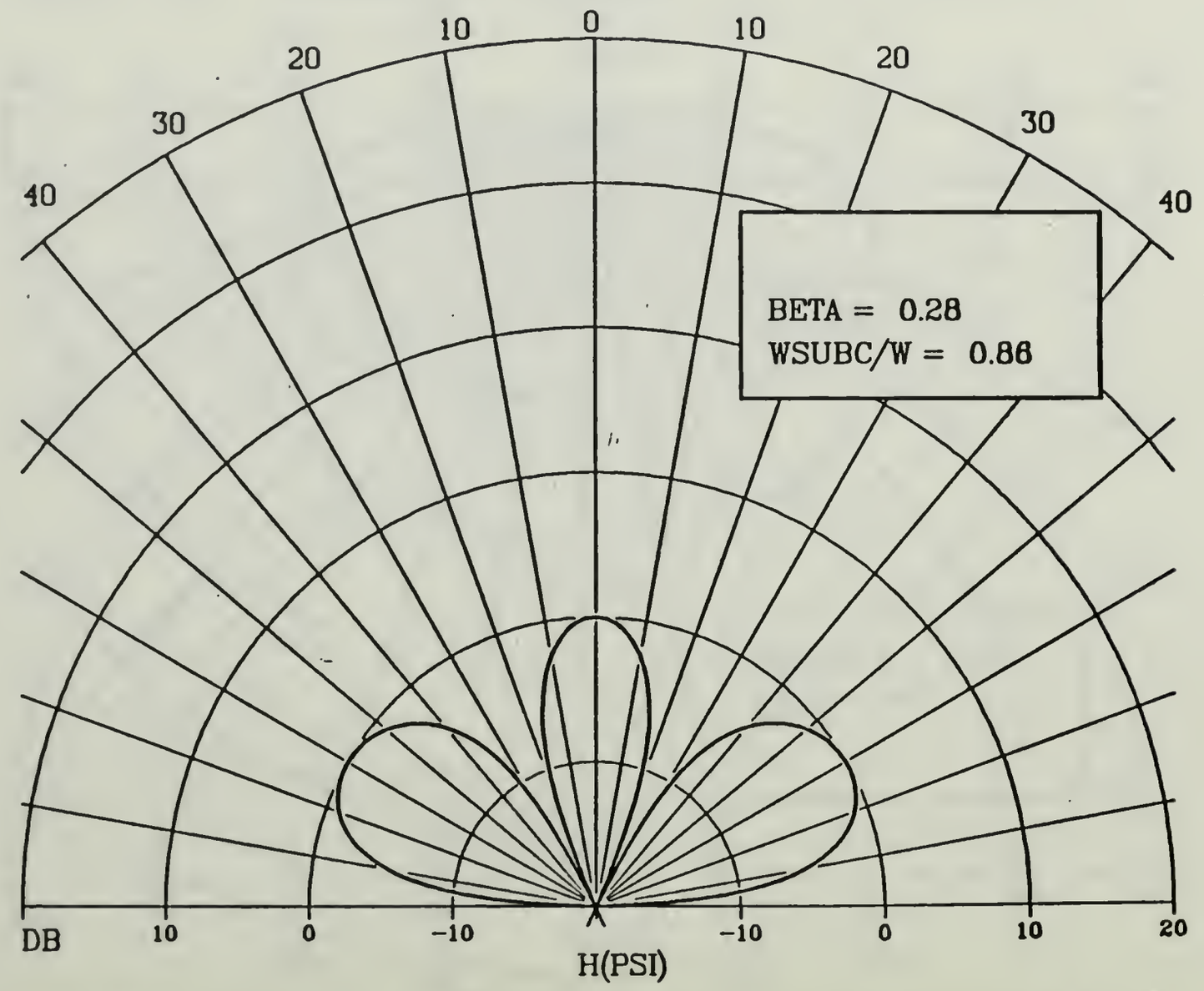

Figure 3.19 Theoretical response, $\beta = 0.28$, $\omega_c/\omega = .86$

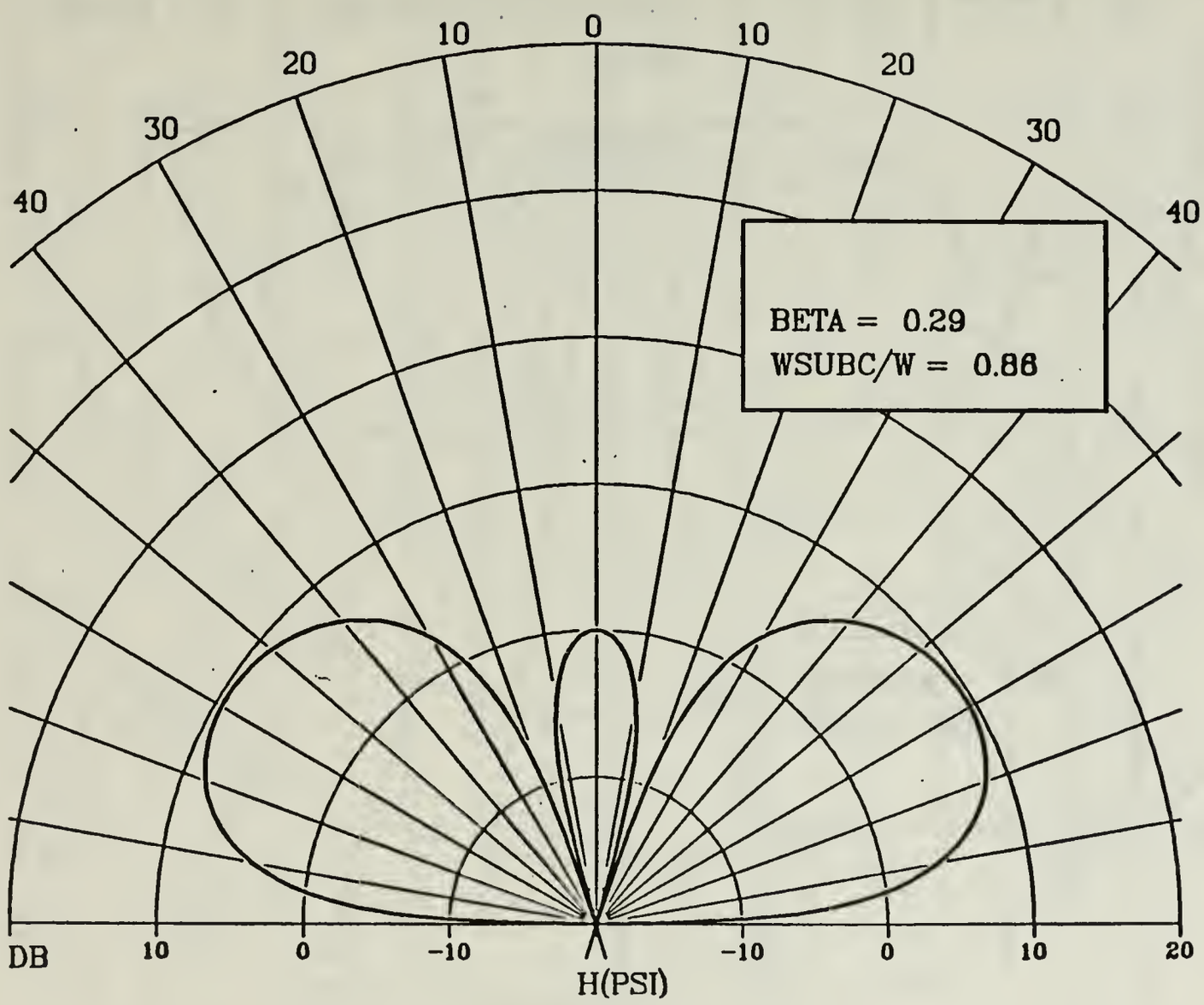

Figure 3.20 Theoretical response, $\beta = 0.29$, $\omega_c/\omega = .86$

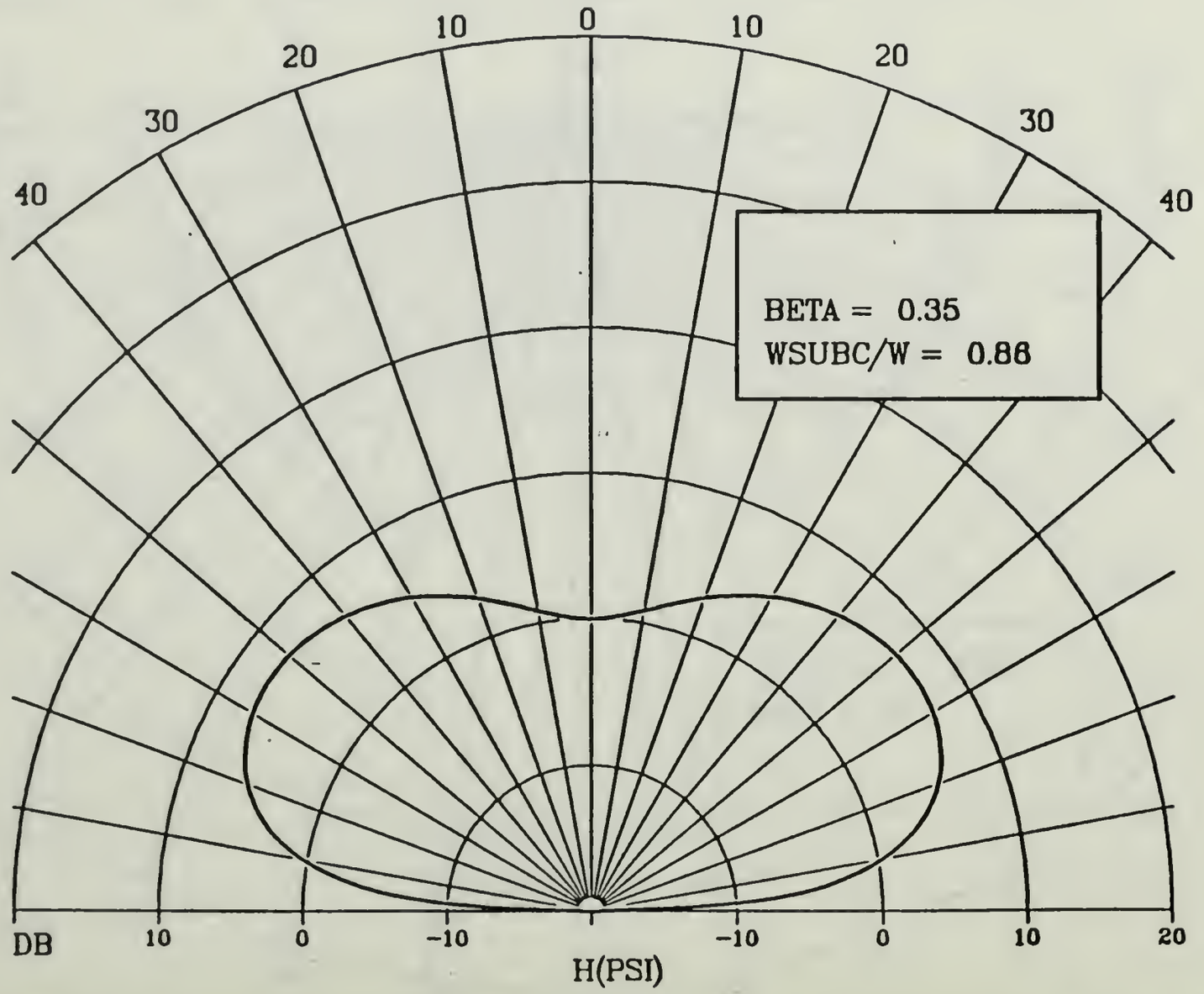

Figure 3.21 Theoretical response, $\beta = 0.35$, $\omega_c/\omega = .86$

which was described as the condition for light fluid loading, small changes in β caused large changes in the radiation patterns.

F. DESCRIPTION OF EXPERIMENT

An experiment was conducted to measure the radiation pattern from a point-driven sheet of plexiglass. See Figure 3.22. A 1/8th-inch thick sheet of plexiglass of dimensions 87cm x 152cm was floated on the surface of a freshwater anechoic tank. A small silicon bead was applied to the edges of the plate to keep it afloat. In the center of the plate a Tonpilz longitudinal vibrator of the author's design[5] and manufacture was bolted to the plate. The vibrator was driven by an HP-3314A function generator operating in the pulse mode. A maximum driving output voltage of 30V was applied.

A schematic cross-section of the Tonpilz vibrator is given in Appendix B. Its tail mass was made out of stainless steel and its head mass out of aluminum. This was to impart as large a signal as possible to the plexiglass sheet while keeping the vibrator's natural resonance frequency fairly high. An admittance circle of susceptance vs. conductance and plots of admittance

---

[5]For an excellent description of the design of Tonpilz vibrators, see Wilson [Ref. 23, Ch. 6].

and susceptance vs. frequency for the vibrator are also given in Appendix B. They show the motional resonance frequency of the vibrator to be 92.4 kHz, and a Q of about 112.

It is stated that although the motional resonance frequency of the vibrator was within the frequency range of interest for this experiment, this was not of key importance because a swept-frequency mode was not used. However, what is of interest in the pulse mode is the Q of the vibrator. The Q of the vibrator showed its effect in the transient response of the vibrator in the pulse mode. The transient response decay time grew when the driving frequency approached the motional resonance frequency of the vibrator. However, in every data set measurement, the pulse length was adjusted to give maximum steady state response time for the given pulse interval.

The head mass of the vibrator was about 1 cm in radius and was attached to the plate with a thin film of silicon grease to ensure positive contact between the head mass and plate. The clamp rod of the vibrator was used to compress the vibrator against the plate.

The radiation pattern from the driven plate was measured with a Celesco LC-10 hydrophone whose output was sent through a Tektronics AM-502 low noise preamplifier to a Kikusui oscilloscope. The LC-10 was mounted on an

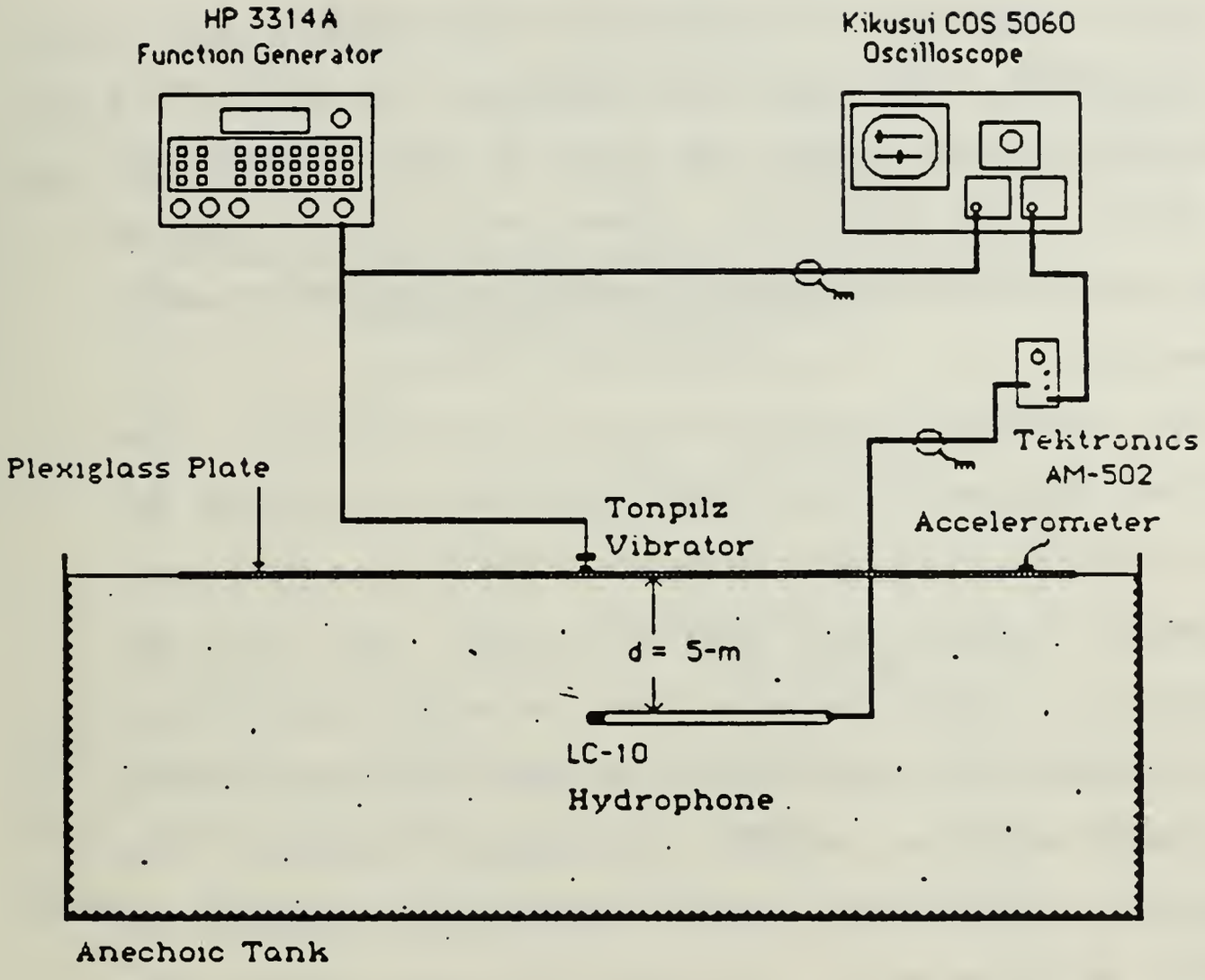

Figure 3.22. Driven Plate Experimental set-up

angular jig that allowed it to be swept from ϕ = -90° to 90° at constant range from the vibrator. An Endevco K920 accelerometer was used at times to probe the plate to obtain attenuation and edge-reflection data.

The pulse mode was used because of a problem of electrical pickup between the leads to the vibrator and the LC-10. The electrical pickup could not be removed even with the use of grounded coaxial cable and shielded connectors.

The length of the pulse varied with frequency. The limiting factors for the pulse length were the pulse interval and the transient response time of the vibrator. The pulse interval was limited because the LC-10 was located at a fixed distance from the source and reception of a pulse by the hydrophone had to be ended before the next began to prevent overlapping signals. The transient response time of the vibrator also limited the length of pulse used. The received pulse showed the transient and stead-state response of the vibrator. However, amplitude data could only be taken on the steady-state portion of the received signal. This further limited the time available in the pulse with which to drive the plate in a steady-state condition.

Both the pulse interval and pulse length were adjusted for each data set measurement to provide the

maximum time available with which to drive the plate in a steady-state condition.

The properties of the plexiglass used were determined experimentally by Johnson and Denny [Ref. 23.] Table 3.1 lists the wave speeds for the three wave types they measured. Note that both the shear wave speed and

TABLE 3.1

Experimental Wave Speeds for Plexiglass

C_p = 2240 m/s

C_s = 1373 m/s

C_b = 700-1150 m/s

therefore the high-frequency asymptote of the flexural wave speed are less than the speed of sound of the water. Therefore, coincidence cannot be reached.

G. EXPERIMENTAL RESULTS

1. Discussion of Plots

Several plots were obtained at frequencies from 50 kHz to 245 kHz with varying degrees of success. As was stated earlier, the high frequency asymptote of the flexural wave speed was less than the speed of sound in the fluid, so the coincidence effect could not be obtained. Still there was a change in the radiation pattern from the plate as frequency was increased.

Figure 3.23 shows the experimental radiation pattern when the plase was driven at f=50 kHz. There are several aberrations in the pattern when the deflection angle increased above 40° . Two plots were made, one with the hydrophone at a range of 0.5 m and the other at a range of 1 m . This was done to see if the distance from the source to the vibrator had an effect on the pattern. It can be seen that it did not, as the two curves appear to have quite similar behavior. Still, the general cosinusoidal pattern of a point-driven plate will below coincidence is seen.

In Figure 3.24, the aberrations of the previous pattern are more pronounced. The next sets of data, Figures 3.25 and 3.26 at 92.3 and 93.5 kHz, respectively show the development of a side lobe at an angle of about 45° . Figure 3.26, where data were taken at angles of -90° to 90°, show an asymmetry in the pattern. This was seen in a few plots and is thought to have been caused by asymmetrical excitation of the plate. This is discussed further in section G.3.

The next three plots, Figures 3.27 to 3.29, at frequencies of 100 kHz, 120 kHz, and 150 kHz show the development of lobes at about 40°. There are multiple aberrations in the pattern which may or may not have been additional minor lobes. Note that only the pattern

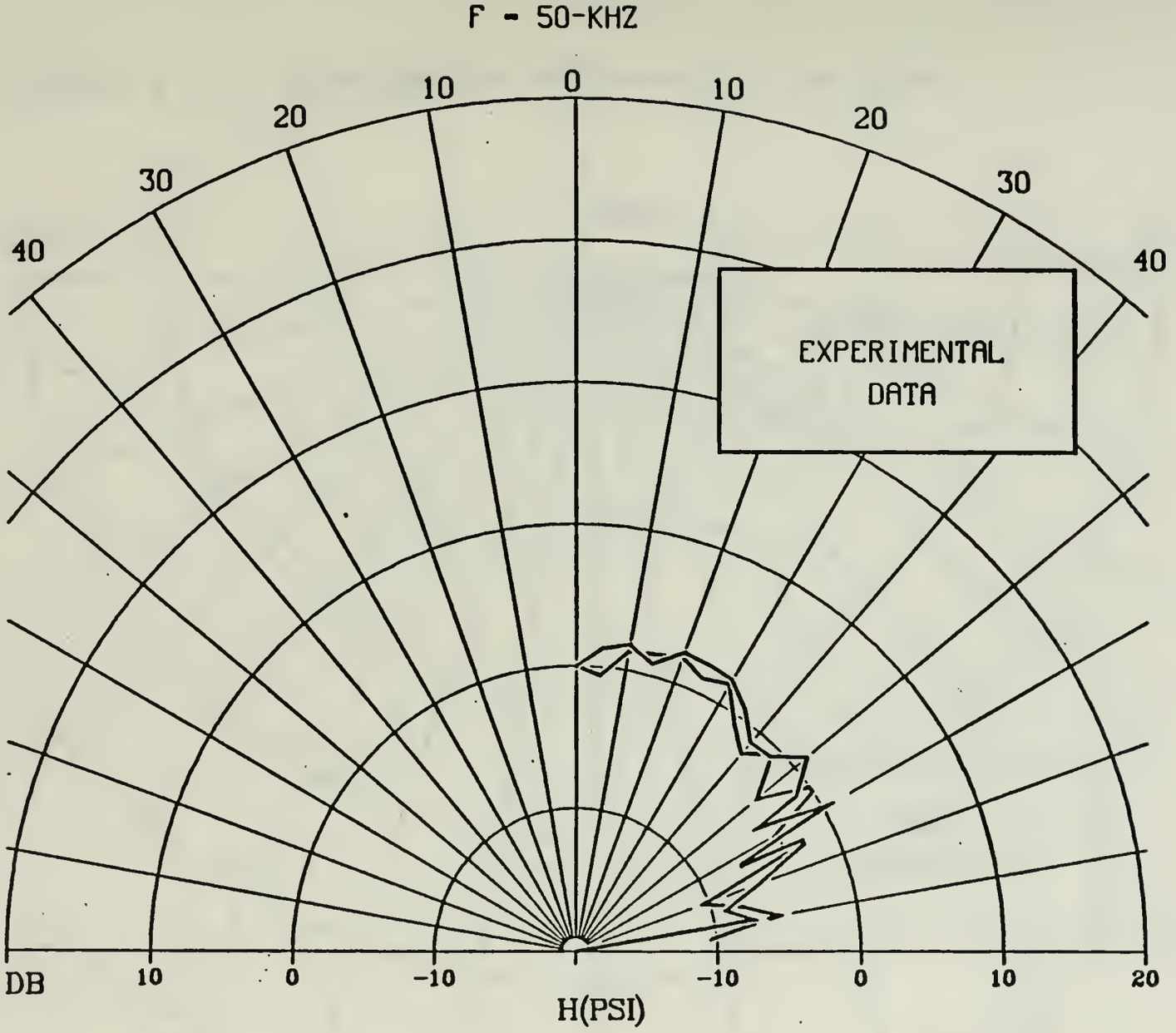

Figure 3.23. Experimental response, f = 50 kHz

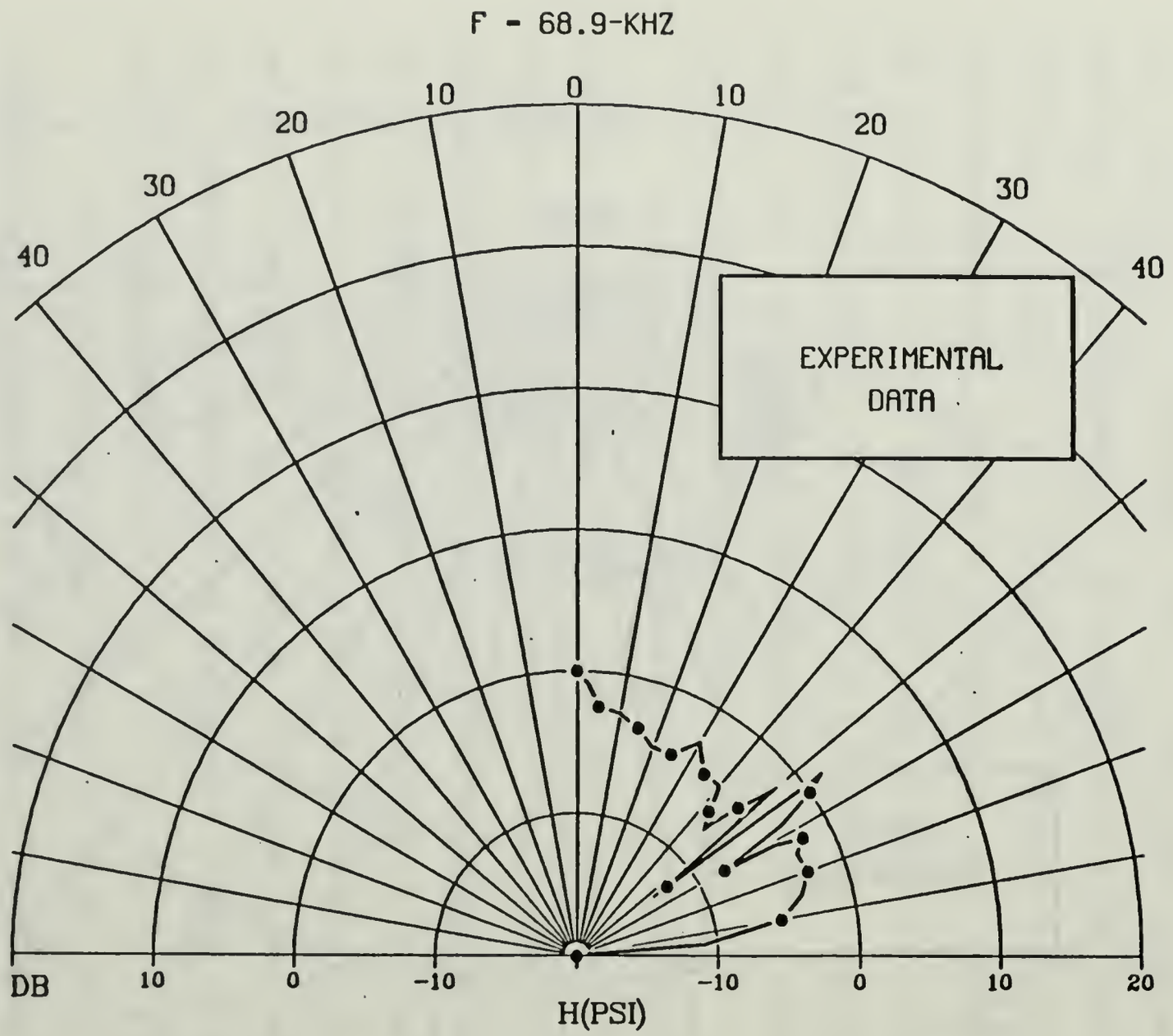

Figure 3.24. Experimental response, f = 68.9 kHz

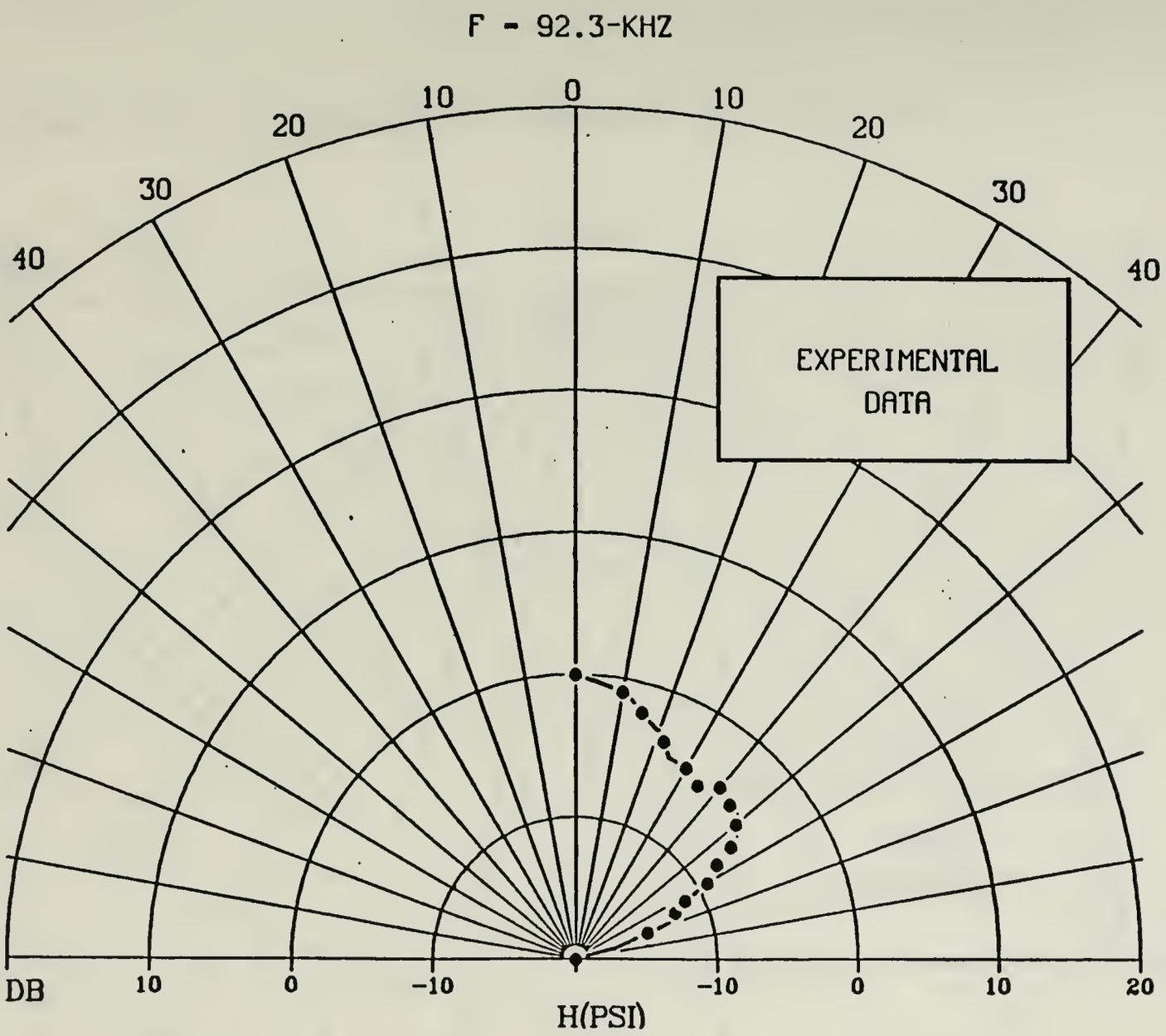

Figure 3.25. Experimental response, f = 92.3 kHz

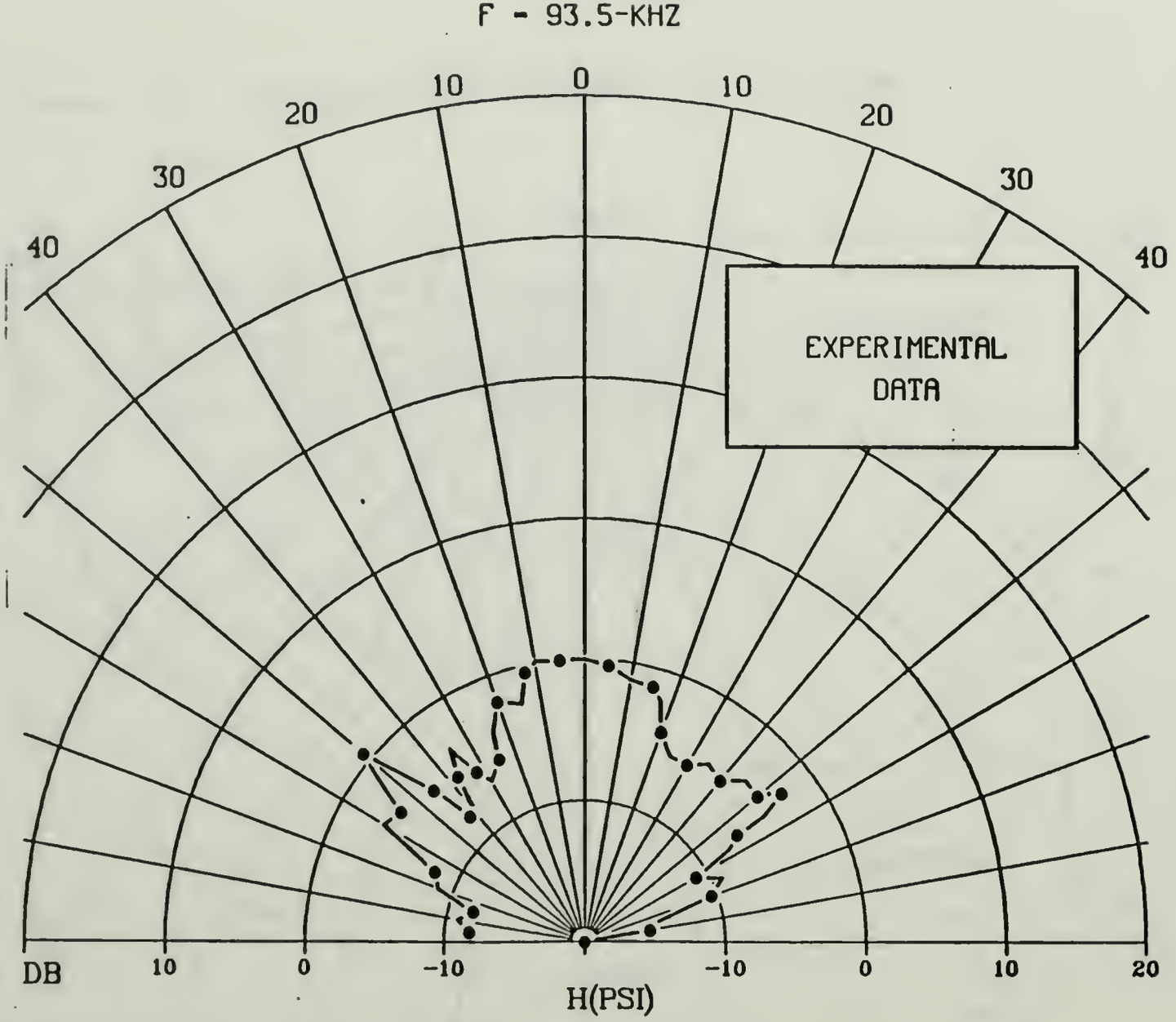

Figure 3.26. Experimental response, f = 93.5 kHz

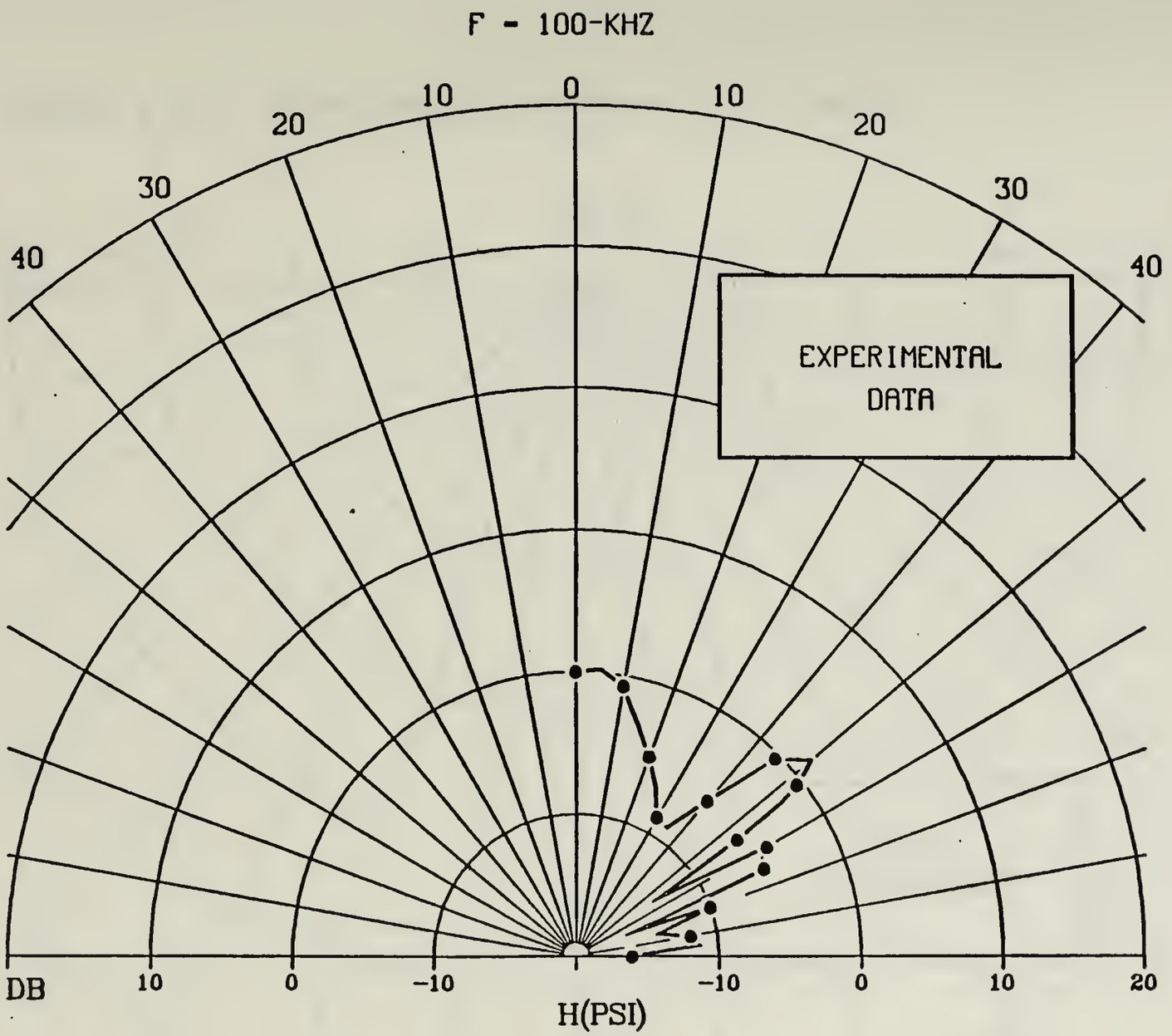

Figure 3.27. Experimental response, f = 100 kHz

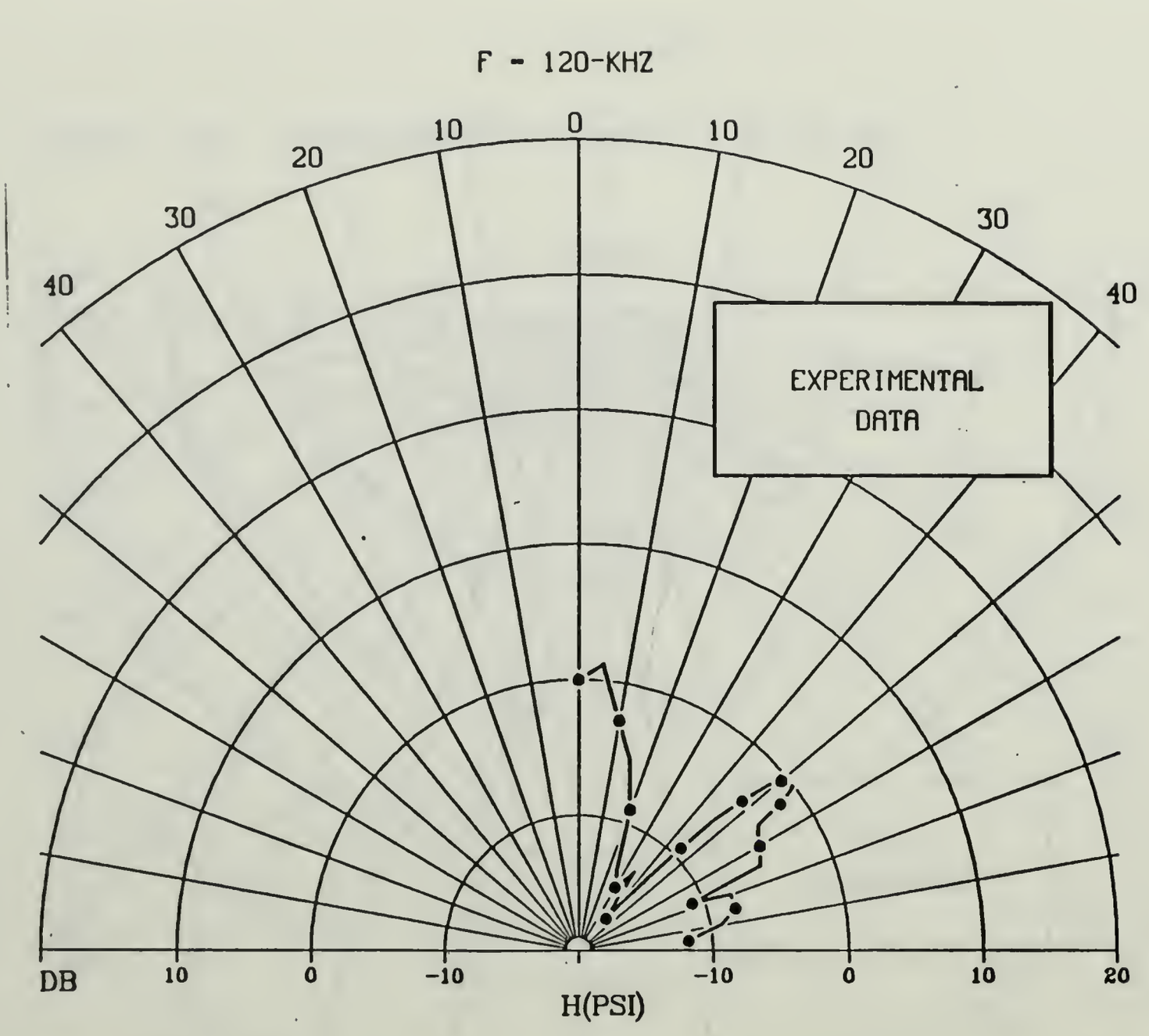

Figure 3.28, Experimental response, f = 120 kHz

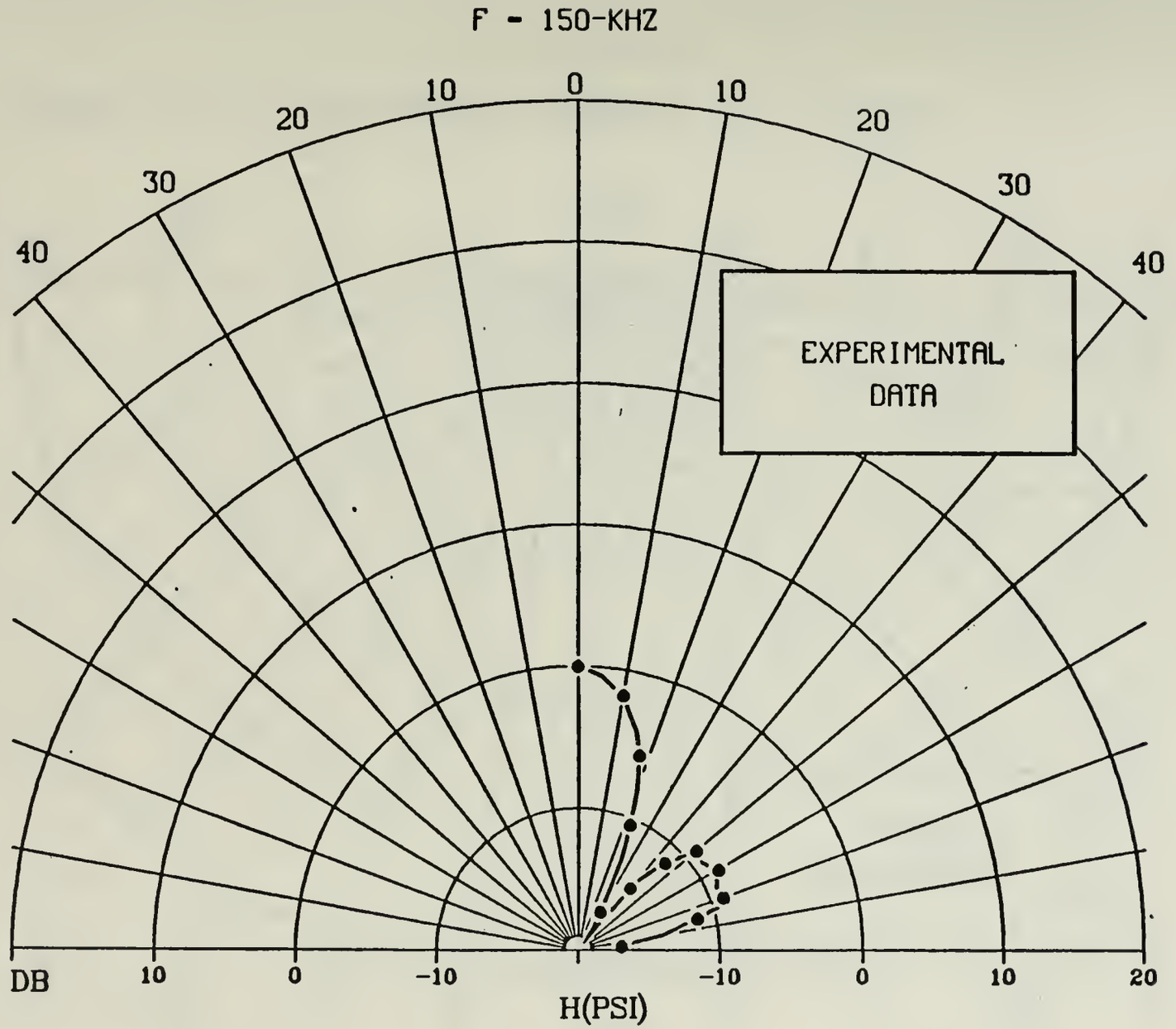

Figure 3.29. Experimental response, f = 150 kHz

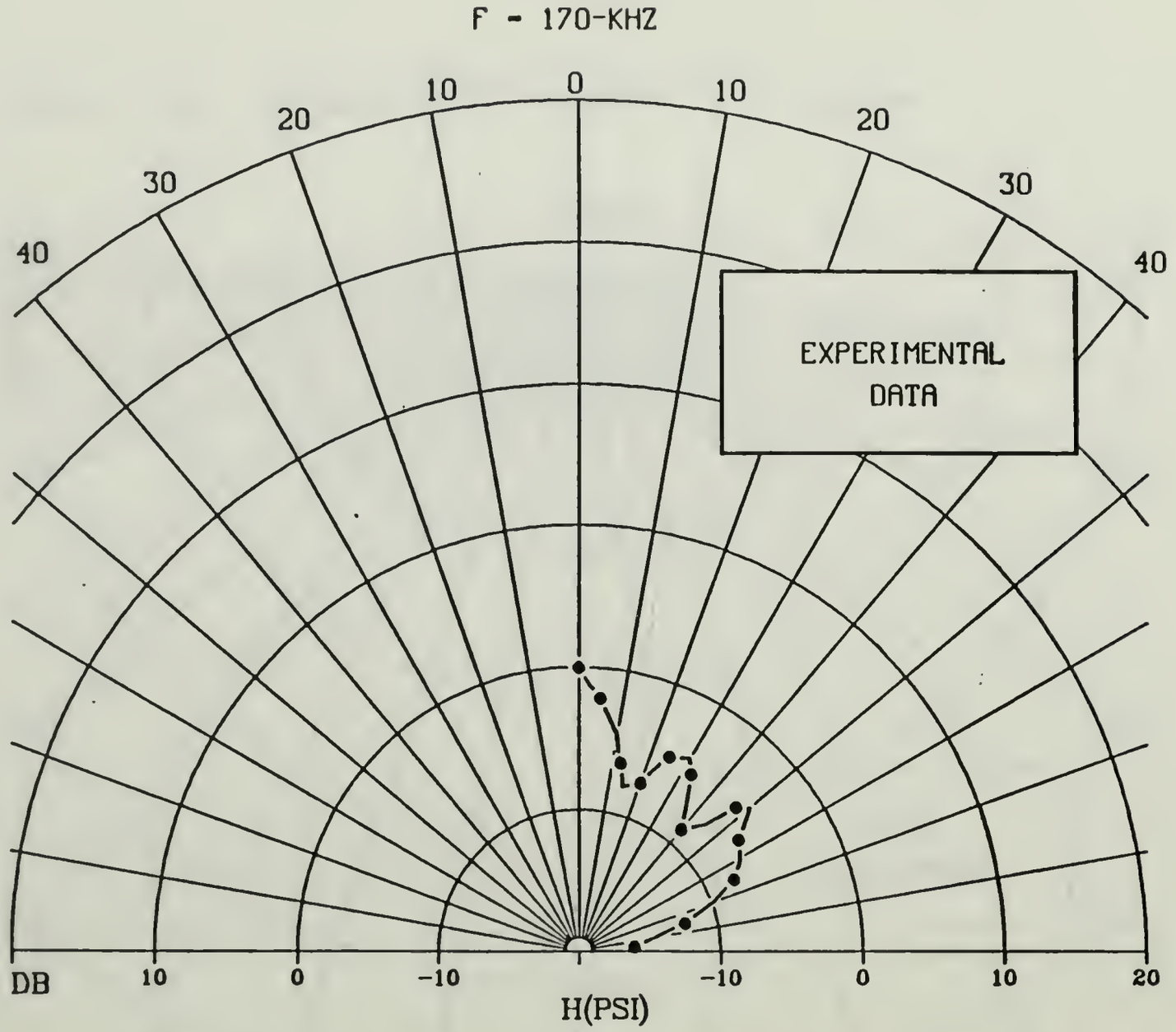

Figure 3.30. Experimental response, f = 170 kHz

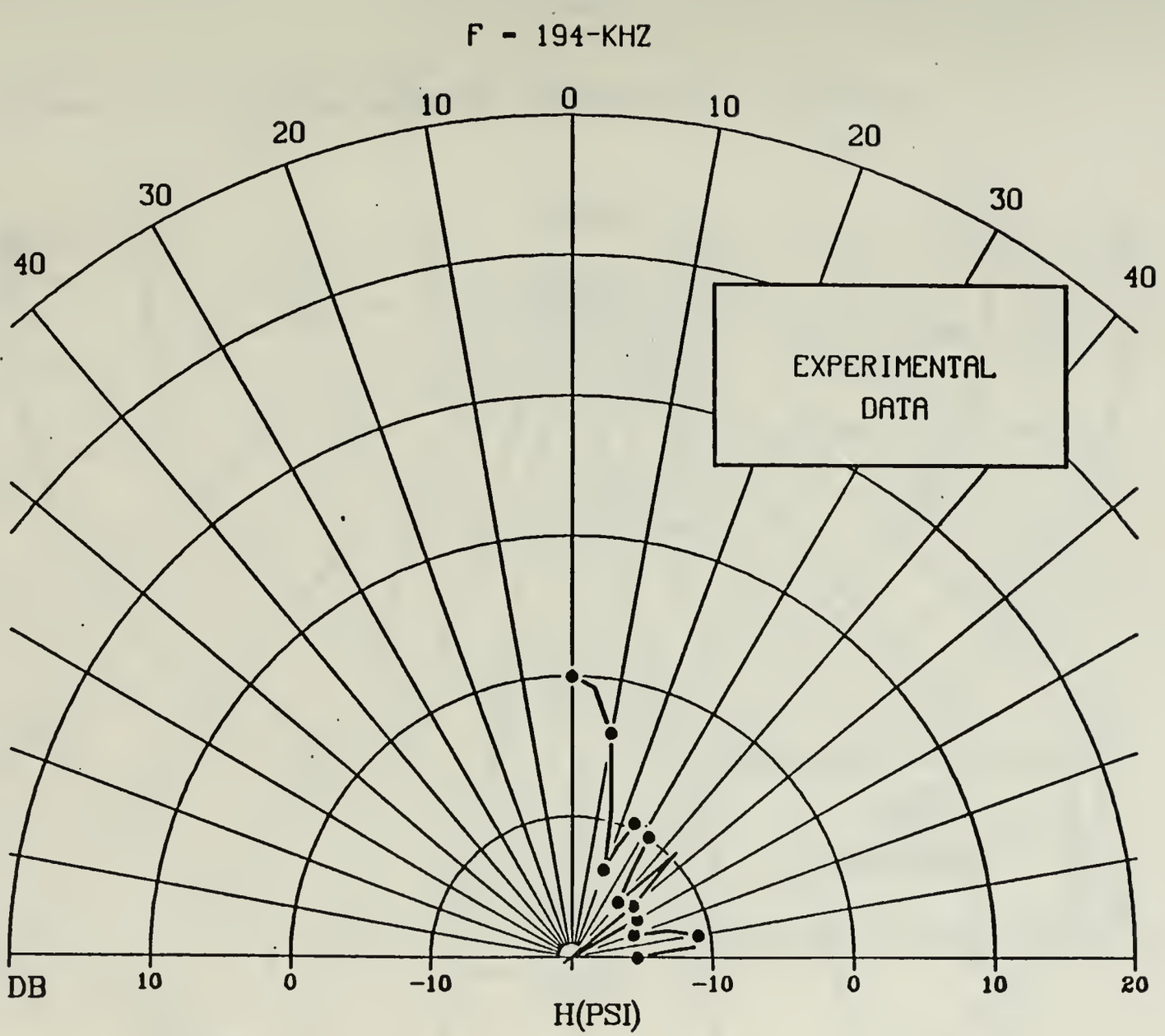

Figure 3.31. Experimental response, f = 194 kHz

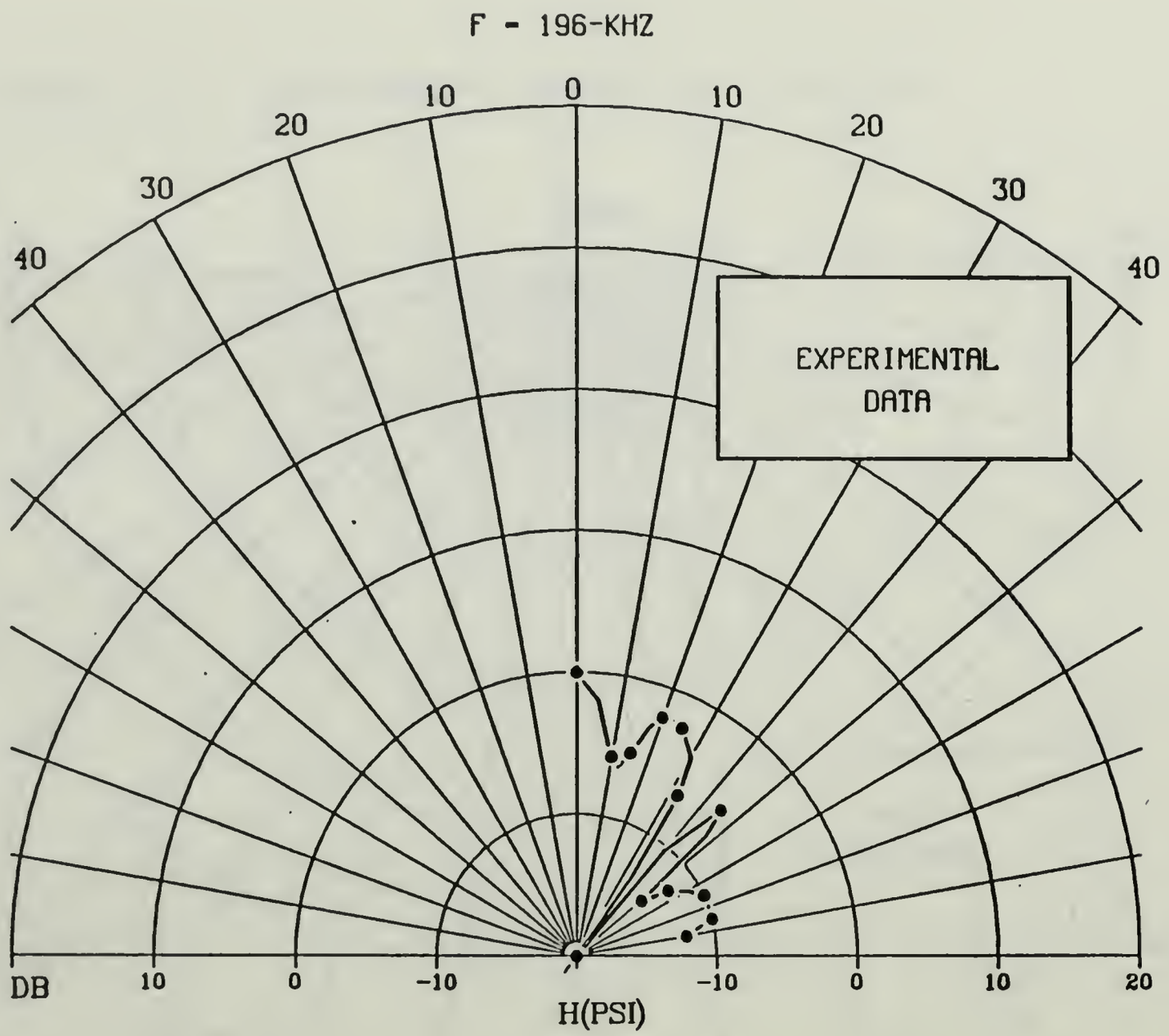

Figure 3.32. Experimental response, f = 196 kHz

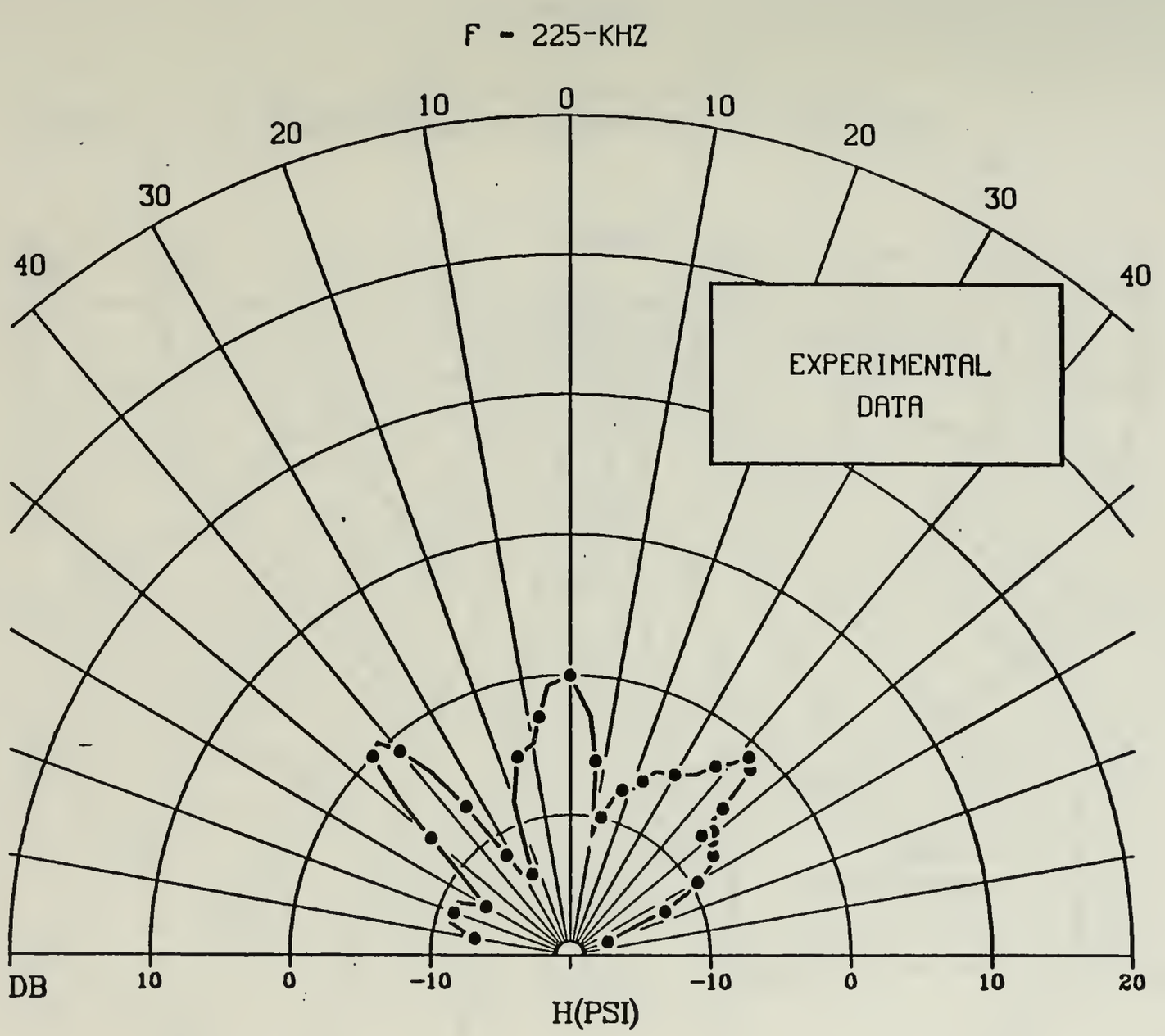

Figure 3.33. Experimental response, f = 225 kHz

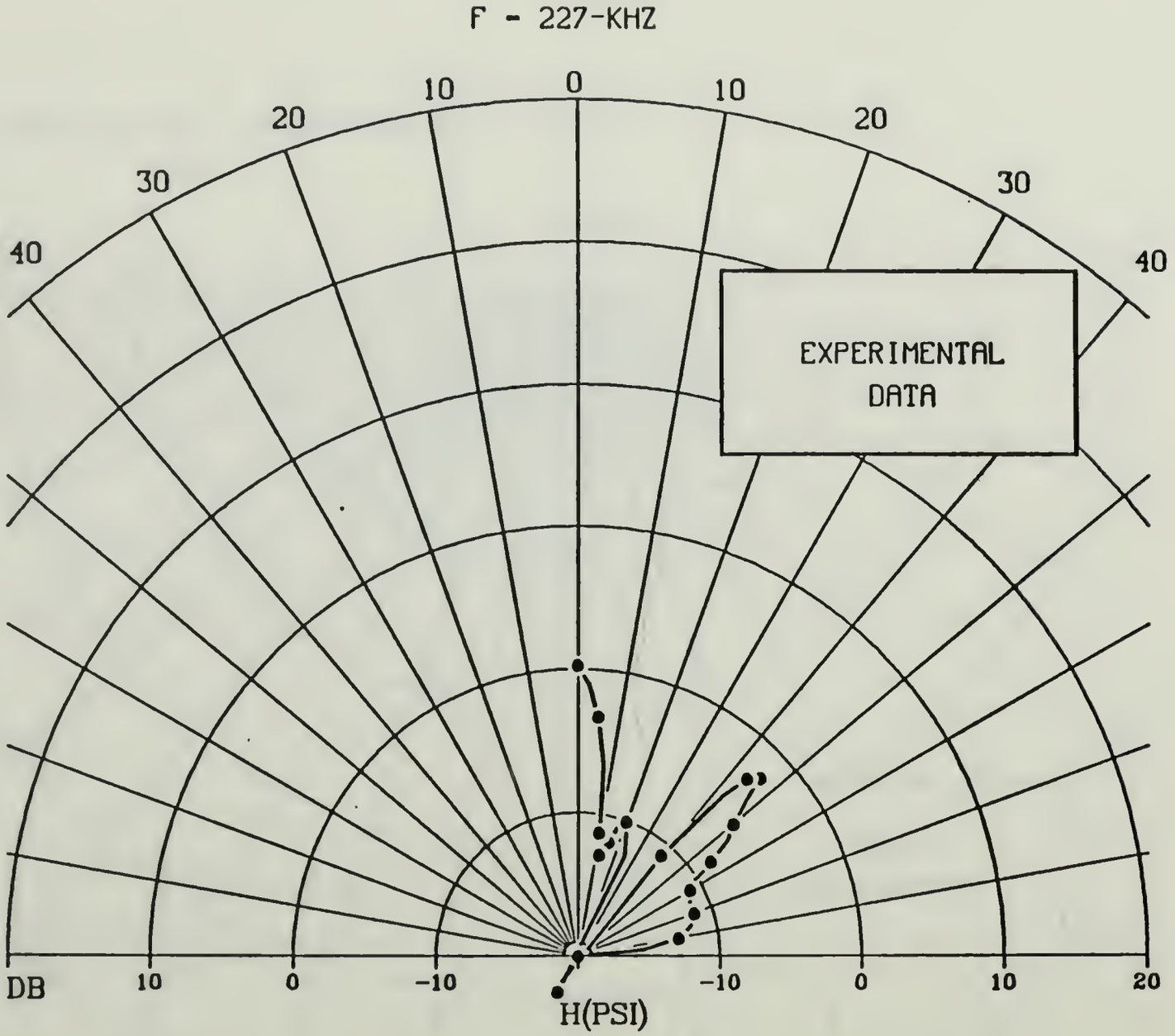

Figure 3.34. Experimental response, f = 227 kHz

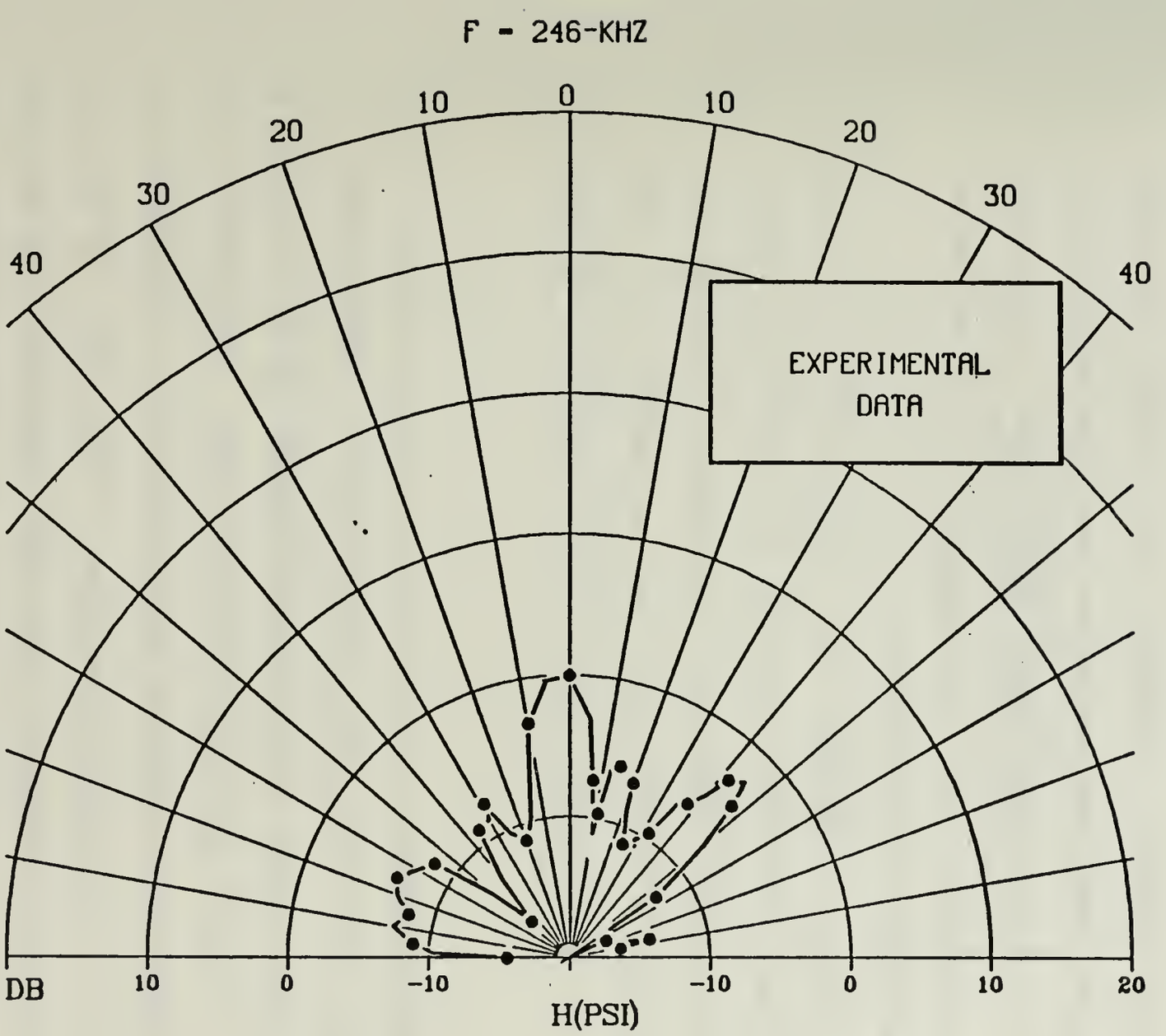

Figure 3.35. Experimental response, f = 246 kHz

at f = 150 kHz show a clean major and minor lobe pattern.

In the following three sets of plots, figures 3.30 to 3.32 at f = 170 kHz, 194 kHz, and 196 kHz, the well-developed pattern of Figure 3.29 is lost and the pattern became more complex, with multiple aberrations which may have represented small minor lobes in the pattern or interference resulting from incomplete and asymmetrical excitation of the plate.

The final three data sets, figures 3.33 to 3.35 at frequencies of 225 kHz, 227 kHz, and 246 kHz, respectively, show patterns that are very complex, and as evidence in figures 3.33 and 3.35, very asymmetrical. The side lobes of the pattern are just as large as the on-axis lobe.

2. Error Analysis

The method of data collection was as follows. For a given frequency, with the hydrophone on-axis (0°) the output voltage of the preamplifier was adjusted to 7.0V. All readings thereafter were immediately corrected to dB re 7.0V. The signal-to-noise ratio (SNR) varied between data runs because of the output response of the vibrator. On the average, however, the SNR was estimated to be 30 dB at zero deflection angle.

Since the data were normalized to the on-axis reading, the error increased with decreasing sound pressure (and hence voltage) levels. Table 3.2 shows the resulting dB error for various levels.

EXPERIMENTAL ERROR

TABLE 3.2

SPL	ERROR
0dB re 7V	± 0.12 dB
-5	± 0.56 dB
-10	± 0.84 dB
-15	± 1.27 dB

Angular measurements were quite precise with the jig that was used. Angles were precise to ±0.1 degree. As precise as the angular measurements were, they were not as accurate. While every attempt was made to accurately position the hydrophone directly underneath the vibrator at the start of each data collection period, parallax and the water refractive effect hampered accurate positioning. It is estimated that the angular accuracy was ±5 degrees. Techniques to improve the accuracy were abandoned because it was reasoned that the

the result of any inaccuracies would be an angular skewing of a pattern, not a change in the pattern itself.

It would seem therefore, that inaccuracies or errors in data collection were not the cause of such large aberrations are asymmetries in the experimental plots.

3. Discussion of Results

Since the high frequency asymptote of the flexural wave speed was less than that of the speed of sound in the fluid, coincidence was not possible. Therefore, the large off-axis pressure maxima associated with the driven plates above coincidence were not obtained. This may, however, be proper modelling of the ice. Stein [Ref. 2, p. 288-289] found in his Arctic ice experiments that ". . . at no point is the first antisymmetric mode [i.e., the flexural wave] supersonic with respect to the water; there is no coincidence frequency above which phase speeds are faster than the water wave speed. This implies that in the plane-wave limit the first antisymmetric mode never radiates and never loses energy to the water."

After a careful search of recent literature on driven plates below coincidence, no theories were found that would suggest a radiation pattern other than that

of a cosinusoidal pattern. Nor were any theories found on the radiation patterns from such acoustically slow plates that coincidence was not possible. Therefore, theoretical plots, such as those developed for earlier sections, were not available. However, some possible explanations are offered about the complexities and asymmetries of the patterns.

Since this was a finite-sized plate it could be argued that plate modes of vibration were set up, which caused nodes in the plate that would affect the pressure field in the fluid. However, the pulse mode of operation was used, which reduces the likelihood that this was responsible for discrepancies. Also, it was found (and stated earlier in this chapter) that no reflections were observed from the plate edge. Therefore, excitation of normal modes of vibration in the plate are thought to be unimportant for the pulse experiment.

Another possible explanation is that the hydrophone was, at 0.5 m, in the "near-field" of the plate. Feit [Ref. 7, p. 1482] used the asymptotic approximation $k_oR>>1$ in the evaluation of the integral, Equation 3.9. At the lowest frequency at which data were taken, 50 kHz, k_oR equals 106, so it would appear that the far-field assumption is valid.

The complexities of the patterns might also be explained by the pulse not being long enough. The pulse

interval was limited to 0.30ms, based on the speed of the pulse through the water to the receiver and the transient response time of the vibrator. Table 3.3 gives values of travel distance that a flexural wave packet would achieve in the plate in 0.30 ms for the frequencies used.

TABLE 3.3

f(kHz)	c_b(m/s)	d(m)
50	725	0.22
100	1026	0.31
200	1150	0.35

The cosinusoidal patterns expected below coincidence are based on an assumption of cylindrical divergence of the flexural wave on an infinite plate. That is,the pressure at a field point in the fluid is made up of the sum of pressures caused by the deflection of each incremental area of the plate. If the entire plate were not excited, this sum would be incomplete. From Table 3.2, a pulse of flexural wave of frequency 50 kHz will only travel out 0.22m in 0.3 m/s. Thus, the entire plate was not being excited. Even at 200 kHz, the entire plate was not excited. This certainly could be one of the contributing factors in the complexity of experimental plots.

Prior to the discovery of the electrical pickup problem mentioned earlier in this chapter, the plate was driven in the CW mode. The complexities in the patterns were still there. This would indicate that use of the pulse mode was only a contributing factor, not the main cause of the complexities of the experimental plots.

A more important factor is thought to be the absorption of the flexural wave in the plexiglass. Following the same argument above, that is, the pressure at a field point is the sum of the pressures caused by the individual deflections of each incremental area of the plate, the effect of the flexural wave absorption would be to greatly reduce the contributions of radiations from the incremental areas far from the source.

The so-called "acoustic mode" of sound propagation, which this experiment was modelling, assumes sound radiation away from the source in the fluid from a lossless plate. Plexiglass is a highly absorptive medium; therefore, the propagating flexural wave decayed in amplitude due to losses as well as divergence as it travelled away from the vibrator. Consequently, the incremental areas of the plate far from the source did not deflect nearly as much as those close to the course, so they did not contribute as much to the pressure at a given point in the fluid.

The plate might be thought of as a complex aperture, or a quasi-piston, with a radius of the head mass radius and a portion of the adjacent plate. A rough estimate of the aperture radius is the head mass radius plus either one-fourth the flexural wave radius plus either one-fourth the flexural wave radius or one plate thickness. Both give similar results. Based on this, $k_o a$ for radiation into the fluid varies from 2.79 for a frequency of 50 kHz to 14 at f = 250 kHz.

Even though the aperture is shaded and phased, it is noteworthy that for a $k_o a$ in excess of 4, a piston is beginning to develop a side lobe, and for a $k_o a$ of 10, it has about two side lobes. This is not inconsistent with the angular scale of the lobelike structure observed.

The asymmetry seen in a few of the radiation patterns might have been caused by radially non-uniform excitation of the plate. As was mentioned in section F of this chapter, the vibrator was compressed against the plate by a bolt. However, asymmetrical compression of the vibrator against the plate was possible. Possible causes of asymmetrical compression are improper machining of the head mass, imperfect centering of the bolt through the vibrator assembly, or a non-uniform layer of

grease between the head mass and plate. A non-uniform radial excitation of the plate seems to be a plausible explanation for asymmetry in the radiation patterns.

Two important points that can be made are that it appears that the radiation pattern is a function of the source, not any flexural wave propagation. Secondly, situations where coincidence is not possible, such as a plexiglass plate on water, present radiation patterns at lower frequencies similar to radiation patterns below coincidence in situations where coincidence is possible.

IV. CONCLUSIONS

This study was a low-cost, "low-tech", first-cut attempt to duplicate a sound source mounted on the ice in the Arctic. The first experiment performed showed that when a plate is introduced at the boundary of a Lloyd's-mirror-type problem, the effect of the plate was only to introduce phase delay, causing a shift in the node and antinode pattern. If any flexural waves were excited in the plate, which might have caused an increase in amplitude in the received signal, they would have been absorbed by the plexiglass.

In the second experiment performed, it was found that even though the theory behind a point-driven fluid-loaded plate is well known and many interesting results can be gleaned from that theory, extracting experimental plots upon which a theory can be based is difficult.

Plexiglass was originally chosen because its specific acoustic impedance is fairly close to both ice and water. However, the flexural wave absorption suffered in commonly available plexiglass and more importantly, its low flexural wave speed render it a poor choice to use in the lab in this type of experiment, where wave generation and propagation are important.

Several interesting types of plastics are available. Often the manufacturer lists the density and Young's modulus of each in its catalog. However, flexural wave attenuation data are never available. It is recommended that the next step in research along these lines be to collect samples of each type of plastic and measure these parameters. The time available for this study prevented such an analysis.

APPENDIX A

COMPUTER PROGRAM

```
C     ************************************************************      BMP00010
C     *                                                          *      BMP00020
C     *                                                          *      BMP00030
C     *                      APPENDIX A                          *      BMP00040
C     *                                                          *      BMP00050
C     *                                                          *      BMP00060
C     ************************************************************      BMP00070
C     THIS PROGRAM IMPLEMENTS ROSS FORMULA 6.63, WHICH IS A               BMP00080
C     SOLUTION FOR THE FAR-FIELD PRESSURE FROM A POINT-DRIVEN             BMP00090
C     FLUID-LOADED PLATE  AS ORIGINALLY DERIVED BY FEIT.                  BMP00100
C                                                                         BMP00110
C     IT IS A NON-INTERACTIVE PROGRAM.  FREQUENCY OF INTEREST, PLATE      BMP00120
C     PARAMETERS, AND WATER SOUND VELOCITY NEED TO BE INSERTED INTO       BMP00130
C     THE PROGRAM BELOW.                                                  BMP00140
C                                                                         BMP00150
C     THE PROGRAM USES DISSPLA VERSION 9.0 (SOFTWARE PRODUCT OF ISSCO,    BMP00160
C     SAN DIEGO, CA)  TO PRODUCE A GRAPHICAL OUTPUT.  THE GRAPH IS A      BMP00170
C     POLAR PLOT WITH THE (-PI TO PI) AXIS BEING THE PLATE AND A POINT    BMP00180
C     SOURCE AT THE ORIGIN.                                               BMP00190
C                                                                         BMP00200
C     THE PROGRAM IS CURRENTLY SET FOR A ONE-EIGHTH INCH SHEET OF PLEXI-  BMP00210
C     GLASS IN FRESHWATER                                                 BMP00220
C                                                                         BMP00230
C     THE PARAMETERS ARE:                                                 BMP00240
C                                                                         BMP00250
C        K IS THE WAVE NUMBER IN THE FLUID                                BMP00260
C        PSI, IPSI   ARE THE REAL AND INTEGER VALUES OF THE ANGLE         BMP00270
C        RPSI IS THE ANGLE EXPRESSED IN RADIANS                           BMP00280
C        PI = 3.14159                                                     BMP00290
C        NORM IS THE NORMALIZATION FACTOR, THE ON-AXIS PRESSURE           BMP00300
C        F IS THE FREQUENCY IN HERTZ                                      BMP00310
C        W, OMEGA, IS THE RADIAL FREQUENCY                                BMP00320
C        RHO IS THE DENSITY OF THE PLATE                                  BMP00330
C        RHOWT IS THE DENSITY OF THE WATER                                BMP00340
C        H IS THE THICKNESS OF THE PLATE                                  BMP00350
C        M IS THE AREA DENSITY OF THE PLATE = RHO * H                     BMP00360
C        C IS THE SPEED OF SOUND IN THE FLUID                             BMP00370
C        CI IS THE PLATE WAVE VELOCITY                                    BMP00380
C                                                                         BMP00390
C            CI = (Y/RHO(1-SIGMA**2))**.5                                 BMP00400
C                                                                         BMP00410
C        PI AND P2 ARE PARAMETERS USED IN THE PROGRAM:                    BMP00420
C                                                                         BMP00430
C            PI IS THE RATIO OF THE SOUND SPEEDS, SQUARED:                BMP00440
C               PI = (C/C1)**2                                            BMP00450
C                                                                         BMP00460
C            P2 IS THE RATIO OF THE FREQUENCIES, SQUARED:                 BMP00470
C               P2 = (W/WSUBC)**2                                         BMP00480
C                                                                         BMP00490
C        GAMMAP IS THE PLATE SHEAR PARAMETER = 1.68 FOR PLEXIGLASS        BMP00500
C                                            = 1.23 FOR STEEL             BMP00510
C                                            = 1.39 FOR ICE               BMP00520
C                                                                         BMP00530
C        WSUBC IS THE RADIAL COINCIDENCE FREQUENCY                        BMP00540
C          WSUBCH IS THE HIGH FREQUENCY APPROXIMATION OF WSUBC            BMP00550
C          WSUBCL IS THE LOW FREQUENCY APPROXIMATION OF WSUBC             BMP00560
C                                                                         BMP00570
C        Q1 THROUGH Q3 ARE INTERMEDIATE QUANTITIES USED IN THE PROGRAM.   BMP00580
C                                                                         BMP00590
C                                                                         BMP00600
C                                                                         BMP00610
C                                                                         BMP00620
      REAL  K,PSI,RPSI,R,PI,NORM,KPM,KH,C2,GAMMAP,WSUBC,KP,               BMP00630
     . PA,P0,PC,PO,A,Q,B,WSUBCH,WSUBCL                                    BMP00640
      DIMENSION P(101),PSI(101),RPSI(101)                                 BMP00650
C     ********************************************************************BMP00660
C     *                                                                  *BMP00670
C     *        ENTER PARAMETER VALUES HERE:                              *BMP00680
C     *                                                                  *BMP00690
      DATA     PI/3.14159/,C/    ./,C1/    .66/,H/       /.             BMP00700
     .  GAMMAP/    /,RHO/     /,RHOWT/    /                              BMP00710
C     *                                                                  *BMP00720
```

```
C     ************************************************************** BMP00730
C     ************************************************************** BMP00740
C     *                                                            * BMP00750
C     *         ENTER THE FREQUENCY HERE (REAL NUMBER, IN HZ.) :   *   BMP00760
C     *                                                            * BMP00770
                F *                                                  BMP00780
C     *                                                            * BMP00790
C     ************************************************************** BMP00800
C                                                                    BMP00810
C     ************************************************************** BMP00820
C     *                                                            * BMP00830
C     *  HERE, THE HF LIMIT OF THE FLEX WAVE SPEED IS COMPUTED       BMP00840
C     *  AND THE PLATE WAVE # BASED ON THAT SPEED                  * BMP00850
C       VPH = 0.92 * CI/ 3.                                          BMP00860
C       KP = W / VPH                                                 BMP00870
C     HERE THE PRODUCT K * H IS COMPUTED:                            BMP00880
C     KH = KP * H                                                    BMP00890
C     THE RADIAL COINCIDENCE FREQUENCY IS CALCULATED HERE:           BMP00900
C     THE LF COINCIDENCE FREQUENCY IS HSUBCL :                       BMP00910
C                                                                    BMP00920
      HSUBCL = (12.**0.5I * (C**2.0) / (H*CI)                        BMP00930
C                                                                    BMP00940
C     HSUBCH IS THE HF LIMIT FOR THE COINCIDENCE FREQUENCY:          BMP00950
      HSUBCH = C1 * (3.46/H) * (C**2./(C1**2. - 2.5 * C**2.))        BMP00960
C                                                                    BMP00970
C                                                                    BMP00980
      HSUBC = HSUBCL                                                 BMP00990
C                                                                    BMP01000
C    CRAT IS THE RATIO CG/CP.( C/C1)                                 BMP01010
C     CRAT = C/CI                                                    BMP01020
C                                                                    BMP01030
C                                                                    BMP01040
C     IFREQK = INT(F/1000.)                                          BMP01050
C     THIS AREA SETS UP THE PAGE AND DIRECTS THE OUTPUT:             BMP01060
      CALL SHERPA ('NEW039K','A'.3)                                  BMP01070
C     CALL TEX618                                                    BMP01080
C     CALL PRTPLT (72,6)                                             BMP01090
      CALL BLOWUP (0.75)                                             BMP01100
      CALL PAGE (11.8.5I                                             BMP01110
      CALL AREA2D(8..6.I                                             BMP01120
C                                                                    BMP01130
C     THIS AREA PRINTS THE ANGLES AND MESSAGES:                      BMP01140
C     CALL MESSAG ('F = $'.100.3.25,6.5)                             BMP01150
C     CALL INTNO (IFREQK.'ABUT'.'ABUT'I                              BMP01160
C     CALL REALNO (F.0,'ABUT','ABUT'I                                BMP01170
C     CALL MESSAG ('-KHZ $'.100.'ABUT','ABUT'I                       BMP01180
      CALL MESSAG ('0'.I,3.92,6.05)                                  BMP01190
      CALL MESSAG ('10',2.2.90,6.)                                   BMP01200
      CALL MESSAG ('10',2,4.95,6.I                                   BMP01210
      CALL MESSAG ('20',2,1.85,5.8)                                  BMP01220
      CALL MESSAG ('20',2,5.95,5.8)                                  BMP01230
      CALL MESSAG ('30',2.0.90,5.35)                                 BMP01240
      CALL MESSAG ('30',2,6.95,5.35)                                 BMP01250
      CALL MESSAG ('40',2,0.00,4.85)                                 BMP01260
      CALL MESSAG ('40',2,7.90,4.80)                                 BMP01270
C                                                                    BMP01280
C                                                                    BMP01290
      CALL COMPLX                                                    BMP01300
      CALL HOCHEK                                                    BMP01310
      CALL POLORG (-20.0)                                            BMP01320
      CALL XNAME ('H(PSI)                                            BMP01330
     .     $',100)                                                   BMP01340
      CALL XAXEND ('NOFIRST')                                        BMP01350
      CALL MESSAG ('DBS',100.0..-8.30I                               BMP01360
      CALL XINTAX                                                    BMP01370
      CALL POLAR(I..10.4..0.I                                        BMP01380
C                                                                    BMP01390
C     THIS AREA IS THE COMPUTATIONAL PART OF THE PROGRAM:            BMP01400
      N = I                                                          BMP01410
      W = 2. * PI * F                                                BMP01420
      PSI   = W/HSUBC                                                BMP01430
      K = N / C                                                      BMP01440
```

```
      BETA = (C * RHONT ) / (M*RHO*M  )                                 BMP01450
      P1 = (C     /  C1    ) ** 2                                       BMP01460
      P2 = (M / MSUBC ) ** 2                                            BMP01470
      DO 18 IPSI   = -90. 90                                            BMP01480
         PSI(M) = FLOAT(IPSI) * PI / 180.                               BMP01490
C                                                                       BMP01500
         RPSI(M) = FLOAT(IPSI+90 ) * PI / 180.                          BMP01510
         G1 = (SIN(PSI(M)))**2-P1                                       BMP01520
         G2 = (SIN(PSI(M)))**2-GAMMAP*P1                                BMP01530
                                                                        BMP01540
         P(M)=COS(PSI(M))*(1.+((COS(PSI(M))/BETA)*((1.-PI*G1*G2)/(1.+P1BMP01550
     .   *P1* GAMMAP*G1))))**2)**(-.5)                                  BMP01560
                                                                        BMP01570
         P(M)= 20. * ALOG10(P(M)/NORM(M,C,C1,MSUBC,GAMMAP,BETA))        BMP01580
C                                                                       BMP01590
C        THIS FORCES THE MINIMUM PRESSURE TO BE -20-DB  (AS A HELP IN   BMP01600
C        SCALING THE AXES)                                              BMP01610
         IF (P(M) .LE. -20.0) P(M) = (-20.0)                            BMP01620
   18    M = M+1                                                        BMP01630
C                                                                       BMP01640
C     THIS AREA PRINTS THE MESSAGE ABOUT THE FLUID LOADING:             BMP01650
      CALL MESSAG  ('M/MSUBC = 1'.100.5.2.3.75)                         BMP01660
      CALL REALNO (     P3.2.'ABUT'.'ABUT')                             BMP01670
      CALL MESSAG  ('BETA = 1'.100.5.2.4.05)                            BMP01680
      CALL REALNO (BETA.2.'ABUT'.'ABUT')                                BMP01690
C     CALL MESSAG  ('CG/CP = 1'.100.5.2.4.35)                           BMP01700
C     CALL REALNO (CRAT.2.'ABUT'.'ABUT')                                BMP01710
C     CALL MESSAG ( 'K = M = 1'.100.5.2.4.65)                           BMP01720
C     CALL REALNO (XM.2.'ABUT'.'ABUT')                                  BMP01730
      CALL BLREC(5..3.5.2.2.1.0.2.0)                                    BMP01740
C                                                                       BMP01750
C     THIS AREA PRINTS OUT THE CURVE:                                   BMP01760
      CALL BLSYM                                                        BMP01770
      CALL BLCURV (0.02,0.0)                                            BMP01780
      CALL MARKER (15)                                                  BMP01790
      CALL TMKCRV (.03)                                                 BMP01800
      CALL CURVE (RPSI  .P.101.0)                                       BMP01810
      CALL RESET ('TMKCRV')                                             BMP01820
      CALL GRID(1.1)                                                    BMP01830
      CALL ENDPL(0)                                                     BMP01840
      CALL DONEPL                                                       BMP01850
                                                                        BMP01860
      STOP                                                              BMP01870
      END                                                               BMP01880
                                                                        BMP01890
                                                                        BMP01900
C     THE FOLLOWING FUNCTION SUBPROGRAM CALCULATES THE NORMALIZATION    BMP01910
C     FACTOR -- ALL THE VALUES ARE NORMALIZED TO THE ON-AXIS PRESSURE   BMP01920
C     FOR THE DESIRED FREQUENCY.  HENCE, ALL PRESSURES AT PSI = 0 DEG   BMP01930
C     ARE 0DB                                                           BMP01940
C                                                                       BMP01950
      FUNCTION NORM (M,C,C1,MSUBC, GAMMAP,BETA)                         BMP01960
      REAL      PSI  ,    P1, NORM                                      BMP01970
      DATA     PI /3.14159/,PSI  /0./                                   BMP01980
                                                                        BMP01990
      P1 = (C     /  CI    ) ** 2                                       BMP02000
      P2 = (M / MSUBC ) ** 2                                            BMP02010
                                                                        BMP02020
      G1 = (SIN(PSI  ))**2-PI                                           BMP02030
      G2 = (SIN(PSI  ))**2-GAMMAP*PI                                    BMP02040
                                                                        BMP02050
      P = COS(PSI  )*(1. + ((COS(PSI  )/BETA)*((1.- PI*G1*G2)/(1.+P1*P2*BMP02060
     . GAMMAP*G1))))**2)**(-.5)                                         BMP02070
      NORM = P                                                          BMP02080
      RETURN                                                            BMP02090
      END                                                               BMP02100
```

APPENDIX B

DATA ON TONPILZ VIBRATOR

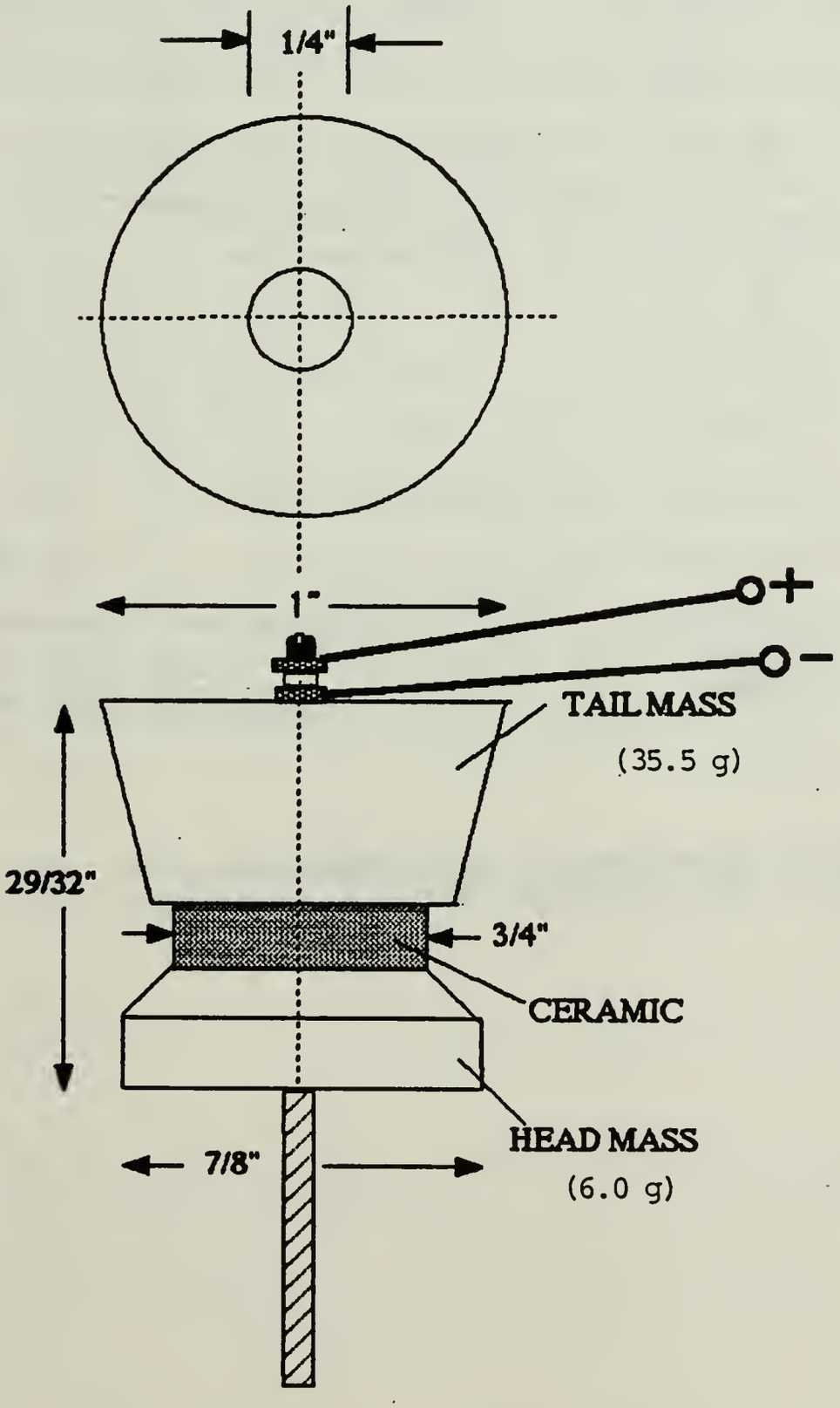

Figure B.1. Diagram of Tonpilz vibrator

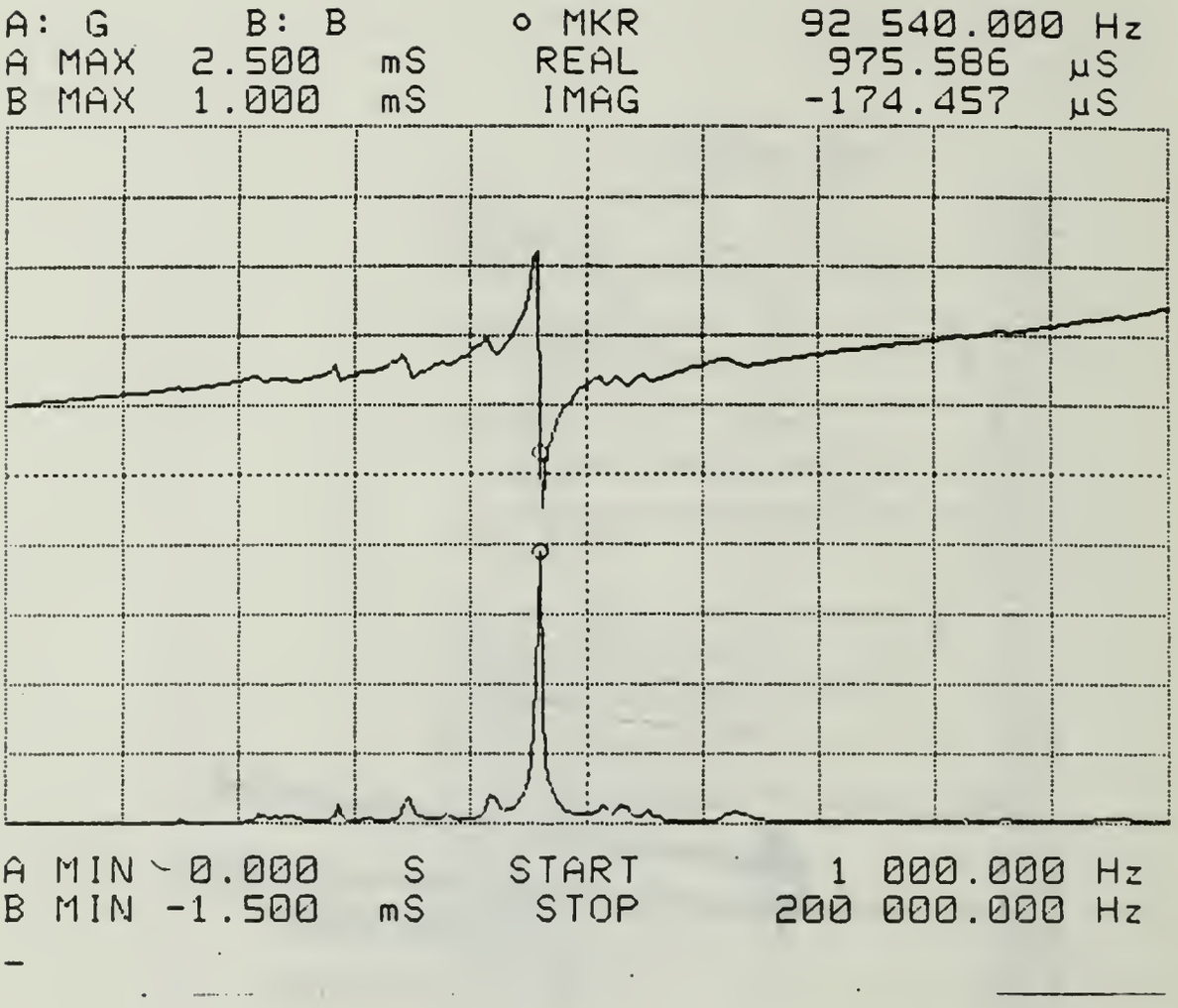

Figure B.2. Susceptance and Conductance vs. Frequency of Tonpilz vibrator

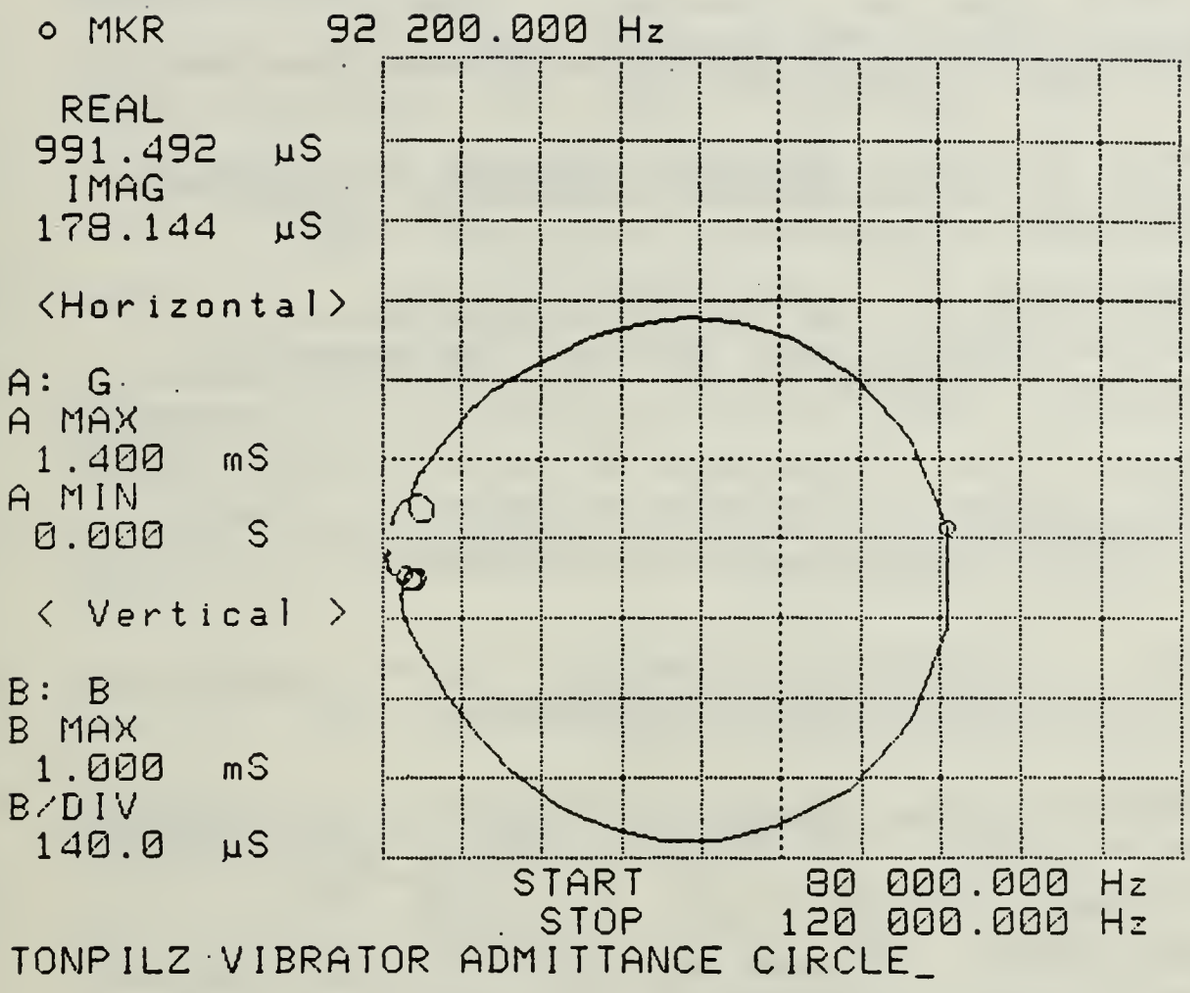

Figure B.3. Complex Admittance circle of Tonpilz vibrator

REFERENCES

1. Press, Frank, and Ewing, Maurice, "Propagation of Elastic Waves in a Floating Ice Sheet," Transactions of the American Geophysical Union, V. 32, N. 5, pp. 673-678, 1951.

2. Stein, Peter J., Acoustic Monopole in a Floating Ice Plate, Ph.D. Dissertation, Massachusetts Institute of Technology, Cambridge, 1986.

3. Timoshenko, S., "On the Transverse Vibration of Bars of Uniform Cross Section," Philosophical Magazine, V. 34.6, 1922.

4. Mindlin, R.D., "Influence of Rotatory Inertia and Shear on flexural Motions of Isotropic, Elastic Plates," Journal of Applied Mechanics, V. 18, pp. 31-38, March 1951.

5. Dyer, I., "Moment Impedance of Plates," Journal of the Acoustical Society of America, V. 32, pp. 1290-1297, (10) Oct 1960.

6. Skudrzyk, Kautz, Green, "Vibration of and Bending-Wave Propagation in Plates," Journal of Acoustical Society of America, V. 33, N. 1, Jan 1961.

7. Feit, David, "Pressure Radiated by a Point-Excited Elastic Plate," Journal of the Acoustical Society of America, V. 40, N. 6, pp. 1489-1494, 1966.

8. Stuart, A.D., "Acoustic Radiation from Submerged Plates," Journal of the Acoustical Society of America, V. 59.5, pp. 1160-1174, 1976.

9. Creighton, D.G., "The Free and Forced Waves on a Fluid-Loaded Elastic Plate," Journal of Sound and Vibration, V. 63, N. 2, 1979.

10. Press, Frank, and Ewing, Maurice, "Theory of Air-Couple Flexural Waves," Journal of Applied Physics, V. 22, N. , pp. 892-899, 1951.

11. Ewing, W.M., Jardetsky, W.S., and Press, F., Elastic Waves in Layered Media, McGraw-Hill, 1957.

12. Ver, I.L. and Holmer, C.I., "Interaction of Sound Waves with Solid Structures," in Noise and Vibration Control, Leo L. Beranek, Ed., McGraw-Hill, 1971.

13. Junger, M.C. and Feit, D., Sound, Structures, and Then Interaction, MIT Press, Cambridge, 1986.

14. Viktorov, I.A., Rayleigh and Lamb Waves, p. 1, Plenun Press, 1967.

15. Medwin, H., personal communication, 27 March 1987.

16. Sanders, J.V., Coppens, A.B., Addendum to Fundamentals of Acoustics, p. 33, 1983, Unpublished.

17. Kinsler, Frey, Coppens, and Sanders, Fundamentals of Acoustics, Section 6.3, John Wiley & Sons, 1982.

18. Brekhovskikh, L.M., Waves in Layered Media, Section 1.5.1, Academic Press, NY, 1960.

19. Officer, C.B., Introduction to the Theory of Sound Transmission, p. 186ff, McGraw-Hill, 1958.

20. Ziomek, L.J., Underwater Acoustics: A Linear Systems Theory Approach, p. 33, 1983, Unpublished.

21. Ross, Donald, Mechanics of Underwater Noise, Ch. 5,6, Pergamon Press, 1976.

22. Ungar, Eric E., "Damping of Panels" in Noise and Vibration Control, Leo L. Baranek, Ed., McGraw-Hill, 1971.

23. Wilson, O.B., An Introduction to the Theory and Design of Sonar Transducers, Government Printing Office, 1985.

24. Denny, P. and Johnson, K., Underwater Acoustic Scattering from a Model of the Arctic Ice Canopy Master's Thesis, Naval Postgraduate School, Monterey, California, December 1986.

INITIAL DISTRIBUTION LIST

		NO. COPIES
1.	Defense Technical Information Center Cameron Station Alexandria, Virginia 22304-6145	2
2.	Library, Code 0142 Naval Postgraduate School Monterey, California 93943-5002	2
3.	Mr. Gerald M. Santos Code 38202, Bldg 104 Naval Underwater Systems Center Newport, Rhode Island 02841-5047	3
4.	Mr. Ken Walsh Code 801, Bldg 990/6 Naval Underwater Systems Center Newport, Rhode Island 02841-5047	1
5.	Professor A. B. Coppens Department of Physics, Code 61Cz Naval Postgraduate School Monterey, California 93943-5000	2
6.	Professor O. B. Wilson Department of Physics, Code 61Wl Naval Postgraduate School Monterey, California 93943-5000	2
7.	Catherine E. Truax Department of Germanic Studies Stanford University Stanford, California 94305	1
8.	LT James G. Stevens, USN Naval Submarine School Code 20, SOAC 87060 Box 700 Groton, Connecticut 06349	2

Thesis
S71265 Stevens
c.1 The temporal and spatial acoustical response of a point-driven, fluid-loaded plate.